

Solutions for Indoor Light Energy Harvesting

STEFANO VIGNATI



KTH Information and
Communication Technology

Degree project in
Communication Systems
Second level, 30.0 HEC
Stockholm, Sweden



*Communication Systems Department
School of Information and Communication Technology
KTH, Kungliga Tekniska Högskolan
SE-164 40 Kista, Stockholm
Sweden*

Solutions for Indoor Light Energy Harvesting

November 20, 2012

Author:
Stefano Vignati
vignati@kth.se

Supervisor at ASSA ABLOY:
Anders Cöster
Examiner at KTH:
Mark T. Smith

Master of Science Thesis
Stockholm, Sweden 2012

Abstract

Energy harvesting (EH) was born few decades ago and evolved during the years, however only recently has found more applications thanks to the advent of wireless sensor networks and the developments in microchips technology.

This thesis investigates energy harvesting potentialities, in particular those related to solar harvesting in indoor applications. Some of the most common challenges are discussed such as: the best maximum power point tracking (MPPT) algorithm for indoor systems; or the effect of partial shading on output performances.

Mathematical and analytical models, for solar panels and batteries, are proposed to simulate at first and simple energy harvesting system.

Furthermore two solar technologies, the present one (silicon cells) and the future one (dye sensitized cells), are simulated and tested to exploit their potentialities.

Finally different commercial solutions are examined and compared to pick the most relevant for this thesis. They are connected to the solar cells and the output characteristics are measured to determine their performances at different illuminances.

Acknowledgements

First of all I would like to thank my supervisor at Assa Abloy AB, Dr. Anders Cöster, for the wonderful working cooperation during the thesis. He is a great and wise person, who gave me support and suggestions during the whole period. Furthermore he was always available and open to solve all the obstacles and help me guiding in the right direction.

I would like to thank also my examiner, Professor Mark T. Smith, who gave me the opportunity to work on this new and interesting topic, and who introduce me to Anders Cöster. During all the courses and the thesis period, Professor Smith's door was always open to me.

Finally I would give a special thanks to my girlfriend Giorgia for the wonderful words she saved for me every night, and her encouragements while I was stuck in difficulties. Lastly, to my family, my friends here in Sweden and all the others spread all over the planet goes my most sincere gratitude.

Stefano Vignati

Contents

1	Introduction	1
1.1	Energy Harvesting	1
1.2	Thesis Plan	2
1.2.1	Problem statement	2
1.2.2	Goals	2
1.2.3	Methodology and Tasks	2
2	Background	5
2.1	Energy Harvesting for Embedded Electronics	5
2.1.1	Specifications	5
2.2	Energy Types and Harvesting Techniques	6
2.2.1	Solar Energy	6
2.2.2	Thermal Energy	6
2.2.3	Vibration Energy	7
2.2.4	Ethernet Energy	7
2.2.5	RF Energy	7
2.2.6	Human Energy	8
2.2.7	Comparisons	8
2.3	Photovoltaic Cells	9
2.3.1	Silicon Cell	9
2.3.2	Dye-Sensitized Solar Cell	11
2.4	Light Measurements	12
2.4.1	Metric Units	12
2.4.2	Illuminance and Irradiance	13
2.5	Power Conversion	14
2.6	Energy Storage	15
3	The Maximum Power Point Tracking	19
3.1	Tracking Problem	19
3.2	MPPT Techniques	20
3.2.1	Ideal	20
3.2.2	Fixed Voltage	20
3.2.3	Fractional Open Circuit Voltage	21
3.2.4	Fractional Short Circuit Current	21
3.2.5	Perturb and Observe	22
3.2.6	Ripple Correlation Control	23
3.2.7	Incremental Conductance	24
3.2.8	Discarded Methods	24

3.3	Technique Selection	25
3.3.1	Selection Rules	25
3.3.2	Analysis of Results	26
3.3.3	Considerations on MPPTs techniques	27
3.4	Available Commercial Solutions	27
4	Modeling and Simulations	29
4.1	PV Cells Models	29
4.1.1	Single diode simple model	29
4.1.2	Single diode detailed model	30
4.1.3	Double diode model	31
4.1.4	DSSC model	32
4.1.5	Parameters Extraction Procedure	33
4.2	Battery Model	34
4.3	SPICE Models	35
4.3.1	a-Si Cell SPICE Model	35
4.3.2	DSSC SPICE Model	37
4.3.3	Battery SPICE Model	37
4.4	Simulations	38
4.4.1	Simulations Setup	38
4.4.2	Measurements Setup	39
4.4.3	a-Si Cell Simulations Results	40
4.4.4	DSSC Simulations	42
4.4.5	Partial Shading	44
4.4.6	Battery Simulations	46
5	PV–Panels Characterization	49
5.1	The Testing Setup	49
5.2	The Characterization	50
5.2.1	Sanyo AM–1815	50
5.2.2	2×Sanyo AM–1454	51
5.2.3	Solarprint SP–7375	52
5.2.4	Solarprint SP–7375–0.5V	53
5.2.5	Partial Shading	54
5.2.6	Nominal Output Power	56
5.2.7	Power Density	57
6	The Harvesting System	59
6.1	Commercial Energy Harvesting Chips	59
6.1.1	BQ25504	59
6.1.2	MAX17710	59
6.1.3	MAS6011	60
6.1.4	LTC4071	60
6.1.5	CBC915	60
6.1.6	ANG1010	61
6.1.7	Considerations	61
6.2	Tested Solutions	63
6.2.1	Energy Harvesting with BQ25504	63
6.2.2	Energy Harvesting with MAS6011	66

6.2.3	Energy Harvesting with MAX17710	67
6.3	Results	70
7	Conclusions	73
7.1	Future Work	74
Bibliography		75
A Schematics of the testing boards		79
B PV panels and testing setup		80

List of Figures

2.1	Typical energy harvesting system elements.	5
2.2	P–n junction silicon solar cell structure.	9
2.3	Atoms arrangement for different silicon cells types. Reused by permission from. .	10
2.4	Different sensitivity spectra for light sources and light absorber. Permissions not granted please refer to fig.11 in [1].	10
2.5	DSSC structure and conversion process. Reused by permission from Macmillan Publishers Ltd: Nature (Applied physics: Solar cells to dye for), copyright (2003). .	11
2.6	Typical spectra of fluorescent light and white LED.	13
2.7	Principle schematic of DC–DC voltage converters, (a) is a linear regulator, (b) is a switching regulator.	15
2.8	Capacity vs. loss diagram. Licensed by Assa Abloy.	17
3.1	P–V (left) and P–I (right) curves at different illuminance levels. Dashed lines show the voltage and current values at each MPP.	20
3.2	Divergence of P&O from MPP.	22
3.3	Working behavior of RCC tracking technique.	23
3.4	Summary methods graph. The numbers on the Y–axis represent the score according the specified classifications system. The highest the score the better. . .	27
3.5	MPPT classification table, with the described parameters	28
4.1	Equivalent circuit of the PV cell representing the <i>single diode simple model</i> parameters and the cell output.	30
4.2	Equivalent circuit of the PV cell representing the <i>single diode detailed model</i> parameters and the cell output.	31
4.3	Equivalent circuit of the PV cell representing the <i>double diode model</i> parameters and the cell output.	31
4.4	Different Interfaces inside a DSSC module.	32
4.5	Equivalent circuit of the DSS cell representing the <i>DSSC model</i> parameters and the cell output.	32
4.6	Discussed battery model with voltage source U_{oc} and series resistance R_i	34
4.7	The circuit model for 4.1.3 (a). The PV module showing inputs and outputs (b). .	35
4.8	Schematic diagram of the described SPICE battery model.	37
4.9	Measurements diagram.	39
4.10	Simulated I–curve of the Sanyo AM–1815 PV panel at 200 lux.	40
4.11	Comparison between simulated and measured values for the Sanyo AM–1815. .	41
4.12	Simulated I–V curve of the Sanyo AM–1815 PV panel, at different illuminance values: (from the bottom) 200, 400, 600, 800, 1000 lux.	41
4.13	Simulated P–V curve of the Sanyo AM–1815 PV panel, at different illuminance values: (from the bottom) 200, 400, 600, 800, 1000 lux.	41

4.14	Simulated I–curve of the G24i DSSC panel at 200 lux.	42
4.15	Comparison between simulated values and measured ones for the G24i DSSC panel. The red line is the simulation and the blue dots are the measured values.	43
4.16	Simulated I–V curve of the G24i DSSC panel, at different illuminance values: (from the bottom) 200, 400, 600, 800, 1000 lux.	43
4.17	Simulated P–V curve of the G24i DSSC panel, at different illuminance values: (from the bottom) 200, 400, 600, 800, 1000 lux.	43
4.18	Four different shading patterns.	44
4.19	Simulated power (up) and current (bottom) curves for a 8 cells a–Si panel, 1 cell shaded (c) scenario, without any bypass diode, at different illuminance values (200, 400, 600, 800, 1000 lux).	45
4.20	Simulated power (up) and current (bottom) curves for a 8 cells a–Si panel, 1 cell shaded (c) scenario, with bypass diode, at different illuminance values (200, 400, 600, 800, 1000 lux).	45
4.21	SOC simulation for a VL2330 connected to a 0.1mA constant load for 24hours. <i>Note: y-axis unit is pure number not V.</i>	47
4.22	SOC simulation for a VL2330 connected to a 10mA pulsed load for 24hours. <i>Note: y-axis unit is pure number not V.</i>	47
4.23	SOC simulation for a VL2330 during charging cycle for 8 working hours for 1 week. <i>Note: y-axis unit is pure number not V.</i>	48
5.1	Current (left) and power (right) curves for Sanyo AM–1815, at different illuminance levels. The black dots represent the MPP.	50
5.2	V_{oc} and V_{mpp} for Sanyo AM–1815, at different illuminance levels.	51
5.3	Current (left) and power (right) curves for 2× Sanyo AM–1454 in parallel, at different illuminance levels. The black dots represent the MPP.	51
5.4	V_{oc} and V_{mpp} for a single Sanyo AM–1454, at different illuminance levels.	52
5.5	Current (left) and power (right) curves for Solarprint SP–7375, at different illuminance levels. The black dots represent the MPP.	52
5.6	V_{oc} and V_{mpp} for Solarprint SP–7375, at different illuminance levels.	53
5.7	Current (left) and power (right) curves for Solarprint SP–7375–0.5V, at different illuminance levels. The black dots represent the MPP.	53
5.8	V_{oc} and V_{mpp} for Solarprint SP–7375–0.5V, at different illuminance levels.	54
5.9	Current (left) and power (right) curves for Sanyo AM–1815, at 185 lux. Every curve is a different shading pattern.	55
5.10	Current (left) and power (right) curves for Solarprint SP–7375, at 185 lux. Every curve is a different shading pattern.	55
5.11	Nominal output power curves (up), normalized curves (down) with respect to Sanyo AM–1815, at different illuminance levels.	56
5.12	Power density curves (up), normalized curves (down) with respect to Sanyo AM–1815, at different illuminance levels.	57
6.1	Thresholds voltages of BQ25504 with respect of the described setup.	64
6.2	Output power of the BQ25504 with a load voltage of 3.0V. Tested performed with 2 types of solar panels.	64
6.3	Power efficiency with respect of the MPP for the BQ25504 at load voltage of 3.0V.	65
6.4	Output power of the BQ25504 with a load voltage of 4.0V. Tested performed with 3 types of solar panels.	65
6.5	Power efficiency with respect of the MPP for the BQ25504 at load voltage of 4.0V.	66

6.6	Output power of the MAS6011 with a load voltage of 3.0V. Tested performed with 2 types of solar panels.	67
6.7	Power efficiency with respect of the MPP for the MAS6011 at load voltage of 3.0V.	67
6.8	Output power of the MAX17710 with a load voltage of 4.0V. Tested performed with 2 types of solar panels.	68
6.9	Power efficiency with respect of the MPP for the MAX17710 at load voltage of 3.0V.	68
6.10	MAX17710 charging behavior. The red line represent the input voltage on the PV panel or on the C5 capacitor, the blue line is the output current to the battery.	69
6.11	MAX17710 output charging current profile.	69
A.1	Circuit schematic used to generate the testing board for MAS6011. The BAT54 diode is used to block reverse current from the battery to the solar cell.	79
B.1	The photovoltaic devices tested in this thesis.	80
B.2	The testing equipment. On top the light controlled chamber, with the lux–meter sensor. On the bottom the two precision multimeters and the DC power supply.	81

List of Tables

2.1	EH techniques comparison chart	9
2.2	Light measures units	13
2.3	Different EH suitable storage solutions families. The symbol (*) means that the value is specific to the model indicated in the text. Data from Assa Abloy	17
3.1	P&O types of perturbations.	22
3.2	Controls for the RCC method according to cases in figure 3.3.	23
4.1	Final parameters for the SPICE model of the Sanyo AM-1815 PV panel.	40
4.2	Final parameters characterized for the SPICE model of the G24i DSSC panel . . .	42
4.3	Panasonic VL2330 specifications.	46
6.1	Summarizing table for EH chips. Prices are for single component and they are extracted from http://www.digikey.com	62
6.2	Summarizing table for EH solutions tested in this chapter. The “–” symbol means that the power value is less than $1\mu W$	71

List of Abbreviations

AC	Alternate Current
ADC	Analog to Digital Converter
DAC	Digital to Analog Converter
DC	Direct Current
DSP	Digital Signal Processor
DSSC	Dye-Sensitized Solar Cell
EH	Energy Harvesting
IC	Integrated Circuit
LD0	Low Drop-out regulator
MEC	Microenergy Cell
MEMS	Micro Electro-Mechanical Systems
MPPT	Maximum Power Point Tracking
PMIC	Power Management Integrated Circuit
PV	Photo-voltaic
SOC	State of Charge
SPICE	Simulation Program with Integrated Circuit Emphasis
STC	Standard Test Conditions
TEG	Thermoelectric Generator
WSN	Wireless Sensors Network

Chapter 1

Introduction

1.1 Energy Harvesting

The idea of Energy Harvesting (EH) is very smart. It consists in using the right means to get the power from the surrounding environment, that would be otherwise wasted.

The world is full of energy sources that are different from the classical non-renewable ones; even human beings are sources of energy. However the difference between energy harvesting and energy mass production is in the aim: the second is needed to power cities, factories, offices, etc. For instance, a power plant produce gigawatts, a small power production system can produce kilowatts, but the power generated by EH source is in the microwatts order. So a billion of devices are needed at least to cover the production amount of a small scale power plant (to power a house). It is clear that EH is not an alternative energy source. Although, if thinking in terms of sustainability, reliability and maintenance costs, EH can give a good contribute to a infrastructure.

The new researches in physics and microelectronics, were able to scale down dramatically the power consumptions of processors and microcontrollers. This reduction gives the possibility to EH sources to power a lot of pocket devices. But also the potential to eliminate the usage of batteries, in the best case. Batteries are good, however only a small number is effectively recycled [2]. They generate waste, that can be extremely dangerous, due to some chemicals inside. If a device is able to scavenge power from the environment, it can prolong its battery life, this translates in less battery substitutions.

Substituting all the batteries in all the electronic door locks of a hotel, for example, will require a huge maintenance cost. Assuming a battery cost of \$4, a battery life of 2 years and an average of 1000 electronic door locks in a hotel. If a maintenance worker is paid \$30 per work hour and he is able to replace 10 batteries per hour the average yearly labour cost will be \$1500 per year. Considering also a product life of the locks of about 8 years and summing up also the battery price, the total cost is \$28,000. This translates into a maintenance cost of \$28 per lock. EH could provide a significant costs reduction, by increasing the battery life, or rather reducing the need of maintenance.

Finally, if a battery completely discharge, the device will not be able to work. In a hybrid system: battery + EH, the device can keep working even if the battery is low. Another possibility is to transmit to the maintenance staff a message alerting the low power status. In this case the system would rely on two power sources conferring it a better reliability.

The first examples of EH devices were the pocket calculators able to work when exposed to light, with just a tiny solar cell, without any battery.

A deeper analysis of the EH sources types is done in next chapter, please refer to section 2.2.

1.2 Thesis Plan

1.2.1 Problem statement

Harvest energy from low power sources is very difficult and not very efficient. There are several sources from which harvest power, such as thermal difference, vibration, movement and radio sources, however this project will focus its attention on small indoor photo-voltaic (PV) cells. The aim of this master thesis is to study, model and test, energy harvesting solutions to the maximize the output power of PV cells, and investigate the feasibility of running an electronic lock with this energy. This project is part of an energy harvesting research, carried out at Assa Abloy AB offices in Stockholm.

1.2.2 Goals

The initial goals were to: *design and find the optimal parameters for the maximum power point tracking (MPPT) circuit, study the best way to control the MPPT and match the load with the charger impedances, in order to harvest the maximum power from a small indoor photo-voltaic cell. All the goals must always follow the initial specifications provided by the Supervisor.*

However after have discovered the fact that a tracking algorithm would not affect positively the energy scavenged from the PV panel, with the approval of the Supervisor and the Examiner, goals were modified in the following elements:

- A wide literature study focused on learning and understanding of: the solar cells topologies, the energy harvesting sources, existing solutions and systems, the light measurements and the current conversion. Study the MPPT topologies and propose a comparison method for those techniques to select them according to the specifications (chapters 2 and 3).
- Model the important elements of a typical EH system: PV panel and battery, in order to have a useful reference for testing and verify on-the-field measurements (chapter 4).
- Implement the models in a simulation environment (PSpice) and test the solutions (chapter 4).
- Using the built testing bench at Assa Abloy AB, acquire data to generate all the useful information regarding: different PV modules current and power curves, investigate the partial shading phenomenon and analyze the power density for the solar modules, especially in relation to the new generations (chapter 5).
- Search, study, list and discuss the commercial solution available and not, for EH aware systems (chapter 6).
- Test deeply the selected commercial solutions in order to acquire more information than what is available on their datasheet, such as: the power output capabilities of the chips and their efficiency for different types of indoor solar panels (chapter 6).
- Draw the thesis conclusions (chapter 7).

1.2.3 Methodology and Tasks

The approach to reach the described goals is first to perform a deep and wide pre-study phase, in order to get the basic knowledge of the field and how the different elements of the EH system behave, for example how the solar panel change the output current at different light levels.

Although the initial pre-study, every time before focusing on a new aspect of the thesis, the author will refine the literature research with new readings. All the components selected or MPPT methodologies are going to be first presented and then selected after careful considerations. Consequently, the performances of the components will be measured and commented within the involved parties. In the final phase all the results will be analyzed and compared to the estimated ones. At the end, there will be the delivery of the final report and a thesis presentation.

Chapter 2

Background

2.1 Energy Harvesting for Embedded Electronics

When designing electronic systems, power management is a crucial aspect to consider. This thesis is focusing the attention on embedded electronics systems such as wireless sensors networks or electronic driven access locks. Those systems require specific electronics input characteristics and can not just be plugged to EH harvester.

A typical energy harvesting system integrates: a harvester, a power conditioning circuit and a storage elements, as showed in figure 2.1. In the following sections all these elements properties and functionalities are discussed. Finally some further digressions are dedicated to photo-voltaic panels and light measurements due to their importance in this thesis.

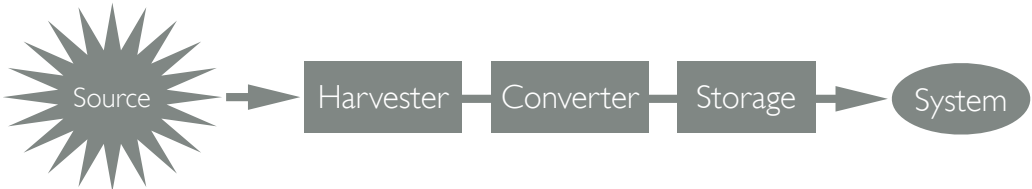


Figure 2.1: Typical energy harvesting system elements.

2.1.1 Specifications

Due to the fact that this thesis work, was part of a preliminary study at Assa Abloy, there were no strict specifications as in already designed products. The main intent was to build an important knowledge, for future developing.

The main characteristic the system should have is to work in indoor environments, such as office spaces or private homes. It must fit on nowadays electronic locks, so the biggest component, which is the PV panel, should not exceed an area of $60mm \times 60mm$. It should be able to work under low light conditions, that translates into the capability of scavenge power with illuminance less than 100 lux. Furthermore the PV panel partial shading should not limit the output power. To avoid this possibility it is helpful to introduce a power tracking algorithm (explained in the next chapter), the algorithm will also set the harvester to work always at the best conditions, in order to maximize the power efficiency.

When it comes to electrical specifications, the system must regulate the input into a stable output to supply the load. The output voltage must be a constant level between 3.0V and 5.0V. The load of the EH system is represented by a constant small power drain ($2 - 10\mu W$), when

the load is in stand-by mode, and aleatory power spikes when the load wake up and run for few milliseconds. However, to what concern the output power, there were no actual specifications, because this thesis was meant to be a research on how much power different technologies are able to harvest from a indoor solar module at low illuminance. In principle all the available power higher than $1\mu W$ is useful to fill up the storage device and build the necessary reservoir to run the load when needed.

2.2 Energy Types and Harvesting Techniques

Electric energy is not available everywhere, however the environment is full of other types of energy sources that need to be processed before being used. This is the fundamental principle on which energy harvesting is based.

This section will describe the various types of energy sources suitable for embedded low power electronics, available at the time this thesis is written. The harvesting techniques and challenges will be discussed and analyzed for the different types.

2.2.1 Solar Energy

Solar harvesting is one of the most mature technology at the moment, in fact it is already possible to find commercial products implementing it. It uses the photo-voltaic effect of the silicon or the electrons generation of the dye layer in dye sensitized solar cells (explained in section: 2.3). Power availability changes according to the positioning of the solar panel with respect of the energy source. For instance, outdoor EH is easily doable thanks to the big power generated by solar irradiation even when overcast conditions, whilst in indoor environments there are more constraints due to the smaller light availability.

The simplest EH method for this solution is to connect the PV panel to the system, throughout a protection diode. Although in most of the cases it is necessary to use a storage device due to the inconsistency of this source if dark light.

A maximum power point should be tracked in order to be able to scavenge the maximum available power at a certain light level.

2.2.2 Thermal Energy

Thermal harvesting is based on the principle that a temperature gradient is found everywhere in different types of environment.

Temperature differences can be utilized to harvest electrical energy using a thermoelectric generator (TEG). The TEG creates electrical power when it is placed between a warm and a cold temperature source. There will be a heat flow from the warm to the cold side and this heat flow makes electrons move within the TEG, creating an electrical voltage that can be harvested. A thermal energy harvester consists in: a Peltier element, a heat sink, a thermal connection and a power conditioning module to match the harvester output with the system input [3].

The Peltier element consists of several p-and n-junctions in series (also called thermocouple); applying a temperature gradient across these results in a charge carrier diffusion from the hot side towards the colder side. This forces electrons (negatives) and hole carriers (positives) to flow and creates a current that generates a voltage across the terminals of the thermocouple [3]. This process is called Seebeck effect.

The output power of a TEG is proportional to the temperature gradient. The challenges for this EH topology are represented by the low output voltage, that would need to design a charge pump circuit to reach higher level, and a maximum power point tracking algorithm.

2.2.3 Vibration Energy

Vibrational harvesting can be used whenever there is a movement. Vibrations are especially available in transportation industry and in industrial machineries. There are three types of harvester mechanisms: piezoelectric, electromagnetic and electrostatic.

Piezoelectric harvester works using a piezoelectric material (or piezo) that accumulates charge when strained and consequently produces a voltage . A piezo can be connected to a button that generates power when stroke it, or can be fixed to one side and connected to free moving mass to the other.

Electromagnetic harvester transforms kinetic movement in electric energy, when a coil is moved around a permanent magnetic field, generating in this way a voltage difference.

Electrostatic harvester converts the mechanical energy generated by the movements of two capacitor plates inside a MEMS (Micro Electro–Mechanical Systems) into electrical energy. The plates movements can be both horizontal and vertical, allowing this device to be useful for three dimensional vibrations. Energy inside a capacitor is equal to $E = 1/2CV^2$ and the charge is $Q = CV$, in this way, when applying a constant charge on the capacitor plates, a capacitance variation produces energy variation to supply the load.

The main constraint with vibrational harvester is the output current, due to their vibrational nature, the current produced is alternate (AC), for this reason a rectifier must be integrated in the circuit design to convert it to a direct current (DC) level. Furthermore, all vibrating systems has a specific resonance frequency at which the AC oscillates, at this frequency the power is maximum, if the harvester is not working at this specific frequency the energy generated will be very low. As consequence, the rectifier must work at the resonance frequency on the AC side.

Piezoelectric devices are easy to fabricate and cheap, they can also be integrated on chips as well as electrostatic devices. The electromagnetic generators can generate high output–current levels but the voltage is very low (typically <1V). Both piezo and electromagnetic harvesting techniques have been shown to be capable of delivering power to the load in the range of μW to mW [3].

2.2.4 Ethernet Energy

Ethernet harvesting consist in collecting packets traveling on a transmission line and use their energy to power other devices. The main difference to other energy harvesting technologies is that energy level does not change according to environmental conditions, however, is expected to vary depending on some factors such as transmission speed [4]. Signals on ethernet cables are analog signals of AC type, for this reason, they need to be rectified to allow the power management IC to accumulate energy.

Currently there are three types of ethernet connections according to the maximum transmission speed. 10Base–T standard provides more energy, however it comes up with disadvantages such as: requiring packet transmission, in fact when the system is idle is not possible to scavenge power, and it is an obsolete standard. On the other hand, 100Base–T provides less energy compared to 10Base–T, but does not require packet transmission because during idle phase current pulses are still sent, furthermore is the most popular ethernet standard nowadays. 1000Base–T also does not require packet transmission and provides energy levels slightly higher than 100Base–TX [4].

2.2.5 RF Energy

RF harvester is based on the fact that nowadays, radio frequency (RF) waves are everywhere scattered all over the air. This area is still under research and there are few experiments done, [5]

and [6]. However it has a lot of challenges: first of all, radio waves spectrum is very wide, starting from audio broadcast, to video broadcast, from GSM and 3G cellular to Wi-Fi. The scavenging antenna is important together with its orientation. The distance between the transmitter and the receiver, is also a challenge together with: obstacles in the path, attenuations in the propagation mean and the source transmitting power.

In [5] they propose two harvesting methods, one for broadband and one for a narrowband of frequencies. They have captured they waves from commercial RF broadcasting stations like GSM, TV, WIFI or Radar in a non precise urban environment. The average of the density in broadband ($1 - 3.5\text{GHz}$) is in the order of $-12\text{dBm}/\text{m}^2$ ($63\mu\text{W}/\text{m}^2$). They claim also that, power density variation is found to be between $-60\text{dBm}/\text{m}^2$ and $-14.5\text{dBm}/\text{m}^2$ ($1\text{nW}/\text{m}^2$ and $35.5\mu\text{W}/\text{m}^2$) and is constant over time. The maximum of this power density has been measured in the $1.8 - 1.9\text{GHz}$ band [5]. However due to several constraints, they were able to scavenge only about 400pW for the narrowband system.

Finally [6], propose a efficient and interesting integrated circuit to harvest RF energy, as well as a corporation, Powercast, is offering some commercial solutions. In conclusion, RF harvesting shows positive signals, but at the moment, it can be feasible only for short range implementations.

2.2.6 Human Energy

Human body is producing a lot of energy everyday in different forms. Since ancient times, humans where used in hard works due to their power. At the moment, there are several researches going on to build a system able of scavenging energy this kind of source.

Mainly human body generates passively two types of energies: thermal and kinetic, for example a foot heel striking on the shoe sole[7]. However [7] lists all the possibilities including harnessing energy from: breathing, blood pressure, exhalation, arm motion, finger motion. The challenges in these cases are: to collect those sources in the most efficient way and to avoid annoying people by wearing invasive probes or to change their living behaviors. The most common way to do that is to implement some kinds of “smart” clothing.

In [8], they converted cotton T-shirt textiles into activated carbon textiles (ACTs) for energy storage applications. After such functionalization, the textile features were well reserved and the obtained ACTs are highly conductive and flexible, enabling an ideal electric double layer capacitor (EDLC or supercapacitor) performance. This achievement will open the road to a new EH field, with the objective of using the wasted energy of human body to power electric devices.

It must be remembered that, human body is not only capable of generating energy passively, but also actively. In fact people can produce it also in other ways, that do not involve wearability. For instance when opening or closing doors or closets, when biking or when strikings buttons on a computer keyboard.

2.2.7 Comparisons

To sum-up, all the techniques are listed in table 2.1. The data in the table is extracted from experimentations, literature (cited in previous subsections) and assumptions, in order to give an idea to the reader, regarding the level of maturity of the different technologies.

The best way to compare techniques is to present their power densities, however it is very difficult to compare those different technologies in such a way. For this reason, the author have chosen to list the typical output power under average conditions. The solar harvesting presents the value at 200 lux of illuminance, which correspond to an office environment with fluorescent

light. Thermal harvesting value is given for a $5^{\circ}K$ temperature gradient. The ethernet harvesting is considered when using 100Base-TX standard; the data speed is not relevant because in the absence of packet transmission, IDLE symbols are transmitted continuously. The piezoelectric and electromagnetic vibrational energies are analyzed when the acceleration of the vibrating system is equal to $\pm 1m/s^2$ [9]. Finally as human energy is considered the [7] experiment of the foot heel striking on a piezoelectric harvesting shoe sole for a 52 kg user.

Table 2.1: EH techniques comparison chart

EH Technology	Voltage [V]	Typical output power [μW]	Challenges
Indoor Solar	0.5 – 6.0	160 at 200lx	MPPT, low light, orientation
Thermal	0 – 5.0	100 for $5^{\circ}K$	MPPT, charge pumping
Piezoelectric	0 – 20	80 for $\pm 1m/s^2$	AC rectification, frequency tuning
Electromagnetic	0 – 10	700 for $\pm 1m/s^2$	AC rectification, frequency tuning
Electrostatic	0 – 2.0	< 50	AC rectification, low charge
Ethernet	0 – 1.0	350	AC rectification, data rate
Radio Frequency	0 – 1.0	< 1	Attenuation, distance, obstacles
Human Energy	0 - 20	1.5×10^6 per step	Materials, wearability, durability

A clarification is important at this point: whilst vibrational energies give a certain power only for the resonance frequency and ethernet is fixed because of its technology; solar and thermal sources change their output according to the energy available. Although thermal variation are usually very slow, solar ones occur more often, for this reason, solar energy is more susceptible to variation and easier to work with. Solar energy is also the most mature at the moment of writing this thesis, those facts justify the choice of this technology in the project.

2.3 Photovoltaic Cells

2.3.1 Silicon Cell

Silicon solar cells has the characteristic of generating power due to the photo-voltaic (PV) effect of semiconductors. When light hit the silicon (Fig. 2.2), reacts with this one and generates positive and negative charges, represented by holes (positive) and electrons (negative). The

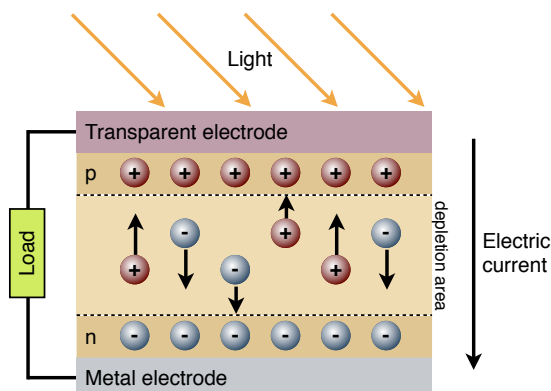


Figure 2.2: P–n junction silicon solar cell structure.

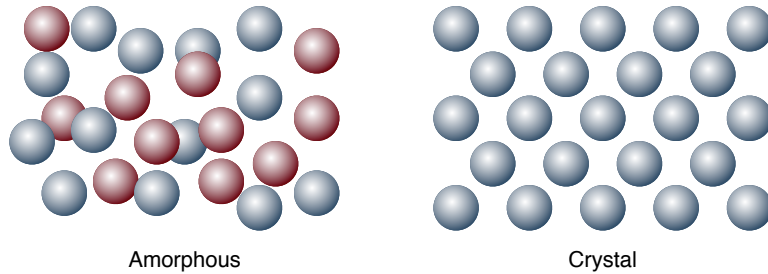


Figure 2.3: Atoms arrangement for different silicon cells types. Reused by permission from.

different doped silicon sections, represent the so called, p–n junction; after the generation, the charges start moving to the respective junction. The holes move towards the p–area and the electrons towards the n–area. This movement generates a depletion area in the middle that results in a voltage difference at the metal electrodes. Sequentiy, if a load is connected to the cell, the electrons move inside the load generating a electric current.

Solar cells are classified according to the material used in the fabrication process, such as: mono-crystalline silicon (c–Si), poly-crystalline silicon or amorphous silicon (a–Si). The silicon cells used in this thesis are the amorphous ones. Unlike crystal silicon, where the atoms inside are placed in structured disposition, in the amorphous one the atoms are scattered (Fig 2.3). As result, the reciprocal action between photons and silicon atoms, occurs more frequently in amorphous silicon than in crystal silicon, allowing much more light to be absorbed [1]. Another important difference between a–Si and c–Si cells, is that they have different spectral sensitivity with respect of absorbed light. As shown in figure 2.4, sunlight and fluorescent light have very different emitting spectra. Also the sensitivity changes a lot according to the sensing device. However it is clear from the figure that a–Si cells are suitable both for indoor use (fluorescent light) and outdoor (sunlight), whilst c–Si ones present a lower sensitivity in the spectral range, where the fluorescent light peaks are.

Silicon cells, as already described, show a behavior typical of the junction diodes, similarly to them, cells have also a similar open circuit voltage around 0.7V. For this reason, in order to achieve different and higher voltages, cells are placed in series. If instead ,the intent is to

Reusing permissions not granted.

Figure 2.4: Different sensitivity spectra for light sources and light absorber. Permissions not granted please refer to fig.11 in [1].

achieve a higher output current, cells are placed in parallel. In outdoor PV panels they use a hybrid solution in order to achieve both high voltage and high current to be able to produce more power. In indoor solutions, due to the limited amount of space, cells are usually placed in series to generate the voltage level to operate digital circuitry.

2.3.2 Dye–Sensitized Solar Cell

Photovoltaic devices are based on the concept of charge separation at the interface of two semiconductive materials differently doped. To date this field has been dominated by solid-state junction devices, usually made of silicon, and profiting from the experience and material availability resulting from the semiconductor industry. The dominance of the photovoltaic field by inorganic solid-state junction devices is now being challenged by the emergence of a third generation of cells, based on nanocrystalline oxide and conducting polymers films [10].

The Dye–Sensitized Solar Cell (DSSC) is a non-silicon based photovoltaic system that operates effectively under low and diffuse light conditions, including indoor artificial light. The DSSC was invented by Michael Grätzel and Brian O'Regan at the École Polytechnique Fédérale de Lausanne EPFL) in 1991. DSSCs are electrochemical devices comprising a light-absorbing dye molecule anchored onto semiconducting titanium dioxide nanoparticles. Though the technology is 20 years old, it has not made an impact commercially due to relatively low performance and poor long term stability compared to existing photovoltaics [11].

The peculiarity that distinguishes the DSSCs from p-n junction solar cells, is that in the latter all the separation, depletion and recombination processes take place in the same material. Although a DSSC has a multilayer structure that physically separates the processes of light absorption and charge-carrier transport (Fig. 2.5). Photons are harvested by dye molecules adsorbed on the surface of a thin gold film (**1**), which is resting on a layer of titanium dioxide (TiO_2). Spontaneous electron flow from the semiconducting TiO_2 layer to the metallic gold layer (**2**) imparts a slight negative charge to the gold, leaving a slight positive charge on the TiO_2 . The

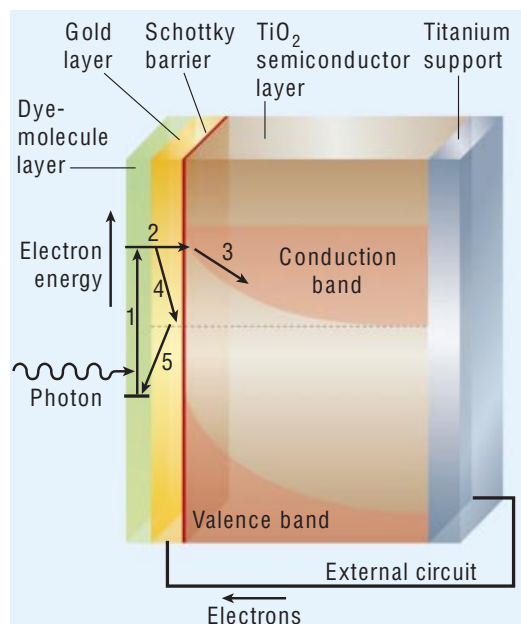


Figure 2.5: DSSC structure and conversion process. Reused by permission from Macmillan Publishers Ltd: Nature (Applied physics: Solar cells to dye for), copyright (2003).

resulting local electrostatic field creates a potential barrier between the TiO_2 and gold layers, called a Schottky barrier. When light falls on the dye layer, electrons are released from the dye molecules and injected into the conduction band of the metal layer (3). To generate electric current through the device, these electrons must have enough energy to travel to (4) and over (5) the Schottky barrier, to reach the TiO_2 conduction band. From there, they are transported to the titanium support layer that acts as a current collector, and then to the external circuit [12].

DSSCs provide us a technically and economically viable alternative way for traditional p-n junction silicon solar cells. Although they use a number of advanced materials (like TiO_2 nanoparticles), these are inexpensive compared to the silicon needed for normal cells because they require no expensive manufacturing steps. TiO_2 , for instance, is already widely used as a paint base.

2.4 Light Measurements

Light is a electromagnetic wave, but it represents only a small part of it. In order for engineer to design a photovoltaic system, they have to know the sunlight availability at certain conditions to correctly size the PV panels. For this reasons some sun standard spectra are defined. AM_x is the standard [13], where AM stays for Air Mass, x is defined as:

$$x = \frac{1}{\cos \vartheta_z} \quad (2.1)$$

where ϑ_z is the angle between the highest point reached by the sun on its apparent orbit and the horizon. For $AM0$ is intended the sun radiation in the outer space, $AM1.5$ is the sea-level spectrum. $AM1.5$ is chosen as standard scenario for on-earth applications with its zenith angle of 48.19° ($x = 1.5$). The total irradiance of this spectrum calculated by integrating it over the wavelengths is equal to $1000W/m^2$. Since it is a standard, all the manufacturers provide the PV cells or panels output values for $AM1.5$. Whilst they do not give performances with respect of fluorescent light spectrum.

Although this considerations, this thesis aim is to develop a indoor EH system. It was clear from the beginning that $AM1.5$ will not give any useful information since it represents the sun radiation, whilst fluorescent spectrum is very different, as seen in figure 2.4. In addition to this measuring radiation is more difficult and expensive, because it requires to measure every wavelength and then integrate the results to get the data.

Measuring illuminance is easier than irradiance. Illuminance is the perceived light by the human eye. In fact the instrument sensitivity curve is adapted to match the one of human eye (the green curve in fig. 2.4). The instrument to measure the illuminance is called *lux-meter* from the name of the measure unit: lux (lx).

2.4.1 Metric Units

Differently from other types of entities, such as temperature, speed, weight; light, due to its nature, is not easy to measure. It can be distinguished in two types of units: *radiometric* consisting in the measure of power at all the wavelength and *photometric* consisting in the measure of light at a certain wavelength weighted with the human eye absorption spectrum.

The most important photometric light quantities are:

- *Luminous flux*: total visible emitted light power;
- *Luminance*: luminous intensity per unit area projected in a given direction;

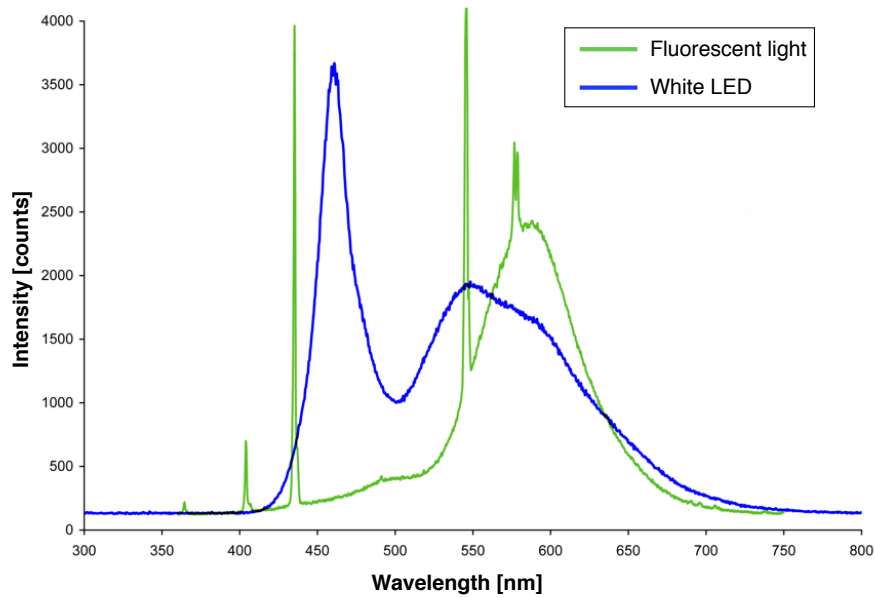


Figure 2.6: Typical spectra of fluorescent light and white LED.

- *Illuminance*: luminous flux incident on a surface per unit area;
- *Luminous intensity*: luminous flux per solid angle.

For the rest of photometric quantities and the relative units, check table 2.2.

Table 2.2: Light measures units

Quantity	Symbol	Units
Wavelength	λ	nanometer (nm)
Luminous energy	Q_v	lumen–seconds (lm–s)
Luminous energy	U_v	lumen–seconds/m ³ (lm–s/m ³)
Luminous flux	Φ_v	lumens (lm)
Illuminance	E_v	lux (lx; lm/m ²)
Luminance	L_l	lumens/m ² /steradians(lm/m ² /sr)
Luminous intensity	I_v	candela (cd; lm/sr)

2.4.2 Illuminance and Irradiance

As stated before, manufacturers provide information about their solar products with respect of the AM1.5 standard. This standard means that the PV panels they produce are tested under an irradiation of $1000\text{W}/\text{m}^2$. This value corresponds approximately to a sunny day condition, and it is obviously very big compared to irradiation levels available in a office or in a house room.

The decision of using *illuminance* instead of *irradiance* for the light information does, however, bring some conversion problems. The lux is one lm/m^2 , and the corresponding radiometric unit, which measures irradiance, is the W/m^2 . There is no single conversion factor between *lux* and W/m^2 ; there is a different conversion factor for every wavelength, and it is not possible to make a conversion unless the spectral composition of the light is known. The peak of the eye-sensitivity curve is at 555nm (green), this means that human eye is more sensitive to this

wavelength than any other. For $1lx$ of light at this wavelength, the correspondent value is $1.464mW/m^2$; in the same way, $1W/m^2$ is equal to $683lx$. From this consideration a primitive conversion rule can be extracted:

$$E_{v(555nm)}[lx] = 683 \times E_{e(555nm)} \quad (2.2)$$

This is only valid if the irradiance (E_e) has a peak at $555nm$ with a value of E_e . Viceversa for a source emitting light only at $555nm$ with an illuminance of E_v , the irradiation is:

$$E_{e(555nm)}[W/m^2] = 1.464 \times 10^{-3} \times E_{v(555nm)} \quad (2.3)$$

Since $555nm$ represents the maximum, where the conversion is direct 1:1, for other wavelengths there is an attenuation, in other words they produce smaller irradiation. Finally if the radiation is in the infrared spectrum there is no possible conversion, because illuminance considers only the visible spectrum.

Furthermore it is useful to remember that both illuminance and irradiation represent the luminous flux or the power, spread over a given area. In this way a flux of $1000lm$, for example, concentrated into an area of $1m^2$, gives an illuminance of $1000lx$. However the same amount of flux spread out over $10m^2$ area, produces a dimmer illuminance of $100lx$.

For the reason that correlating the illuminance with the irradiance is very difficult and requires assumptions, in this thesis was abandoned the irradiation measure. Furthermore all the tested solar panels have a sensitivity curve close to the human eye one, and the sensitivity peaks are all within the $555nm$ wavelength [1, 14]. All the data are provided in this thesis are measured with respect to the illuminance. Illuminance is also better to quantize the light levels for indoor environments, and the reader could easily understand it.

2.5 Power Conversion

In the past years, power management, was an important part of a electronic device, but not as critical as nowadays. Due to improvements into microchips fabrication processes, ICs became more susceptible to power noise, for this reason it is very important to process the input power in order to provide a constant supply to the chips.

The role of power management circuits or ICs (PMIC –Power Management Integrated Circuits), is to convert an unstable, noisy, intermittent input current, into a regulated one (DC, direct current).

According to section 2.2 there are two kinds of energy sources, the *DC* and the *AC*. The PMIC needs to be able to convert the respective currents into a DC one with the properly characteristic of the system load or of a storage device. The conversion must be the most efficient as possible, otherwise a power loss will degrade significantly the output energy. Efficiency is an important parameter in the selection and implementation of a PMIC.

There are different solutions to convert an input DC voltage into a suitable output level, however the two main typologies used in this thesis are: the *linear regulator* and the *switching regulator*.

A *linear regulator* (fig. 2.7a) is used to maintain a stable voltage by adjusting a resistor according to the load. A closed loop is controlling the adjustment by comparing the output voltage to a reference level. The main characteristics is to take an higher DC unstable level, and converting it into a smaller stable DC, however some energy is dissipated as heat in the conversion, decreasing the efficiency. An improvement to the linear regulator is the *low-dropout regulator* (LDO). It can operate at smaller DC voltages difference, resulting in a higher flexibility

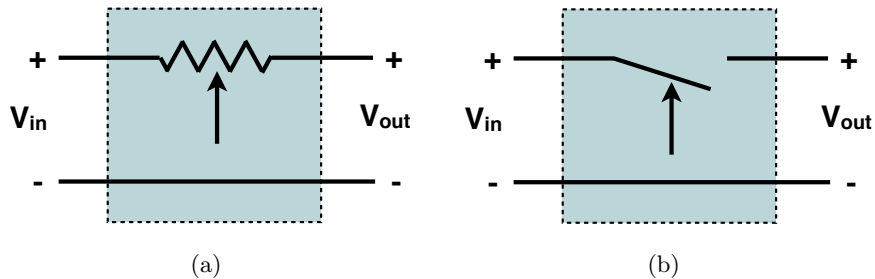


Figure 2.7: Principle schematic of DC-DC voltage converters, (a) is a linear regulator, (b) is a switching regulator.

and less heat dissipation. In general linear regulation is used for input voltages close to the load one and small load systems, in this case they consumes less power than switching regulators.

The *switching regulator* (fig. 2.7b) is basically a switch that goes on and off. The time that the switch close the circuit (duty cycle), determine the output voltage. According to the output voltage, the switching converter are divided into two categories: *buck converter* and *boost converter*. A buck converter is a step-down DC-DC converter, meaning that the output voltage is lower than the input one. Otherwise, a boost converter is a step-up DC-DC converter, where the output voltage is higher than the input one. However this considerations, for both converter the power formula $P = VI$ is always valid. That translates into a power balance between the input and the output: if the $V_{out} > V_{in}$ at the same time $I_{out} < I_{in}$, and viceversa. Anyway, certain amount of power is lost in the conversion due to internal resistance of components and the switching circuit, but a good switching regulator can give efficiency as high as 80% – 95%.

Another important characteristic that PMIC connected to batteries should have, is the represented by charging thresholds. These thresholds do not allow the load or the energy source to overdischarge or overcharge a battery, avoiding to persistently damage the storage device. However this feature is not easy to implement, because there are several battery families with different voltages and properties. One solution that manufacturers adopt is to have agreements with battery supplier and design their ICs suitable only for a battery type. Another solution is to produce ICs with programmable charging thresholds.

Finally due to market demand and also to stand-out the other competitors, PMICs manufacturers are adding several additional features (such as MPPT, voltage regulators, clocks, microcontrollers), enriching the design possibilities and reduce the number of other external components need, bringing down the costs and the power consumption.

2.6 Energy Storage

Energy sources, as seen in section 2.2, are very rare and inconsistent over time. A system would stop working in the night if relying only on the output of a solar cell. For this reason storing harvested energy is very important. Storage elements field is very broad, so it is necessary to remember that in this thesis are all devices suitable for low power electronics (less than 1W consumption). Sequentiy, when are used terms as high power or peak power are intended power values of $> 10mW$, on the other hand, small power is everything below 1mW.

There are several types of storage elements such as *batteries* or *capacitors*, however the crucial characteristic for this thesis, is that they must be able to be charged and discharged several times, since this is most likely how they are going to be used. The main physical difference between capacitors and batteries, is how the energy is stored: in the capacitor the

energy is stored on the plates thanks to a electric field, in the battery instead the energy is stored in chemical format and then converted into electrical energy. This justify also that batteries performances decays after charging cycles, due to chemical deterioration, instead capacitor can be charged more than a million of times without significant deterioration.

The are two main batteries families: primary batteries and secondary batteries. The primary ones are able to produce current flowing immediately upon assembly, due to the chemical reactions. The secondary batteries are called also rechargeable, because they need to be charged before being used, but they have the property of being to be charged several times. There are several types of batteries according to the materials used, some examples are: alkaline, lithium-ion (Li-Ion), lithium-cobalt, lithium-vanadium (LiVa), lithium, nickel-metal hydride (NiMH), thinfilm lithium.

Capacitors are passive components and they store the energy thanks to an electric field. They discharge and re-charge very quickly, in this way they can provide a lot of power but only for a short time. So capacitors have a lot of power capability but small energy capacity. On the other hand, batteries are slow devices, providing less power but for longer periods, they are not able to stand high peaks of power demand, but they work efficiently in constant load conditions. Supercapacitors are a evolution of capacitors with higher energy, but still not able to reach energy level in batteries. The important parameter to take into account when considering supercapacitors is the leakage current, proportional to capacity, temperature and voltage. Initial leakage is quite high, but declines over time. Since this current is usually high, it can rapidly discharge a capacitor.

When choosing a storage element there are some important characteristics to evaluate them:

- *Nominal voltage* is the voltage at which a battery is rated to operate by the manufacturer. Although the real operating voltage varies between two values according to the state of charge. To what concerns capacitors, they only have a maximum voltage, so they can work to every DC level from 0V to V_{max} .
- *Capacity* is the specific energy expressed in Ampere-hours (Ah). It means that in 1 hour a battery provides the specified amount of current.
- *Energy* is how much power can be delivered during a certain amount of time and it is measured in watt-hour (Wh).
- *Self discharge* is a chemical reaction that reduces the stored charge without connecting the two electrodes. It is measured as a current in Ampere (A). Since it is a chemical reaction it is more effective at higher temperatures.
- *Internal resistance* is an internal series resistance that oppose to the internal flow of current, it is expressed in Ohms (Ω).
- *Life Cycles* are the number of times a storage element is able to complete a cycle (charge and discharge).

In table 2.3 is reported a study at Assa Abloy on energy harvesting specific storage solutions. All the data comes from several experiments and measurements. Some solutions are hybrid versions such as: combination of several cells stacked in parallel ($10 \times$ Thinfilms) or combination of battery and supercapacitor. As thinfilm battery was used a 2.5mAh capacity one, like for the 10 stacked thinfilms. As LiVa battery was used a 50mAh capacity one, whilst for the Li-Ion a 40mAh one. Analyzing the table is clear that Li-Ions are not suitable for EH due to their low level of life cycles, in fact an EH system could be charged and discharged several times per day,

Table 2.3: Different EH suitable storage solutions families. The symbol (*) means that the value is specific to the model indicated in the text. Data from Assa Abloy.

Storage type	Nominal voltage [V]	Capacity [mA·h]	Energy [mWh]	Self discharge [μA]	Internal resistance [Ω]	Life Cycles
Thinfilm	4.1	0.13-2.5	0.5-10	0.3	15*	10^5
10×Thinfilms	4.1	25*	100*	3*	1.5*	10^5
Supercapacitor	2.5	0.01-0.5	0.025-0.5	1-5	< 0.5	Unlimited
Thinfilm and supercapacitor	4.1	0.13-2.5	0.5-10	1-5	< 0.5	10^5
LiVa	3.0	1.5-100	4.5-300	0.12*	30*	2×10^4
LiVa and supercapacitor	3.0	1.5-100	4.5-300	1-5	< 0.5	2×10^4
Li-Ion	3.7	10-2800	40-10 ⁴	2*	2*	500

thus compromising battery life. Thinfilm and LiVa batteries are good candidates, they are both going to be considered because, as showed later, PMICs are using those technologies. Finally, a supercapacitor alone has low level of energy instead when associated to a secondary battery, the lack is compensated. This hybrid system will be more capable of addressing both energy and power demands. Losses (due to internal resistance) inside a storage element are very important because they will determine how fast will react to peak current. High loss systems will not work with high peak currents.

The last consideration is about the size of storage elements. In fact it is clear in figure 2.8, that smaller batteries not only have smaller capacities, but also higher losses than the bigger counterparts. For this reason a tradeoff among the specifications is always necessary, to choose the best solution.

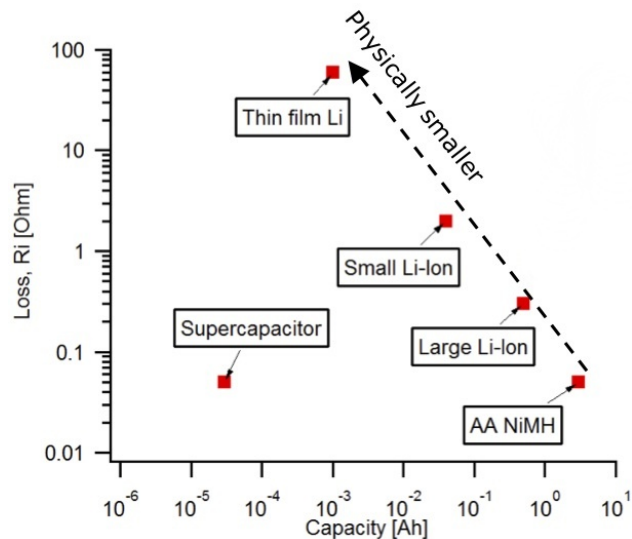


Figure 2.8: Capacity vs. loss diagram. Licensed by Assa Abloy.

Chapter 3

The Maximum Power Point Tracking

Unfortunately, PV generation systems have two major problems: the conversion efficiency of electric power generation, which is very low (9–17%) especially under low irradiation conditions, and the amount of electric power generated by solar arrays, which changes continuously with environmental conditions [15].

Tracking the maximum power point (MPP) of a photovoltaic (PV) array is usually an essential part of a PV system. As such, many MPP tracking (MPPT) methods have been developed and implemented. The methods vary in complexity, sensors required, convergence speed, cost, range of effectiveness, implementation hardware, popularity, and in other aspects [16].

The aim of this thesis is to focus on the Energy Harvesting (EH) field. All the MPPT techniques analyzed in [16], are taking into account PV systems employed to generate high amounts of power, in order to power house, commercial or industrial facilities. Energy Harvesting MPPT techniques and algorithms have to deal with harder constraints, such as: low generated power, voltage conversion, leakages, efficiency and power consumptions.

There are several researches on this field using different methods but not all of them are suitable for energy harvesting. This chapter will investigate different MPPT techniques, developed originally for large PV systems, but can be feasible also on low power PV cells.

3.1 Tracking Problem

Tracking the maximum power point of a dynamic system is important, otherwise the power loss can become very big, making the system not efficient. The voltage–current curve of a PV cell is varying according to different light conditions. When calculating power values with the formula $P = V \times I$, the voltage–power graph looks like the one in figure 3.1 (left). The graph shows that there is usually only one power peak at a certain voltage V_{MPP} . The voltage coordinate of the peak is changing every time light changes. Because of this, the MPPT system should track the changes and be able to promptly react to keep the circuit working at the maximum power point. If MPP is not tracked, the system would not receive the maximum available power at that certain time. The same considerations done for the power–voltage (P–V) characteristics are valid for the power–current (P–I) ones. Power relates together current and voltage, this means that for a certain MPP there is not only an optimal voltage value V_{MPP} , but also an optimal current I_{MPP} as show in figure 3.1 (right).

According to [16], the partial shading of a PV panel, could affect the PV curves and in some cases it is possible to have multiple local maxima. What is happening inside a shaded solar module is deeply explained in section 4.4.5. The end result is that the tracking system would no longer be able to extract the MPP under such conditions [17]. MPPT devices that take into

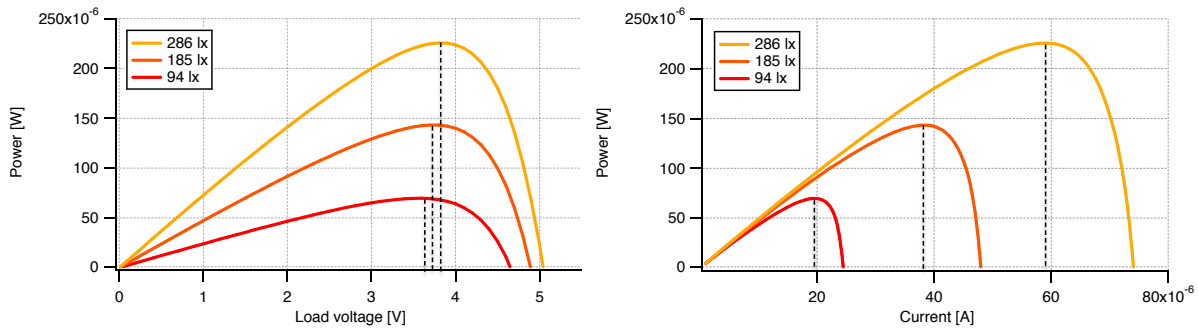


Figure 3.1: P–V (left) and P–I (right) curves at different illuminance levels. Dashed lines show the voltage and current values at each MPP.

account partial shading are more complex. A radical solution to this problem is using a single large PV cell (as discussed in section 5.2.5) but it will also sacrifice the voltage output.

The principal requirements for a MPPT are: to be able to track always the true MPP also under changing light conditions; to be fast enough in order to keep track of sudden changes; to be not very complex to not increase costs and power consumptions; to be efficient in order to deliver all the available energy; to consume low power otherwise it is not useful anymore and finally to be cost effective.

In the following paragraphs some techniques will be investigated and evaluated according to established parameters.

3.2 MPPT Techniques

3.2.1 Ideal

The *ideal* tracking system would have very good performances with low realizations and components costs, high efficiency and low power consumption, it would track MPPT even in partial shading light conditions. It would be also technology independent, being able to use both a-Si and DSSC panels.

3.2.2 Fixed Voltage

The *fixed voltage* is the simplest possible implementation. Instead of tracking always V_{MPP} , it is selected the average V_{MPP} for the most common scenario. This method is an empirical method, based on several experiments and measurements in different light conditions, in order to determine the average value of V_{MPP} . A big problem with this method is that the PV cells characteristics differs from one to the other, even for the same production family.

In some cases this value is programmed by an external resistor connected to a current source pin of the control IC. In this case, this resistor can be part of a network that includes a NTC (Negative Temperature Coefficient) thermistor so the value can be temperature compensated [18]. A temperature variation will shift the showed P–V curves resulting in a different V_{MPP} .

The pros of fixed voltage method are: low power consumptions and zero costs for the MPPT. On the other hand, it is not a tracking techniques, but in some conditions, where is not requested to track the real V_{MPP} every instant, it can be worth. Reference [15] gives fixed voltage an overall rating of about 80% for outdoor PV cells. This means that for the various different irradiance variations, the method will collect about 80% of the available maximum power. The actual

performance will be determined by the average level of irradiance. In the cases of low levels of irradiance the results can be better.

This technique sometimes is combined with other techniques thanks to its low power and cost.

3.2.3 Fractional Open Circuit Voltage

The evolution of the fixed voltage method, is the *fractional open circuit voltage* (V_{OC}). Literature is full of studies and tests concerning this MPPT for energy harvesting systems, such as [19], [20], [21], [22] and [23]. It is based on the experimental characteristic of PV cells, that show a nearly linear relationship between voltage of the MPP V_{MPP} and the open circuit voltage V_{OC} , under varying irradiance and temperature levels. The relationship is given by:

$$V_{MPP} \approx k_1 \times V_{OC} \quad (3.1)$$

where k_1 is a constant of proportionality. This constant is dependent on the PV cell characteristics, so it has to be empirically determined for every cell and is never reaching the exact MPPT, but for tolerant systems, can be a fine approximation. There are several variations of this method, implemented with different circuitry. The most common requires the use of a secondary smaller PV cell, or pilot cell, to obtain the V_{OC} , [20] and [24]. It needs few components, and no digital ones, such as microcontroller or DSP, which makes it low power and not complex.

In [25] the V_{MPP} is computed from measuring periodically V_{OC} , obtained by disconnecting every time the load from the cell. This brings down the complexity, but causes also more losses in power transferring. The pros about this technique are that is analog and not requires a pilot cell.

Another research [21] claims that the voltage generated by p–n junction diodes is approximately 75% of V_{OC} . Once V_{MPP} has been approximated, a closed-loop control on the array power converter can be used to asymptotically reach this desired voltage. This technique will not give a trustworthy result for DSSC, because these cells take time to settle the output voltage when a perturbation occur. So the circuit can miss the real V_{MPP} by setting the voltage before stabilization.

3.2.4 Fractional Short Circuit Current

According to what illustrated in section 3.1, it is possible to determine also the MPP by checking the current amount. Similarly to the fractional open circuit voltage, the *fractional short circuit current*, use a relationship to estimate I_{MPP} :

$$I_{MPP} \approx k_2 \times I_{SC} \quad (3.2)$$

where k_2 is a proportionality constant. This method uses a short load pulse to generate a short circuit condition. During the short circuit pulse, the input voltage will go to zero, so the power conversion circuit must be powered from some other source [18].

An additional switch usually has to be added to the power converter to periodically short the PV array so that I_{SC} can be measured using a current sensor. This increases the number of components and cost [16]. It is a more complex and costly implementation of the 3.2.3, for this reason in most of the cases it is preferable to use the fractional open circuit voltage.

3.2.5 Perturb and Observe

The *perturb and observe* (P&O) algorithm works by periodically perturb the cell output voltage or current and measure the power generated. In the next cycle the algorithm perturb again and measure again the power to determine whether it is a positive or a negative power change so as to establish the sign of the next perturbation. The table 3.1 summarize the described behavior. For instance the controller applies a positive voltage perturbation to the solar panel, if the change in output power is positive, it means that the perturbation is towards the MPP; on the other hand, if the power change is negative, the perturbation passed the maximum point, and next perturbation should be negative.

Table 3.1: P&O types of perturbations.

Voltage Perturbation	Change in Power	Next Perturbation
Positive	Positive	Positive
Positive	Negative	Negative
Negative	Positive	Negative
Negative	Negative	Positive

In this way the MPP is never reached, because the system is always modifying the voltage or the current. Therefore it will keep oscillating around it, resulting in small power loss and lower efficiency. A solution to this conflicting situation is to have a variable perturbation size ΔV that gets smaller towards the MPP [16]. There can be also issues when there are fast changes in the irradiance which can result in initially choosing the wrong direction of search [18]. As shown in the figure 3.2: instead of going from point A to C, the system will go from point A to B.

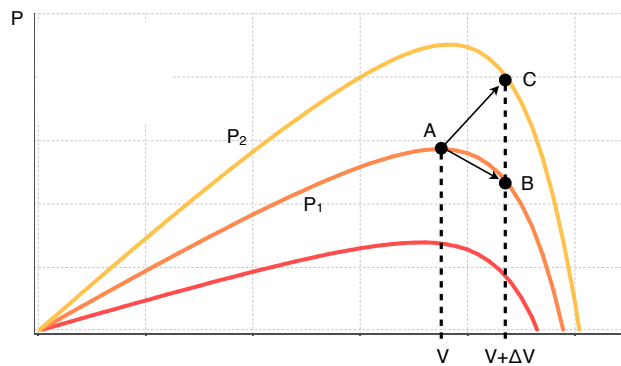


Figure 3.2: Divergence of P&O from MPP.

P&O method can have an analog or digital implementation and, as already said before, it requires voltage and current sensors. The stated problems can be overcame by using some variants such as: an average of several samples of the power [15] or by comparing the PV output power on three points of the P-V curve [16]. It is not complex method with a decent efficiency, but power consumptions and costs are components dependent. For what concerns the speed, choosing the proper step size for the perturbations is important. Too large will result in oscillation about the maximum power point and too small will result in slow response to irradiance changes [18].

3.2.6 Ripple Correlation Control

The *ripple correlation control (RCC)* makes use of the current and voltage ripple from DC–DC switching converter to perform the MPPT.

RCC correlates the time derivative of the power from the solar module p' (dp/dt), with the time derivative of the current i' (di/dt) or voltage v' (dv/dt), to drive the power gradient to zero, thus reaching the MPP [16]. In this way, the system will be able to recognize any change (thanks to the derivative) in the parameters. For instance, if considering case 1 in figure 3.3 where both power and voltage variations are positives, it means that MPP is not reached thus voltage must increase. For the other cases, please refer to figure 3.3 and table 3.2. The products $p'v'$ or $p'i'$ are positive to the left of the MPP and negative on the right and zero when the MPP is reached. The RCC method operates by controlling the duty cycle of the boost converter. In this way the RCC is a true MPPT technique, because the MPP will be always tracked.

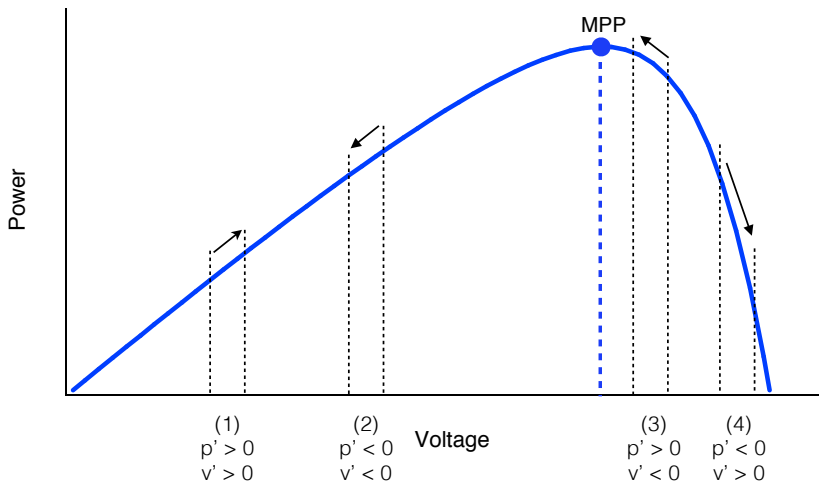


Figure 3.3: Working behavior of RCC tracking technique.

The exact derivatives are difficult to achieve without a DSP, but they can also be approximated by high pass filter with cut-off frequency higher than the ripple frequency [26]. The filter or differentiator is made with an operational amplifier with a capacitor and a resistor as external components. Capacitors oppose to voltage change by generating a current equal to $i = C(dv/dt)$. Another method is to sense the inductor voltage of the boost converter, which is proportional to the current derivative. For this reason RCC systems can be designed also with analog circuitry, experimental results [27] showed that it can accurately track MPP even under varying light conditions.

One more positive aspect of the RCC method is: that it does not require any information about the PV cells characteristics, making it more flexible and able to work both with a-Si and DSSC cells.

Table 3.2: Controls for the RCC method according to cases in figure 3.3.

Case	Condition	p'	v'	to reach MPP
1	$v \leq V_{mpp}$	> 0	> 0	v increases
2	$v \leq V_{mpp}$	≤ 0	≤ 0	v increases
3	$v > V_{mpp}$	> 0	≤ 0	v decreases
4	$v > V_{mpp}$	≤ 0	> 0	v decreases

3.2.7 Incremental Conductance

Incremental conductance method is based on the fact that, the slope of the P–V curve is equal to zero, when the MPP is reached, positive on the left of MPP and negative on the right. The following equations hold the MPP:

$$\frac{dI_{PV}}{dV_{PV}} + \frac{I_{PV}}{V_{PV}} = 0 \quad (3.3)$$

where I_{PV} and V_{PV} , are respectively the current and the voltage of the PV cell. The equation can be rewritten as:

$$\frac{\Delta I_{PV}}{\Delta V_{PV}} = -\frac{I_{PV}}{V_{PV}} \quad (3.4)$$

this means that the incremental conductance is equal to the negative ratio of current over voltage, and it has the following solutions:

$$\begin{cases} \Delta I_{PV}/\Delta V_{PV} = -I_{PV}/V_{PV} & \text{at MPP} \\ \Delta I_{PV}/\Delta V_{PV} > -I_{PV}/V_{PV} & \text{left of MPP} \\ \Delta I_{PV}/\Delta V_{PV} < -I_{PV}/V_{PV} & \text{right of MPP} \end{cases} \quad (3.5)$$

The PV panel is set to be working at a fixed voltage V_{ref} . Then the system start tracking the MPP by comparing the instantaneous conductance (I/V) to the incremental conductance ($\Delta I/\Delta V$). Once MPP has been reached ($V_{ref} = V_{MPP}$), the operation of PV array is maintained at this point and the perturbation stopped unless a change in ΔI_{PV} is noted. In this case, the algorithm decrements or increments V_{ref} to track the new MPP. The increment size determines how fast the MPP is tracked [15]. Fast tracking might lead for the system to not operate exactly at the MPP, thus a tradeoff should be found. Some references propose another method to use the fractional V_{OC} or the fractional I_{SC} methods to approach the MPP and then refine the result with the incremental conductance method. With this last variant, the system could also work in presence of various local maxima.

According to [15] experimental study, for outdoor solar system, the incremental conductance method gives an efficiency of 98.73% without taking into account power needed to run the tracking device. However this is a remarkable result, but also the indoor performances have to be tested. Voltage and current sensors are required for the computations of the described equations, in additions to this a DSP and microcontroller are needed. This components will increase the costs and power consumption.

3.2.8 Discarded Methods

Among all the techniques analyzed in [16], there are several which are not feasible for the purpose of this research due to several reasons. For completeness, they are going to be shortly listed in this paragraph and explained why they are not possible to be used.

Fuzzy Logic method has the advantage of working with imprecise inputs, not needing an accurate mathematical model, and handling nonlinearity; however it is very complex and power consuming. *Neural networks* is very high level implementation, but at the same time very complex. Since PV cells have different characteristics, they have to be trained periodically, and they take time to learn the behavior of cells. The tracking will be very tight, but the costs in terms of money, time and power consumption are too high compared to the aim of this system. *DC-link capacitor drop control* works only with systems using inverters, which is not this case. *OCC MPPT* also requires an inverter. *Array reconfiguration* needs big arrays

of different configurations (parallel and series) of PV cells. The *current sweep* method is too power consuming and highly complex. Another method is to compute the *slope of the power curve*, dP/dV or dP/dI , but it will need DSP and microcontroller being able to handle complex computations. The *linear current control* requires sensing the level of irradiance and some digital control and processing. Another technique proposed, involve *temperature and irradiance level sense* to find the optimal values of the MPP, this also require complex computations.

3.3 Technique Selection

3.3.1 Selection Rules

In order to be able to select the most suitable techniques for the EH application, it is necessary to analyze them together and give some methodologies to be able to rank them. The analysis carried out in this chapter is considering previous literatures of the MPPT methods performances and it does not involve any real data. So it is good to keep in mind, that the scores given to determined parameters are based on the author and the supervisor evaluations of feasibility of a certain method. Therefore this classification does not want to be a selection of the best MPPT, but a selection of the more suitable to test MPPT according to project specifications.

The selection parameters evaluated are the followings:

- *Analog or Digital*: analog system sometimes can be implemented with lower complexity, lower power consumption and lower costs than digital ones. However nowadays is it possible to find low power digital components that can suit in this work. The highest rank is given to MPPT that are able to work with both digital and analog circuitry, in order to have a choice possibility, whilst the choice of only one family is limiting the design.
- *Real Tracking*: some implementations, such as fixed voltage or fractional voltage, does not really track the MPP, but rather use a formula to determine it, or use an average. On the other hand real tracking can be power consuming and costly.
- *Speed*: to get an high tracking accuracy it is necessary to have high speed MPP tracking. The higher the speed the better.
- *Complexity*: complexity is a difficult parameter to define, in this case it was considered complex, for example, the use of a microcontroller (due to the necessity of be programmed first and the requirement of additional circuitry), or the use of a current sensing circuit (due to the additional components involved). In general all the components and aspects that increase the difficulty of designing a system. Low complexity is preferable and gets a high rank, as well as solutions already implemented in the literature.
- *Sensed Parameters*: the tracking algorithm usually works by acquiring data from the PV cell and then control an actuator to reach the MPP. To get the data, sensors are crucial: voltage can be easily handled, instead current needs a conditioning circuit. According to this considerations, sensing voltage is more desirable. No other types of sensors were described in the methodologies, so they are not taken into account in the evaluation.
- *Cost*: this parameter is straightforward: the lower the cost the better, without compromising on performances, of course.
- *Efficiency*: is the capacity of tracking the real MPP. This parameters it is really dependent on weather is a real tracking or not, or the speed of the algorithm. It does not take into

account power consumed by the tracking device itself. It is given in any case to have an immediate idea of performances, but at this point it is not based only on literature references such as [15]. High efficiency gets the highest rank.

- *Power Consumption*: the power used by the MPPT technique is crucial to decide if a method is worth or not. It must be also compared to the total power output of the PV cell. For this analysis the power consumption is estimated by considering the type components involved in the circuit. Low power consumption is the highest rank.
- *Robustness*: characterize the resistance of the system to both mechanical and electrical perturbations and disturbs. High robustness indicates a high rank.
- *Handle Partial Shading*: is an important parameters for indoor PV cells, which are smaller and more subjected to be partially shaded by some agents. A good system will be able to handle the partial shading which, as explained in the beginning, can result in different maxima. According to this considerations if the system can handle it, it will get a positive rank.
- *DSSC Capable*: a DSSC panel change slower its output characteristics compared to a-Si ones. This result for some tracking algorithm to miss the real MPP, since the DSSC would take more time to stabilize the output values. The purpose of this work is to study also this new generation of cells, so if the MPPT is capable of handle them it would be a plus point.

The number associated to every feature is listed in the legend of fig. 3.4.

3.3.2 Analysis of Results

On the summarizing table 3.5 are listed all the methods analyzed so far, including the ideal MPPT. The described selection parameters are also indicated and a value is assigned for every ranking level (see fig. 3.4). Then simple additions are carried out and the sum is represented by the blue columns. The higher the rank is, the more suitable for the application.

As expected the ideal case represents the reference: the best model achievable for this system. Interestingly the fixed voltage also achieve an high rank, meaning that even if it is not a proper method itself, it must be taken into account, but only simulations and real data in several conditions can shows its real value.

With enough confidence according to the analysis incremental conductance method can be discarded due to its lowest rank. Literature study shows a very recurrent use of fractional open circuit voltage algorithm for EH systems, this results seems reasonable also from this analysis. The high rank justify a large implementation of this method. Its simplicity and average efficiency are plus points, that play an important role in choosing it, on the other hand is not supporting partial shading and real tracking.

The P&O method also find a big support in literature, but less compared to the fractional voltage. Nevertheless it has good tracking performances, but sometimes it fails when conditions change fast or under partial shading.

RCC techniques studied were implemented on outdoor PV cells successfully [26]. The paper shows really good properties: multiple maxima tracking, real MPP and independent from PV cell topology. An amorphous silicon or DSSC cell can be used with RCC method. It is a bit complex, but according to the analysis it is worth to test it.

Finally the fractional short circuit current is in the lowest rank of the possible implementations excluding the already discarded ones. This is because the method is similar in principle

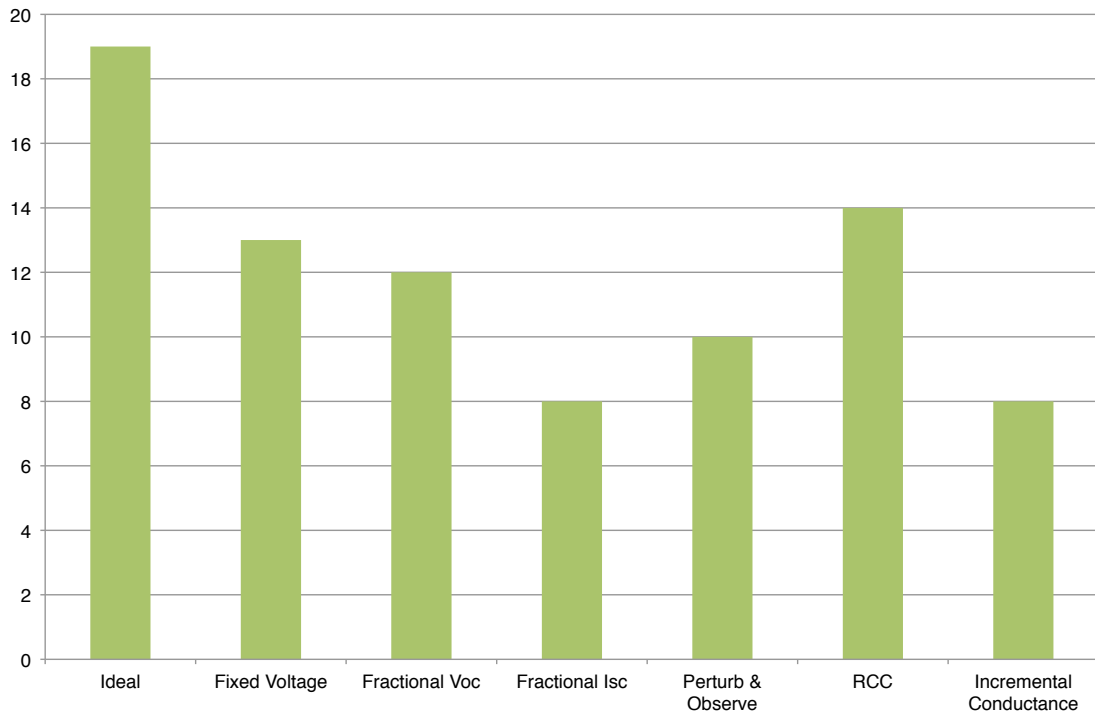


Figure 3.4: Summary methods graph. The numbers on the Y-axis represent the score according the specified classifications system. The highest the score the better.

to fractional voltage, but it has some constraints that make it more complex to be adopted. Current sensor and microcontroller also add costs and power consumption.

3.3.3 Considerations on MPPTs techniques

When the previous analysis was done, nothing was simulated or tested because it was based on literature study, however during the first measurements in chapter 6, it came out that a MPP tracking circuit was not necessary at all. In fact at low illuminance levels, the light is so dim that the power generated by the tested PV panels is too low to run a tracking algorithm. Furthermore the techniques used in the tests were the simpler ones: *fixed voltage* and *open circuit voltage*. For instance, fig. 6.7 shows that with a simple, yet very efficient linear regulator, even at low light it is possible to harvest the most out of a PV panel, without the requirement of a MPPT. At high light level, efficiency is good even without any MPPT, for different cases.

3.4 Available Commercial Solutions

The offer of Energy Harvesting microchips in the market is increasing everyday. These integrated solutions are very interesting. They start with a basic “diode architecture”, reaching a complex and handful “energy processor”, capable of being programmed and communicate the status of the system via serial port.

Most of these chips integrate a DC–DC converter, to modify the voltage and make it compatible with the rest of the system and the load. However few of them, at the time this thesis was written, are capable of tracking the MPP of an energy source. To complete this discussion about the MPPT, the commercial solutions will be listed in section 6.1 and shortly described.

MPPT classification techniques suitable for indoor Energy Harvesting

MPPT Technique	Analog or Digital	Real tracking	Speed	Complexity	Sensed parameters	Cost	Efficiency	Power consumption	Robustness	Handle partial shading	DSSC Capable	Total score
Ideal	Both	Yes	High	Low	Voltage	Low	High	Low	High	Yes	Yes	19
Fixed Voltage	Analog	No	High	Low	None	Low	Medium	Low	Medium	No	No	13
Fractional Voc	Analog	No	Medium	Low	Voltage	Low	Medium	Low	Medium	No	No	12
Fractional Isc	Analog	No	Medium	Medium	Current	Medium	Medium	Medium	Medium	No	No	8
Perturb & Observe	Both	Yes	Medium	Medium	Voltage, Current	Low	Medium	Medium	Medium	No	No	10
RCC	Both	Yes	High	Medium	Voltage, Current	Medium	High	Medium	High	Yes	Yes	14
Incremental Conduct	Digital	Yes	Medium	Medium	Voltage, Current	High	High	Medium	Medium	No	No	8

Figure 3.5: MPPT classification table, with the described parameters

Legend:

Analog = 1
 Digital = 1
 Both = 2
 No = 0
 Others = 0
 None = 2

High = 2
 Medium = 1
 Low = 0
 Voltage = 2
 Medium = 1
 Current = 1
 Both = 0
 High = 0
 Others = 0

Chapter 4

Modeling and Simulations

Before focusing on the whole system, the design of the circuits and the tests, it is necessary to understand first the behaviors of the main components: the energy source (PV cell), and the load (battery). Circuit simulation is generally more accurate than simple circuit idealization, used in manual calculus to analyze circuits behavior. It is good practice in engineering before facing the concrete problem, to model and simulate the components involved in the project. This is very important to understand the circuit functionality and check for any design errors. The main blocks in simulations are the models of selected devices. Unfortunately not all electronic components manufacturers, provide models for simulation tools, as in this case, it was necessary to create them from scratch.

In this chapter, it will be discussed a model to simulate the two different types of PV cells: a-Si and DSSC, and battery. Later the results will be compared to real measurements in order to match the curves. Particular attention will be focused on the understanding of the PV cells behavior under partial shading conditions.

4.1 PV Cells Models

Most of the PV cells models available in the tools libraries or on-line, are suited for big solar power plants systems. However [28] and [13] give a good overview to build a specific model that will work also for indoor solar cells. Manufacturers typically provide only few operational data for photovoltaic panels, such as: the open circuit voltage (V_{OC}), the short circuit current (I_{SC}), and the maximum power point voltage (V_{MPP}) and current (I_{MPP}). Those data are usually available at Standard Test Condition (STC), at which the irradiance is $1000W/m^2$ and panel temperature (T_C) is $25^\circ C$ [28]. Although, this irradiance level is not a standard in indoor environments. For these reasons it is necessary to have an accurate, reliable and simple model for variable indoor working conditions.

There are several existing models described in the literature, [29] gives an overview of the most commons. All those models vary in complexity according to the level of accuracy and closeness to reality. A good model is something that takes into account the most important parameters of the concrete case.

4.1.1 Single diode simple model

The single diode model (or four-parameter model), can be described by the superposition of the responses of the device to two excitations: voltage and light. Therefore, as shown in figure 4.1, the model consists of a constant current source, varying the current according to the incident

radiation on the cell, in parallel with a diode that accounts the typical knee of the current–voltage relation through the reverse saturation current. The series resistance R_s emulates the intrinsic losses because of resistive semiconductor material, both in the base region, not heavily doped in general, and in the emitter region, and also losses due to connections with other cells.

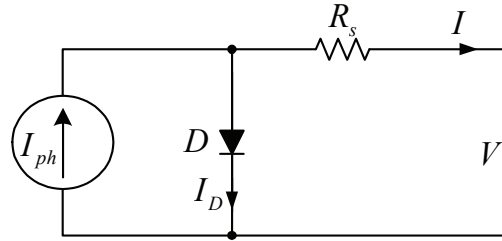


Figure 4.1: Equivalent circuit of the PV cell representing the *single diode simple model* parameters and the cell output.

The equations controlling this model are:

$$I = I_{ph} - I_0(e^{\frac{V+IR_s}{V_t}} - 1) \quad (4.1)$$

where I_{ph} and I_0 relate to their respective current densities J_{ph} and J_0 as follows:

$$I_{ph} = AJ_{ph} \quad (4.2)$$

$$I_0 = AJ_0 \quad (4.3)$$

A is the total area of the device neglecting the metal covered area. V_t in 4.1 is the thermal voltage, which is equal to:

$$V_t = \frac{n_s A k T}{q} \quad (4.4)$$

where n_s is the number of cells connected in series, k is the Boltzmann's constant, T is the temperature in Kelvin and q is the electron charge in Coulomb.

It is clear that both short circuit current (J_{ph}) and dark current (J_0), scales linearly with the area, helping to easily scale the system according to the requirements. This model is rather simple, but it gives reasonably good results. It is possible to work with it, obtaining a good approximation without sacrificing simplicity.

4.1.2 Single diode detailed model

In industry, a solar cell is the result of mass production of devices generally made out of large area wafers, or of large area thin film material. A number of parallel resistive losses, such as localized shorts at the emitter layer or perimeter shunts along cell borders, are among the most common [13].

The single diode detailed model (or single-exponential five-parameter model), adds to the previous one the shunt resistance R_{sh} , in parallel with the diode and the current source, to simulate the losses due to leakage currents across the junction inside the solar cell. The circuit is shown in figure 4.2.

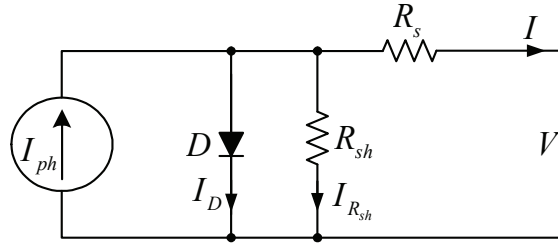


Figure 4.2: Equivalent circuit of the PV cell representing the *single diode detailed model* parameters and the cell output.

The control equation is:

$$I = I_{ph} - I_0 (e^{\frac{V+IR_s}{V_t}} - 1) - \frac{V + IR_s}{R_{sh}} \quad (4.5)$$

where R_{sh} is the shunt resistance.

4.1.3 Double diode model

The double diode model (or double-exponential model), adds another parallel diode in order to consider the recombination phenomena. The recombination, at the space charge region of solar cells, explains non-ohmic current paths in parallel with the intrinsic solar cell. This is relevant at low bias voltage and can be represented in an equivalent circuit by a second diode term with a saturation density current I_{02} , which is different from the saturation density current of the ideal solar cell diode [13]. The figure 4.3 shows the circuit.

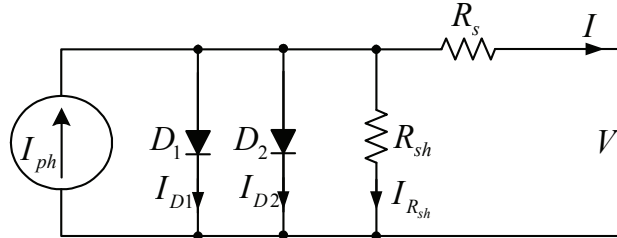


Figure 4.3: Equivalent circuit of the PV cell representing the *double diode model* parameters and the cell output.

The control equation is:

$$I = I_{ph} - I_{01} (e^{\frac{V+IR_s}{V_t}} - 1) - I_{02} (e^{\frac{V+IR_s}{2V_t}} - 1) - \frac{V + IR_s}{R_{sh}} \quad (4.6)$$

where I_{01} is the dark saturation current of the first diode representing the diffusion current, and I_{02} is the dark saturation current of the second diode representing the recombination in the space charge region.

This model was chosen for all the analysis performed in this thesis, because it is the closer to the reality behavior and reflects the most important behavior of a typical PV cell. The parameters and the actual implementation are discussed in section 4.3.

4.1.4 DSSC model

For the dye-sensitized solar cells, both models described in sections 4.1.2 and 4.1.3 work fine, though they need an additional component to replicate the exact behavior of this cell family. In [30], are briefly discussed some old models for DSSC using similar circuits to the ones proposed for p–n junction a–Si solar cells.

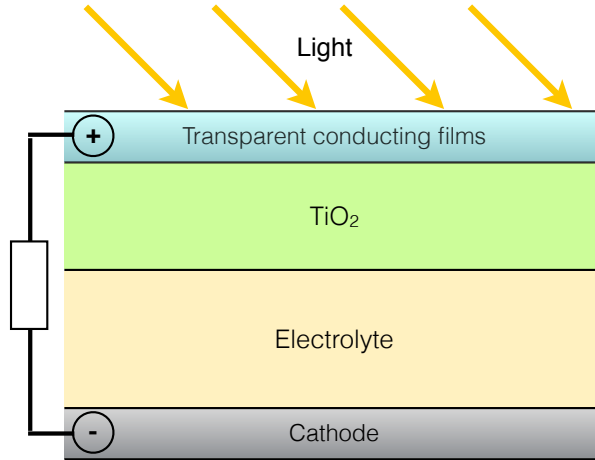


Figure 4.4: Different Interfaces inside a DSSC module.

As to figure 4.4 standard DSSC typically contains three interfaces:

- Transparent conducting films/ TiO_2 ;
- TiO_2 /electrolyte;
- Electrolyte/Cathod.

The second interface is modeled as rectifying diode (D_1) and a double layer capacitance (C_i). A recombination diode (D_2) is used to emulate the interfacial charge recombination (when charges are combined with their opposites thus eliminating each other), as for the p–n junction cells, for the dye (which is scattered in the electrolyte) and electrolyte. The shunt resistance (R_{sh}) takes into account the losses such as leakage current. Finally, [30] models the interconnection, with other cells, as a complex series of RLC circuit in order to reproduce the high frequency behavior. In this case, using a series resistance (R_s) will be more than enough to model the interconnections losses. The figure 4.5 shows the circuit.

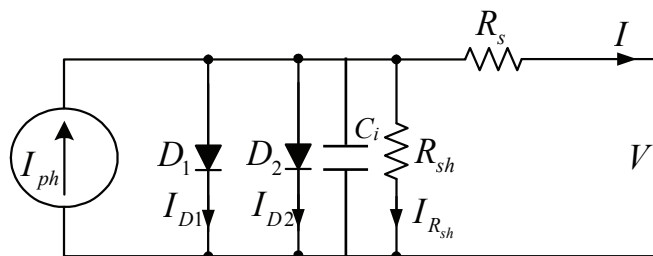


Figure 4.5: Equivalent circuit of the DSSC cell representing the *DSSC model* parameters and the cell output.

The simplified control equation is:

$$I = I_{ph} - I_{01}(e^{\frac{V+IR_s}{V_t}} - 1) - I_{02}(e^{\frac{V+IR_s}{2V_t}} - 1) - \frac{V + IR_s}{R_{sh}}(j\omega C_i + 1/R_{sh}) \quad (4.7)$$

4.1.5 Parameters Extraction Procedure

The double diode model (Section 4.1.3) presents complex equation to solve (Eq. 4.7). For this reason the following analysis to extract the parameters will consider the single diode detailed model (Section 4.1.2) and the equation 4.5. Although during the simulations the double diode mode is used, and the remaining parameters are extracted from the experimental results.

This section analysis follows the procedure described in [28] and it will show only the main passages, because it is not meant for demonstration reasons, but just for better understanding.

The current–voltage relationship at a fixed cell temperature and solar insolation for the circuit in Fig. 4.2 is expressed in Eq. 4.5. Five parameters must be known in order to determine the current and voltage to evaluate the power delivered to the load. Those parameters are: the diode reverse saturation current (I_0), the current generated due to irradiation (I_{ph}), the series resistance (R_s), the shunt resistance (R_{sh}), and the thermal voltage drift (V_t). We report the Eq. 4.5 for semplicity:

$$I = I_{ph} - I_0(e^{\frac{V+IR_s}{V_t}} - 1) - \frac{V + IR_s}{R_{sh}} \quad (4.8)$$

$$V_t = \frac{n_s A k T}{q} \quad (4.9)$$

For the explanation of these parameters refer to previous sections: 4.1 and 4.2. The previously described five parameters are functions of the light irradiation and the panel temperature. To determine them it is necessary to define a five independent equation system and evaluate the equations at STC. But as shown in [28], this approach is difficult and complex to apply, so they proposed a simplified extraction procedure. The extraction of parameters like R_s and R_{sh} , is possible but doing some correct current–voltage measurements. It can be assumed also that the short circuit current (I_{sc}) initially is equal to the light dependent current (I_{ph}), so the eq. 4.8 becomes:

$$I_{sc} = I_0(e^{\frac{qV_{oc}}{kT}} - 1) + \frac{V_{oc}}{R_{sh}} \quad (4.10)$$

The last term of this equation, between V_{oc} and R_{sh} , can be neglected, because usually R_{sh} is several $k\Omega$. So, since the diode saturation current determines the open–circuit voltage (V_{oc}), we can solve for this last:

$$V_{oc} = \left(\frac{kT}{q} \right) \ln \left(\frac{I_{sc}}{I_0} + 1 \right) \quad (4.11)$$

The next step is to extract the irradiation and the temperature parameters. Here there will be reported the equations from [28]:

$$I_0 = I_{0,STC} \left(\frac{T}{T_{ref}} \right)^3 e^{\left(\frac{qE_G}{kT} \right) \frac{1}{T_{ref}} - \frac{1}{T}} \quad (4.12)$$

$$I_L = I_{L,STC} S + V_{T(I_{sc})} \left(\frac{1}{T_{ref}} - \frac{1}{T} \right) \quad (4.13)$$

where S is the light irradiation expressed in $[W/m^2]$, T is the PV panel working temperature in $[K]$ and T_{ref} is the reference temperature for the manufacturers data, also in $[K]$. $I_{0,STC}$ is derived by imposing the STC, and $I_{L,STC}$ can be obtained by imposing the output voltage to zero, so $I_L = I_{sc}$. $V_{T(I_{sc})}$ is the thermal drift coefficient obtained at short circuit current mode.

By solving those equations and follow the previous assumptions, it is possible to determine the parameters used to create a PV cell model. Although it is important to stress that this extracting method is based on simplifications and idealizations, so the parameters should be double checked, after with real-life measurements.

4.2 Battery Model

The most common load for a PV system, is a battery. The battery is a very important and useful element, in fact it allows the system to run when the light availability is very low, such as night time. Thus it stores energy when the load power demand is less than the generated one by the solar cell.

Model a battery behavior is very complicated due to a lot of parameters to consider such as: temperature, state of charge (*SOC*) and chemical composition. However with the following assumptions, the model could be simplified enough to have a good balance between real characteristics and ideal ones. Furthermore batteries from the same producer and same family can behave differently due to manufacturing imprecisions. Costly batteries obviously show a closer behavior between different samples, whilst cheap ones can differ a lot. So, it is not always wise to aim at the most accurate model, because it could also lead to wrong results. Moreover, [31] says that models change according to the specific purposes, for instance: battery design, performance estimation and circuit simulation.

The first simplification is to assume the battery working in two possible modes: charging and discharging. In charging mode, the current I_{bat} flows in the positive terminal of the battery, the battery voltage V_{bat} increases slowly and the charge stored increases. In discharging mode, the current flows out of the positive terminal, the battery voltage and the charge decrease. There are two other important modes: undercharge and overcharge, however they will not be considered, because if the battery (depending on the technology) enters in those modes, it could be reduced in capacity or damaged irreparably.

The main parameters used for describing a battery model are: the nominal capacity, the charge/discharge rates and the state of charge (SOC). The nominal capacity is defined as the total charge that can be stored. The charge or discharge rates are defined as the ratio between the nominal capacity and the charging or discharging current. For discharging, usually this value represents the time length that the battery takes to discharge at constant current. The SOC is defined as the amount of electric charge stored in the battery at a certain time. It is the ratio between the maximum capacity and the present capacity, so:

$$0 \leq SOC \leq 1 \quad (4.14)$$

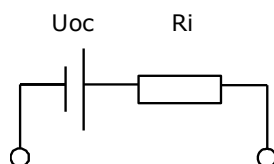


Figure 4.6: Discussed battery model with voltage source U_{oc} and series resistance R_i

The electrical battery model used in this thesis, is composed by a voltage source in series with a resistance, as show in figure 4.6. These two components vary according the modes described before.

4.3 SPICE Models

SPICE (Simulation Program with Integrated Circuit Emphasis) [32] is an open source analog circuit simulator. It is very powerful and rather simple to use. It offers a lot of tools and the possibility to create own libraries. The Cadence student version of SPICE, called PSpice [32], has evolved into an analog mixed signal simulator. It offers automatic optimization, encryption, a model editor, support for parametrized models, auto-convergence and checkpoint restart and several internal solvers.

4.3.1 a-Si Cell SPICE Model

First of all, a library was created for the model described in 4.1.3, in order to have the possibility of reusing the PV cell model in several projects. A library model will also facilitate the connection of the module in series or in parallel. The illustrated method, reported in this thesis, follows the steps listed in [13].

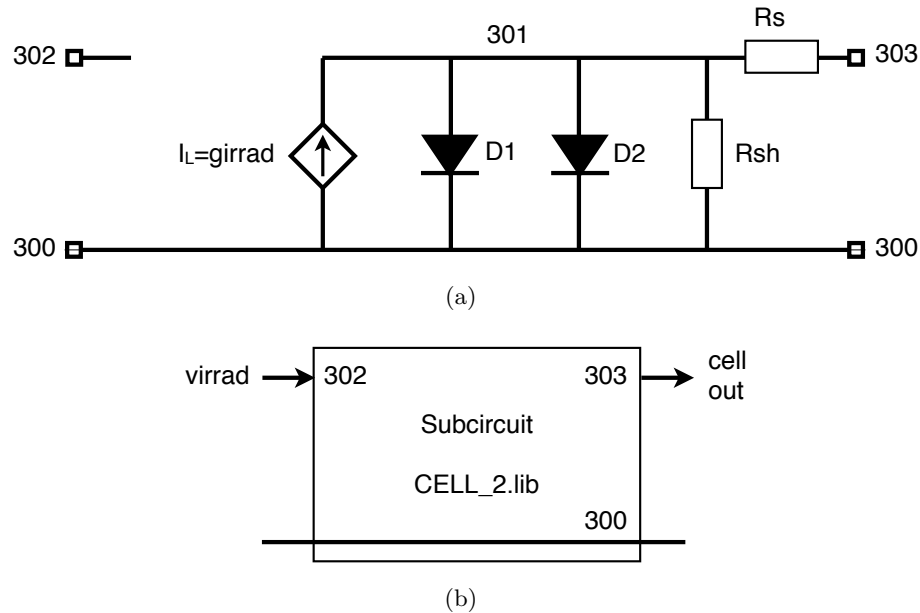


Figure 4.7: The circuit model for 4.1.3 (a). The PV module showing inputs and outputs (b).

A solar cell short circuit current will be proportional to a given irradiation value. To bring these phenomena to the PSpice model, it is used a G-device (as show in figure 4.7): a voltage-controlled current source. The mathematical formula describing this relationship is:

$$I_L = girrad = \frac{J_{sc}A}{1000}G \quad (4.15)$$

where G is the value of irradiance in W/m^2 , A is the area of the cell unit in cm^2 and J_{sc} is the short circuit current given at STC, that means: $G = 1000W/m^2$ and $T_{cell} = 25^\circ C$. However this is true for outdoor solar cells, since the solar cells used in this work are for indoor use, an

irradiation value of $1000W/m^2$ is quite high parameter. In fact, in indoor conditions most of the manufacturers gives the specifications according to illuminance (*lux*) levels. For a deeper analysis and comparison between illuminance and irradiation the reader should refer to section 2.4.2. Although this considerations it was decided to simply keep the expression 4.15 as it is, and using typical irradiation values scaled down to match indoors levels.

Equation 4.15 returns the value of the short circuit current at any irradiance value G , because of the proportionality between irradiance and short circuit current. This is usually the case verified that low injection conditions are satisfied and the relative PSpice code is:

```
girrad 300 301 value={(jsc/1000)*v(302)*area}
```

The first parameter *girrad* is the name of the G-Device, the second is the *+node*, the third is the *-node* and the last is the actual expression to calculate the value of the output current. Nodes in Pspice are used to connect devices together.

Figure 4.7 shows that the next component to add is the diode to simulate the p–n junction. The saturation current value for the diode was expressed in equation 4.3, which is the product of the current density and the cell area.

```
d1 301 300 diode
.model diode d(is={j0*area})
```

The first line creates the PSpice diode component and connects it to the G-Device using the *+node* and *-node*; whilst the second line define diode model and the relative current. The same procedure is done for the diode simulating the recombination effect.

```
d2 301 300 diode2
.model diode2 d(is={j02*area}, n=2)
```

Finally the two resistances, taking into account the cell's losses, are added to the library file in this way:

```
rs 301 303 {rs}
rsh 301 300 {rsh}
```

The *rs* resistance is connected in series and *rsh* in parallel. Both of the values are defined by the user, so the program is limited to just copy the entered values onto the variables *rs* and *rsh*.

The input parameters for the PV model are:

- $area(cm^2)$: the PV module active area;
- $J_0(A)$: the dark current;
- $J_{sc}(A)$: the short-circuit current;
- $J_{02}(A)$: the recombination current;
- $r_s(\Omega)$: the series resistance;
- $r_{sh}(\Omega)$: the shunt resistance.

This SPICE model gives a rather accurate simulation results (as showed later fig. 4.11), thanks to the various environment parameters introduced. The temperature drift effects are not needed to be specified in the model because PSpice gives the possibility of defining them in the analysis file.

4.3.2 DSSC SPICE Model

According to what was shown and demonstrated in section 4.1.4, a-Si cells model and DSSC one, differ only for a capacitor connect in parallel to the current generator and the diodes. So for the library definition refer to previous section: 4.3.1.

```
c 301 300 {c}
```

The capacitance c is connected in parallel and the value is defined by the user. All the others parameters are the same as a-Si cell model.

4.3.3 Battery SPICE Model

The battery SPICE circuit, will follow the considerations done in section 4.2 and the guide provided by [13]. The figure 4.8 shows the schematic.

Node 3 is the positive terminal of the battery and node 2 is the negative one. Node 1 is the output indicating the SOC at certain instant. The model needs the parameters:

- n_s : number of 2V cells (since is designed on a 2V cell, but it can be easily used for other voltages);
- $SOC_m(Wh)$: the absolute maximum capacity;
- k : charge/discharge battery efficiency (depending on battery characteristics);
- $D(h^{-1})$: battery self discharge rate (determined empirically);
- $SOC_1(\%)$: the available charge.

The first assumption made is that the series resistance (R_s), is equal for both charging and discharging modes. This can reduce the accuracy when simulating, but also give shorter simulation times. Furthermore, studies made at ASSA ABLOY, teached that for a some Li-Ion batteries the series resistance is more or less the same for both modes.

The voltage source **ebat**, instead, changes value to **eVch** or **eVdch**, whether if charging or discharging. The variable $i(vcurrent)$ senses if the current is drawn from or injected in the battery.

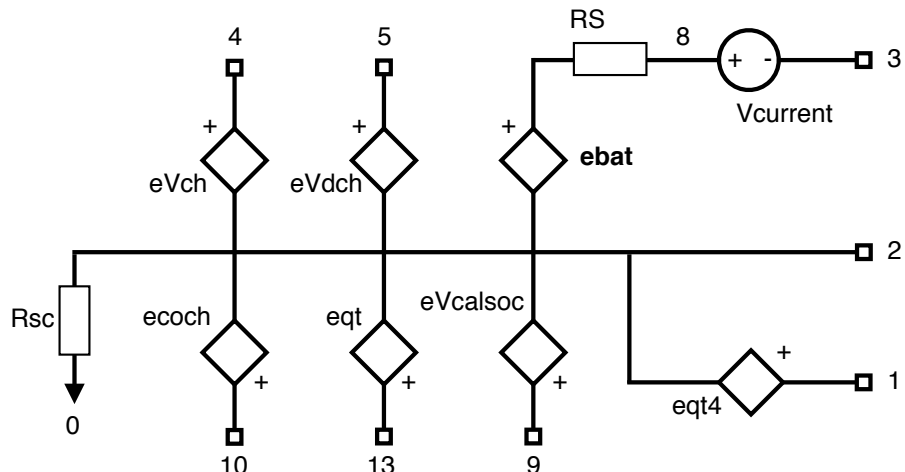


Figure 4.8: Schematic diagram of the described SPICE battery model.

```

evch 4 2 value={(2+(0.16*v(1)))*ns}
evdch 5 2 value={(1.926+(0.248*v(1)))*ns}
ebat 88 2 value={IF(i(vcurrent)>0,v(4),v(5))}

```

Finally **eqt4** gives as output the current SOC, expressed in volts between 0V and 1V, which indicates respectively 0% and 100% of the SOC. This is how it is evaluated:

```

ecoh 10 2 value={IF(i(vcurrent)>0,v(4),v(5))}
evcalculsoc 9 2 value={(k*v(10)*i(vcurrent)/3600)-(D*SOCm*v(13)/3600)}
eqt 13 2 value={SOC1 +(sdt(v(9))/SOCm)}
eqt4 1 2 value={limit (v(13), 0 , 1)}

```

4.4 Simulations

This section collects the simulations and compares them with measurements, in order to test the validity of the developed models.

4.4.1 Simulations Setup

First, it is helpful to introduce how the simulation was performed with PSpice and how the data was acquired in order to be compared with the simulated results.

To use the model described in section 4.3, the library should be included first. The library for the solar cell needs to be connected to the circuit and the parameters assigned. To reproduce a solar array, the cell library must be connected in series with the following syntax:

```
xcell1 -node +node irrad cell_3 params:area=3.53 j0=2e-16 jsc=4e-2 j02=0 rs=8e2
rsh=7e4
```

Where the first parameter is the cell-object's name; the second and the third are the `-node`s; the fourth is the irradiation value. Following, all the others values stay respectively for: area, dark current, short circuit current, series resistance and shunt resistance.

To emulate the different values of irradiation, in PSpice is it possible to do, by using a voltage controlled source and varying it using a step parameters list.

```

.param IR=1
virrad 32 0 dc {IR}
*** restpectively lux: 200, 400, 600, 800, 1000 *****
.step param IR list 0.29 0.45 0.68 0.89 1.11

```

The code shows how the irradiation parameter (*IR*) is initialized, connected to the *irrad* input of the cell module and a list of irradiation created. The comment in the code shows that the written values are equal respectively to the illuminance values of: 200, 400, 600, 800, 1000. These values are empirically determined by measuring the cell output.

Finally SPICE needs to know which type of analysis has to perform. There are several types of possible analysis, that SPICE can perform, such as [33]:

- *AC analysis*: linear small signal frequency domain analysis;
- *DC analysis*: nonlinear biased point calculation;

- *DC transfer*: generate curve from nonlinear operating points calculated while sweeping an input voltage or current, or a circuit parameter;
- *Noise analysis*: small signal analysis which sums uncorrelated noise currents at a chosen output point;
- *Transfer function analysis*: a small-signal input/output gain and impedance calculation;
- *Transient analysis*: time-domain large-signal solution of nonlinear differential algebraic equations.

In the following cases, the analysis is DC transfer, in order to bias the solar panel with variable voltage and generate a plot for the voltage-current. The command is:

```
.dc vbias 0 5.7 0.01
```

This shows that the voltage generator *vbias*, is going to sweep from 0V to 5.7V within an interval step of 100mV.

4.4.2 Measurements Setup

In order to match the solar cell models to the commercial samples, several measurements were performed. In figure 4.9 is shown the used setup for the data acquisition. This measuring approach was necessary because the DC current meter of the FLUKE 8842A [34], was not giving accurate enough results. The DC current lowest resolution is $1\mu A$ at $200mA$ range, whilst accuracy is 0.08% of reading + 40 counts for the $200mA$ range. If for example the measure gives $50\mu A$, the error will be $50 \times 0.08/100 + 40 = 40.04\mu A$. So the actual current could be any value between 10 and 90 μA , which can represent also more the 100% error for certain light levels.

For this reason it was decided to change the measuring approach and go for the measurement of the voltage drop across a known resistance. The resistor value was measured with a extremely precise RLC meter, giving 987Ω value. The voltage source is used to bias the PV cell by sweeping the level from 0V, until the voltage level at which current was getting negative. The FLUKE 8842A for DC voltage measurements has a resolution of $1\mu V$ at $200mV$ range, whilst the accuracy calculation gives an error 0.01% on a $40mV$ value. A voltage drop correspond to a current equal to: $I = V \times R$. The switch was used to compensate the static error.

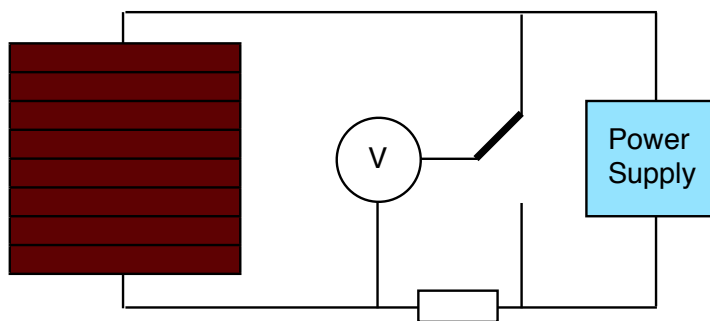


Figure 4.9: Measurements diagram.

4.4.3 a-Si Cell Simulations Results

The sample used for the analysis of the a-Si family cell, is a Sanyo AM-1815 (dimensions $58.1\text{mm} \times 48.6\text{mm}$). This panel is composed by 8 solar cells in series, so eight modeled cells were connected together in PSpice. At first the parameters computed with the method described in section 4.1.5, were inserted in the code, but after few measurements it was discovered that the generated I-V curve was not fitting properly the real data. This was due to the not accurate computation, rather than a wrong model. To fix the problem model parameters where adjusted to match the real curve. Table 4.1 presents the final obtained parameters.

Table 4.1: Final parameters for the SPICE model of the Sanyo AM-1815 PV panel.

Parameter name	Value
Single cell area (A)	$3.53[\text{cm}^2]$
Dark reverse current (J_0)	$2 \times 10^{-16}[\text{A}]$
Short circuit current (J_{sc})	$40[\mu\text{A}]$
Series resistance (R_s)	$800[\Omega]$
Shunt resistance (R_{sh})	$70[\text{k}\Omega]$

The graphs 4.10 and 4.11 will present the simulations and measurements results.

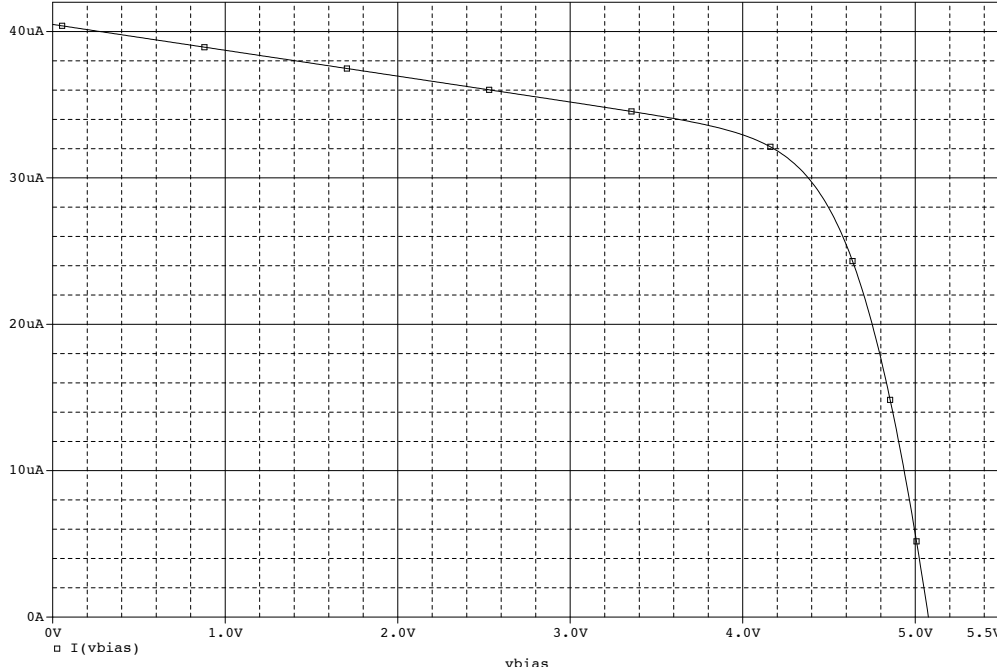


Figure 4.10: Simulated I-V curve of the Sanyo AM-1815 PV panel at 200 lux.

The match was quite accurate, with an average of 95% correspondent to the measured values. After matched the real array behavior with the simulated one, further analysis were performed at different illuminance level. In figures 4.12 and 4.13, the current and power curves, respectively, are plotted. The power curve in 4.13, gives an overview of the available power for the system; for example at 200 lux of illuminance, at the MPP there about $133\mu\text{W}$ of available power.

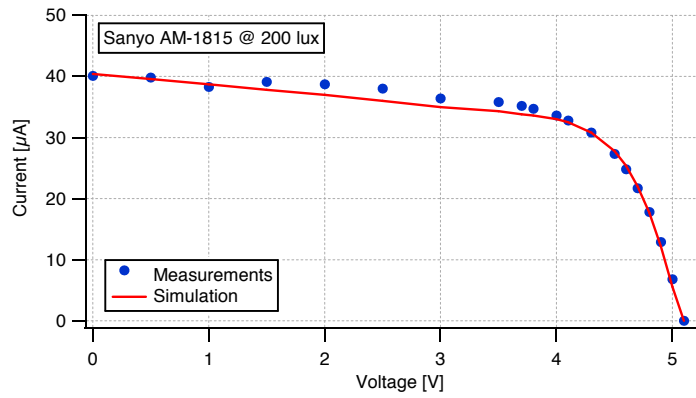


Figure 4.11: Comparison between simulated and measured values for the Sanyo AM–1815.

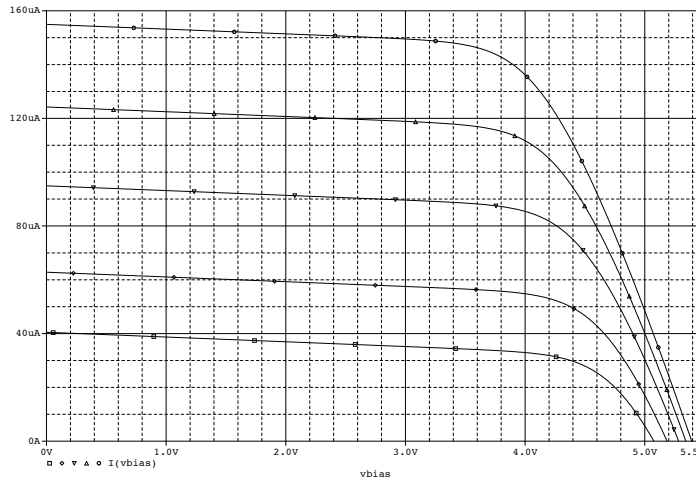


Figure 4.12: Simulated I–V curve of the Sanyo AM–1815 PV panel, at different illuminance values: (from the bottom) 200, 400, 600, 800, 1000 lux.

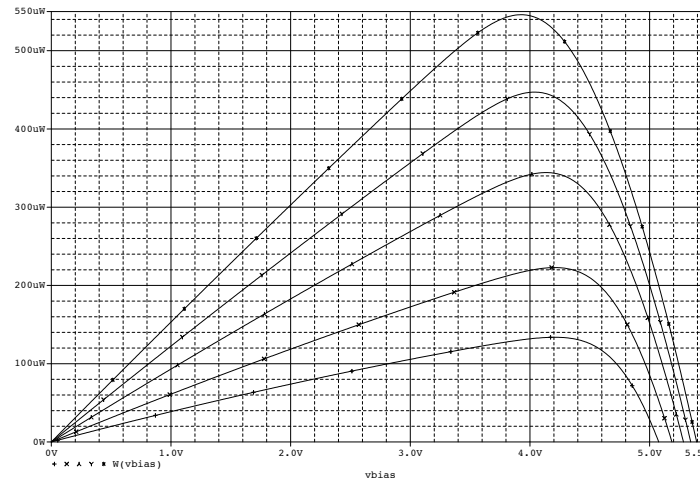


Figure 4.13: Simulated P–V curve of the Sanyo AM–1815 PV panel, at different illuminance values: (from the bottom) 200, 400, 600, 800, 1000 lux.

4.4.4 DSSC Simulations

The sample used for the analysis of the DSSC family cell, is pre-production by G24i (effective dimensions $70mm \times 10mm$). Its area is more than the double than the Sanyo AM-1815 PV panel, but instead of using a glass support, is mounted on a transparent plastic materiel that gives it big flexibility, but would probably absorb part of the incident radiation due to impurities. This panel is composed by 7 solar cells in series, so seven modeled cell were connected together in PSpice. It was performed the same procedure to tune the model with the measurements data for the a-Si panel to match the curves. Table 4.2 presents the final obtained parameters.

Table 4.2: Final parameters characterized for the SPICE model of the G24i DSSC panel.

Parameter name	Value
Single cell area (A)	$7[cm^2]$
Dark reverse current (J_0)	$4 \times 10^{-15}[A]$
Short circuit current (J_{sc})	$25.5[\mu A]$
Series resistance (R_s)	$600[\Omega]$
Shunt resistance (R_{sh})	$60[k\Omega]$
Shunt capacitance (C_i)	$10[\mu F]$

The graphs 4.14 and 4.15 will present the simulations and measurements results.

The match was quite accurate, with an average of 98% correspondent to the measured values. In figures 4.16 and 4.17, the current and power curves, respectively, are plotted. The power curve in 4.17, gives an overview of the available power for the system; for example at 200 lux of illuminance, at the MPP there about $129\mu W$ of available power. This data show a worse results than the Sanyo AM-1815 PV panel, but it must be considered that is a pre-production sample of a technology still in research level.

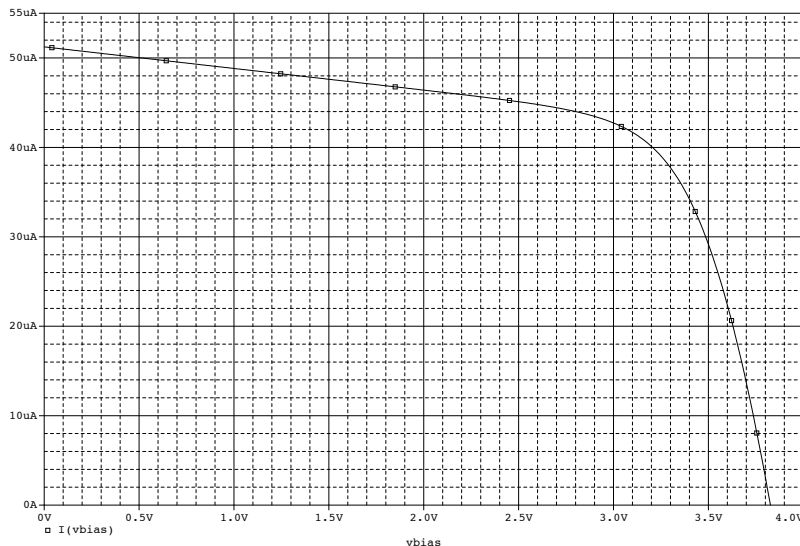


Figure 4.14: Simulated I–curve of the G24i DSSC panel at 200 lux.

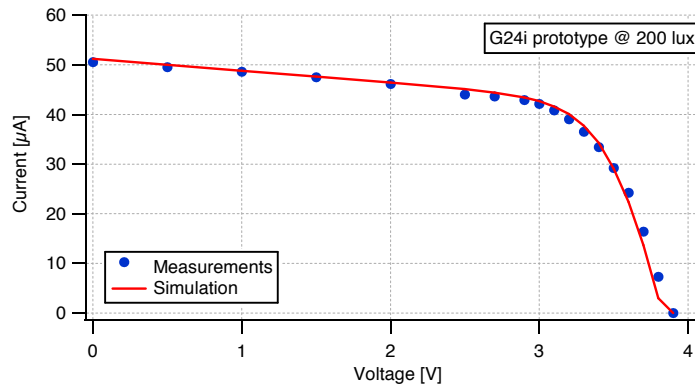


Figure 4.15: Comparison between simulated values and measured ones for the G24i DSSC panel. The red line is the simulation and the blue dots are the measured values.

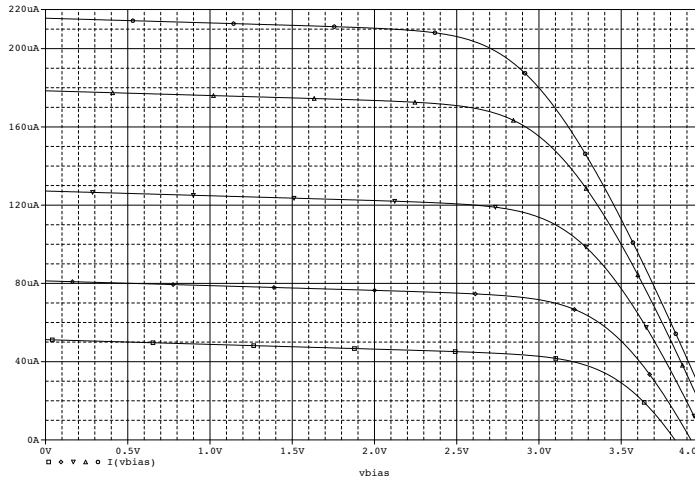


Figure 4.16: Simulated I-V curve of the G24i DSSC panel, at different illuminance values: (from the bottom) 200, 400, 600, 800, 1000 lux.

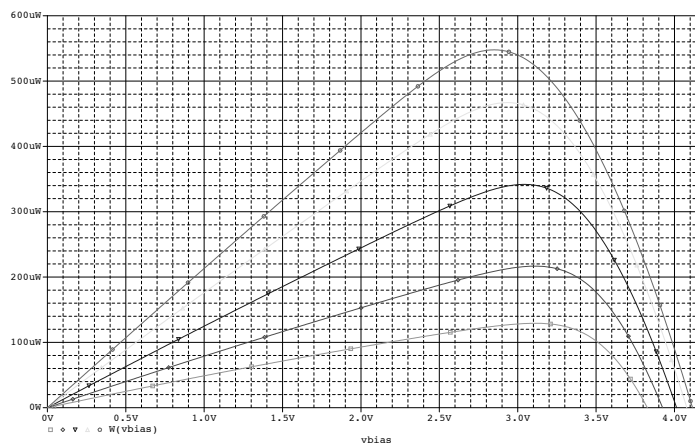


Figure 4.17: Simulated P-V curve of the G24i DSSC panel, at different illuminance values: (from the bottom) 200, 400, 600, 800, 1000 lux.

4.4.5 Partial Shading

As discussed briefly in chapter 3, partial shading can represent a problem for a MPPT algorithm. However in this section will be investigated, with simulations, how crucial is it in practice. In [17], they claim to have demonstrated, for DSSC cells, the presence of multiple maxima, under shading conditions.

Partial shading means that a portion of the PV panel surface is shaded. According to the shading object shape, there are infinite types of shading patterns, but not all of them are relevant in this analysis.

Shadow intensity is also a parameter, but is not critical since it can be seen as a negative light value. For example 20 lux can be considered as shadow in respect to a 300 lux ambient illuminance. This effect is not disruptive for this PV cells. For this reason in this thesis, shadow is considered when a fully dark area, such as an object on the panel, will totally obstruct the light.

Figure 4.18 different types of shading patterns. For example, covering the panel perpendicularly with respect to the cells length, as shown in figure 4.18(a), reflects in a decreased size of the panel's active area. The consequence is that the I-V and P-V curves looks like the same but can output less current and power. Even for shadows that have strange shapes like the one in figure 4.18(b), the result is the same, because no complete cell is shaded. Equally for (a) and (b), there is no issue for parallel or series cell connection.

The problem is different in figures 4.18(c) and (d): in both cases the cells are completely shaded. In figure (c), for example only one cell is covered, however even if the area is less than case (a) and (b), this scenario can be very critical. The solar panels considered in this project, are all arrays of PV cells in series. Photons work as an activator and allow the p-n junction of

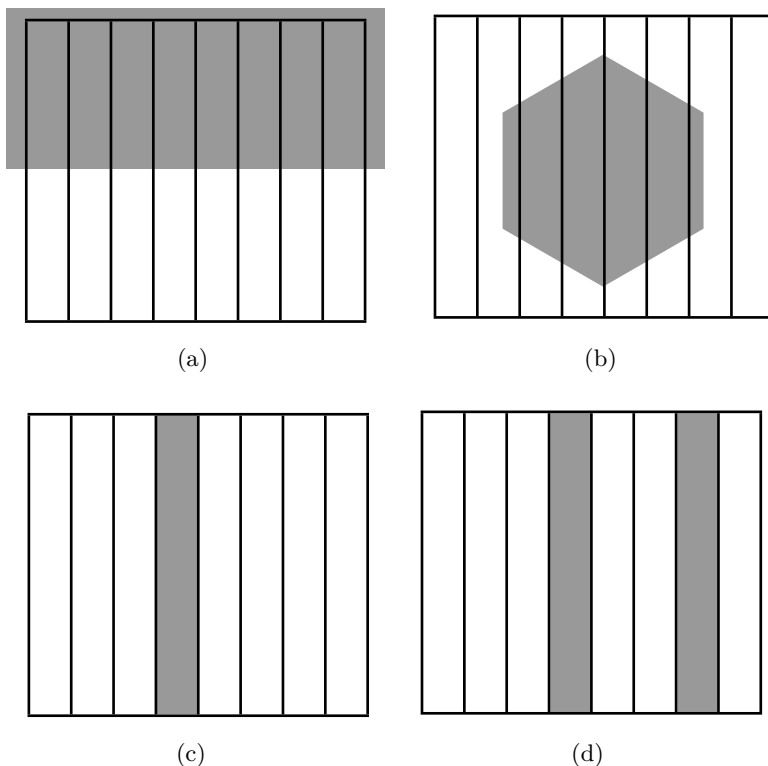


Figure 4.18: Four different shading patterns.

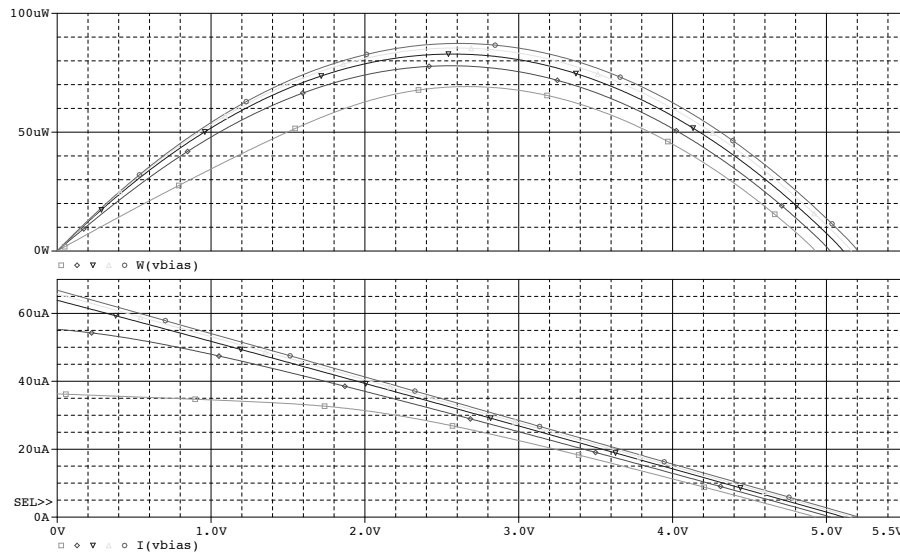


Figure 4.19: Simulated power (up) and current (bottom) curves for a 8 cells a-Si panel, 1 cell shaded (c) scenario, without any bypass diode, at different illuminance values (200, 400, 600, 800, 1000 lux).

every doped cell to work as a diode. Completely shading one cell, will be like interrupting the circuit. In reality since the silicon is doped, the current is still able to transit, but it will face a very high resistance. This resistance will degrade significantly the performances of the whole panel, even if only one cell is shaded. In case the scenario is like the one in (d), the effect will be even worse.

After those considerations, only case (c) is examined in the next simulations, because it is

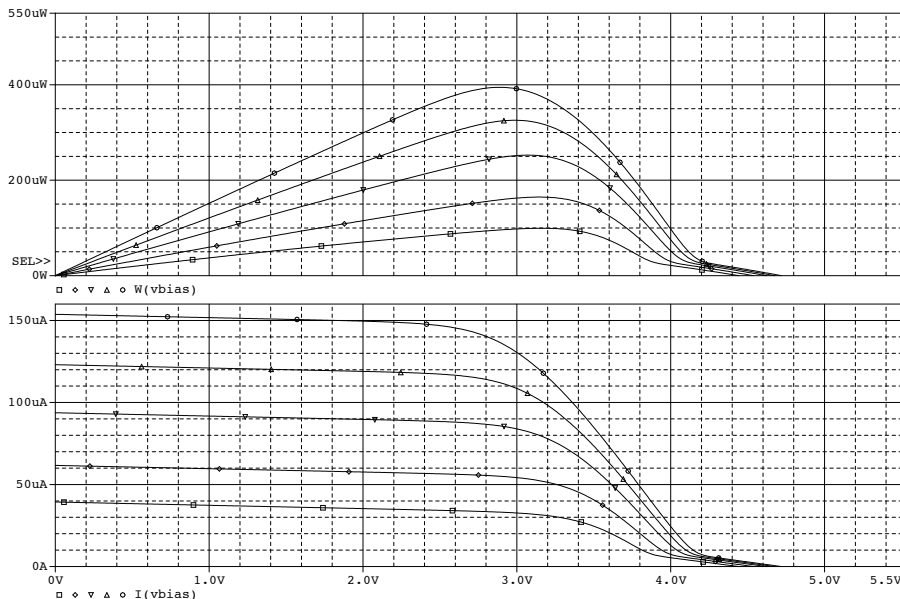


Figure 4.20: Simulated power (up) and current (bottom) curves for a 8 cells a-Si panel, 1 cell shaded (c) scenario, with bypass diode, at different illuminance values (200, 400, 600, 800, 1000 lux).

taken as the worst case. More shaded cells will differ from the (c) case for more degraded curves, whilst area shading (a) and (b) will result as if the panel gets a lower illuminance.

Figure 4.19 shows what happen for a 8 cells a-Si panel with one shaded cell. Both power and current curves are dramatically degraded, even at 1000 lux. Whilst at 1000 lux the power was about $550\mu W$, now it is approximately 100. The short circuit current at 1000 lux, is almost equal to the single cell one at 200 lux.

To solve this critic issue, the methodology used in the outdoor solar arrays, is to bypass some cell groups, or better, every cell, with a diode. This solution is more expensive and leading to a higher manufacturing cost, but will also assure less degradation of the power curve. The idea behind this method is to bypass the off cell and let the current flow throughout the diode, even if the p-n junction is not active.

Figure 4.20 demonstrates that with bypass diode, the one cell shading is less critical than the one in figure 4.19. In this case the output is proportional to the number of not shaded cells.

This partial shading analysis is performed to give the reader the overview of the phenomena, however, for more accurate results and considerations on a concrete case, measurements could be found in section 5.2.5.

4.4.6 Battery Simulations

The battery for the simulation modeled on the characteristics of: Panasonic Lithium Vanadium Pentoxide coin battery (VL2330). The battery specifications are listed in table 4.3.

Table 4.3: Panasonic VL2330 specifications.

Parameter name	Value
Nominal voltage [V]	3
Nominal capacity [mAh]	50
Continuos standard load [mA]	0.1
Operating temperature [$^{\circ}C$]	-20 ~ +60

The VL2330 was modeled using the method described in 4.3.3. This model is very simple and will not reflect the real battery behavior, however is it useful to understand how will work in the final the system: PV panel + battery. The model in section 4.3.3, needs the input parameters. The number of 2V cells is set to 1.5 in order to achieve a output voltage of 3V; the nominal capacity of $50mAh$; a charge/discharge efficiency, determined with iterative simulations, of 0.325; a discharge rate of 0.001 and an initial capacity of 100%.

```
xbat1 3 2 1 bat params: ns=1.5, S0Cm=0.05, k=0.325, D=1e-3, SOC1=1
```

The simplest load type is a constant load, so a $0.1mA$ current were applied to the battery for 24 hours to simulate the continuos standard load. Figure 4.21 shows that the energy consumed by this load is 7.4% of the full capacity. This gives an autonomy of 324 working hours.

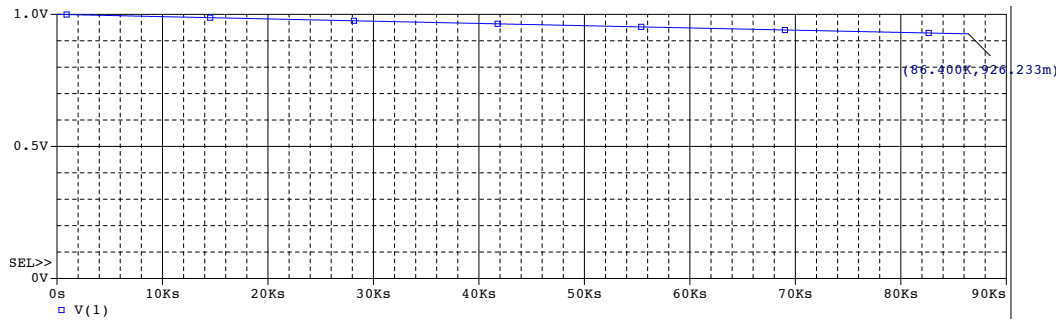


Figure 4.21: SOC simulation for a VL2330 connected to a $0.1mA$ constant load for 24hours.
Note: *y*-axis unit is pure number not *V*.

Another load type is a square wave, obtained in SPICE with the *pulse* command and with the following syntax:

```
iload 3 2 pulse(0 10mA 0s 1us 1us 100ms 5s)
```

The first parameter inside the round bracket indicates the low wave limit, the second is the high limit, the third is the delay time, the fourth and the fifth are the rising and falling time, the sixth is the high time and the last is the period. In this case, the pulsed load has the values of $10mA$, applied for $100ms$ every $5s$. The average current is $0.2mA$. This case represents a common load situation rather than a constant one. It will emulate a system that wakes up periodically, perform some actions, and goes to sleep again. The simulation time is 24 hours. Figure 4.22 shows that the energy consumed by this load is 33.7% of the full capacity.

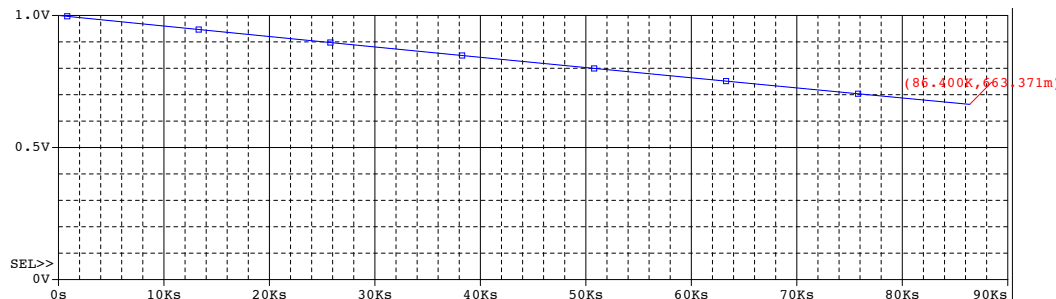


Figure 4.22: SOC simulation for a VL2330 connected to a $10mA$ pulsed load for 24hours. Note: *y*-axis unit is pure number not *V*.

The aim of the last simulation, was to test the simplest charging system using: a-Si 8 cells array, BAT54 protecting diode and a battery. The models used for the PV panel and the battery are the ones previously described, instead for the BAT54 was used a model provided by a diode manufacturer.

The diode is included to protect the PV cell from reverse current during low light conditions. Among the commercially available low power Schottky diodes, there is a trade-off between leakage current and forward voltage. Diodes with low forward voltage have high leakage current and viceversa. However the BAT54 diode is the most common choice in these types of systems thanks to its low leakage current. For 8-cells solar panels, voltage is less critical requirement since the V_{oc} is usually more than $4.0V$.

In this case the battery is the load: instead of providing energy to the system, it is absorbing current to regenerate the internal charge. The hypothetical scenario is to have the solar panel

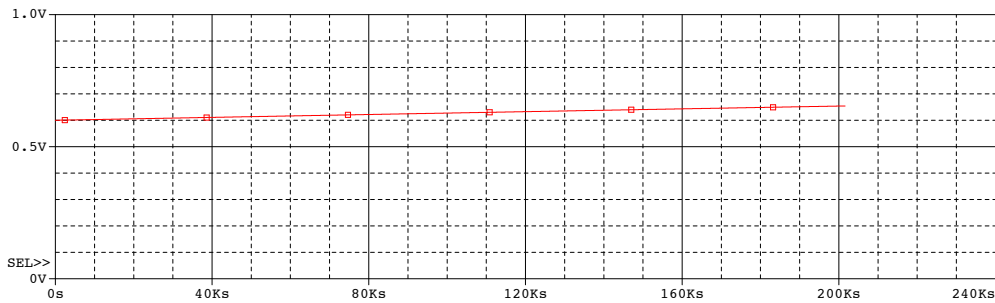


Figure 4.23: SOC simulation for a VL2330 during charging cycle for 8 working hours for 1 week.
Note: y -axis unit is pure number not V .

in a office with an average illuminance of 400 lux, during the 8 working hours cycle. The test simulates one week of charging and the resulting SOC level is showed in figure 4.23. The charging current during optimal light conditions is $78\mu A$, but the resulting average due to the dark not working hours is only $3.25\mu A$. This demonstrate also why is very important to have a very efficient system. In the figure 4.23, the SOC level varies from 60% starting condition to 65.42%, so the system was able to charge the battery of 5.42% of the full capacity.

Chapter 5

PV–Panels Characterization

In this chapter the simulation results are going to be demonstrated and presented. Furthermore not only the different cell characteristics are showed, but also their response to shading, their nominal output power and the power density.

5.1 The Testing Setup

The testing equipment (showed in the appendix, fig. B.2) consists in: a closed box (320mm width $\times 290\text{mm}$ depth $\times 380\text{mm}$ height) with 12 white LEDs on the ceiling to generate constant diffused light. Inside the chamber, are placed a lux–meter (model LX02 manufactured by Lutron Ltd) and the PV module under test. The device is connected to a controllable voltage source and to a multimeter to measure the output DC current.

The data presented in the next sections are obtained by measuring the output current at different bias voltages (like it was done in simulations to generate the PV panel characteristics). The light level is varied between 10 and around 1000 lux, in 22 steps. At every step the light level is incremented by 25%, resulting in a logarithmic increment scale. It was chosen to use logarithmic to be able to present more data in the graphs and mostly because it better reflects the sensitivity of human eye. As a matter of fact, human eye can discern the difference between 10 lux (dark), 1000lux (bright room), 10000 lux (outdoor sun), whilst a difference between 900 lux and 1000 lux, is less discernible by human eye. The same works for logarithmic scale where 900 and 1000 are close. In conclusion, a linear variation will be more difficult to be interpreted by the reader.

All the information gathered from the instruments are collected into text files. The computer program, developed internal to Assa Abloy., generates 22 files, one for every illuminance step. Inside every file are collected the values of bias voltage and output current. The program is also generating a useful summary files with information on: illuminance, short circuit current, open circuit voltage, and maximum power point coordinates. The power is obtained by simply multiply voltage times current. Those files are then imported in the processing tool, analyzed and displayed in the following sections and chapters. The voltage resolution used in the measurements is variable depending on the maximum voltage the PV–panel provides. For every module will be specified the resolution.

The used multimeter for measuring the DC current level is a Fluke 8846A, set to operate with a maximum of $1mA$ range and a resolution of $1nA$. However the accuracy from the datasheet [35], is 0.05% of measurement + 0.005% of range. For a $100\mu A$ will give an error of $0.1\mu A$ (0.1%).

In the next sections the results are presented and discussed for the different solar panels

models and technologies.

5.2 The Characterization

The current–voltage and power–voltage characteristics are usually included in every datasheet. The problem with them is that manufacturers usually do not plot graphs for low light levels. For this reason the first experiment to do to understand solar arrays behaviors, is to generate the characteristics and compare the output powers.

The tradeoff in solar panels is between output voltage and output current. In fact for the same area, the higher the cells number, the higher the output voltage, but the smaller the current. Contrary, with a single solar cell, of the same size, the output voltage will be very small ($0.5\text{--}0.7V$ depending on the technology), but the current will be higher.

This is a crucial point, that is why in this thesis was chosen to investigate both of the possibilities:

- panels with 8 cells in series;
- panels with one cell, or 4 cells in parallel.

Besides this consideration, the size is also important. At last, most considerations are common to all the PV–panels, for this reason they are going to be discussed deeply in section 5.2.1, and briefly denoted in the next sections. The solar panels used in this thesis are showed in fig. B.1, where they are collected together to easy compare their different sizes.

5.2.1 Sanyo AM–1815

This PV module was exhaustively analyzed before. It is an amorphous silicon panel especially tuned to respond to indoor artificial light. Compared to outdoor ones it shows a brownish color, instead of black. It is considered as market leader in its sector, so it is very worth to take it into exam.

The dimensions for this model are $58.1\text{mm} \times 48.6\text{mm}$, which give a total area of 28.23cm^2 . It is composed by 8 PV–cells in series.

First interesting graphs are the I–V and P–V characteristics. In figure 5.1, they are presented for different light levels. The graphs seem interrupted, but what is actually happening here is that for higher bias voltage, the diode architecture inside the solar cells is entering the breakdown region and current goes negative. Negative logarithmic arguments result in complex numbers. Furthermore this solar array shows that the maximum voltage is around $5.5V$ for an illuminance

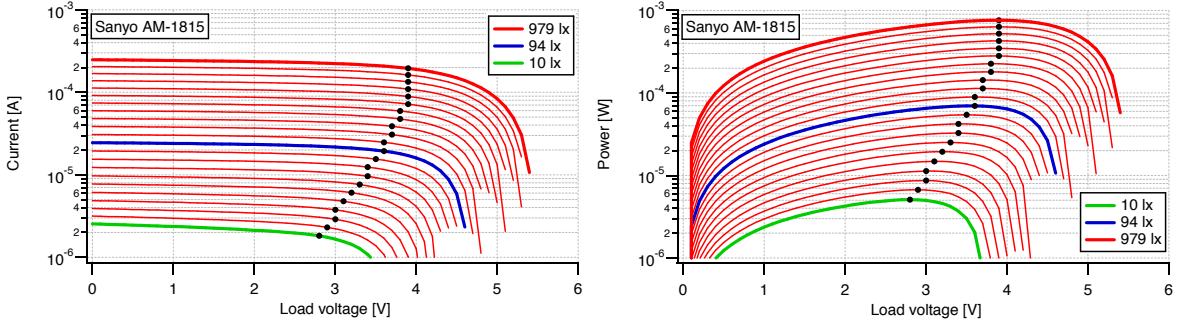


Figure 5.1: Current (left) and power (right) curves for Sanyo AM–1815, at different illuminance levels. The black dots represent the MPP.

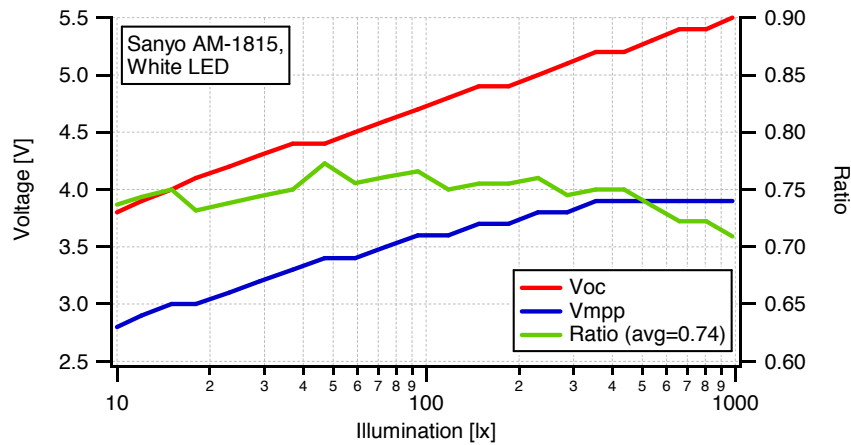


Figure 5.2: V_{oc} and V_{mpp} for Sanyo AM-1815, at different illuminance levels.

of around 1000 lux. The current varies between $2.5\mu A$ (at 10 lux) and $250\mu A$ (at 979 lux). The power varies between $5.1\mu W$ (at 10 lux) and $760\mu W$ (at 979 lux).

A interesting particularity noticeable in figure 5.1, is the position of the MPP: its voltage point is increasing as well as power. Further tests showed that for higher light level (sun shining on the panel around 35000 lux), the voltage at MPP was less than the one at 979 lux. However this high levels are not relevant in this project, so there will not be any related graph.

In figure 5.2 are plotted the open circuit voltage V_{oc} and the MPP voltage V_{mpp} . It is very evident the almost constant ratio between them: they both vary the same amount with the increment of the illuminance. The fractional open circuit voltage MPPT method is demonstrated to make sense. The average ratio among all the samples is 0.74.

The sampling resolution for this module is $0.1V$, it represents the load voltage step on the voltage source, depending on the maximum V_{oc} , the quantization error is between 1.8–2.6%.

5.2.2 2×Sanyo AM-1454

The initial consideration done for the Sanyo AM-1815, are the same for this model. The differences between the two products are the dimensions and the number of cells.

This module has 4 cells in series and smaller dimensions: $41.6mm \times 26.3mm$, which give a total area of $10.94cm^2$, 3 times smaller than AM-1815. For this reason in order to have a comparable size device, **all tests using the AM-1454, are actually made using a 2×**

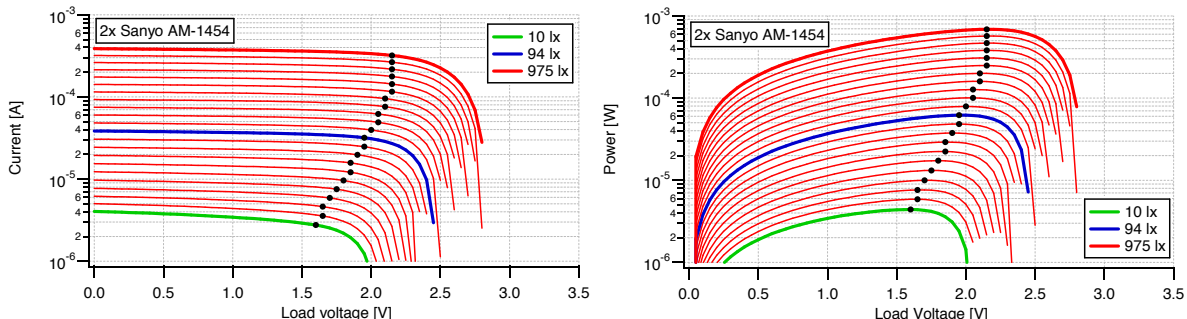


Figure 5.3: Current (left) and power (right) curves for 2× Sanyo AM-1454 in parallel, at different illuminance levels. The black dots represent the MPP.

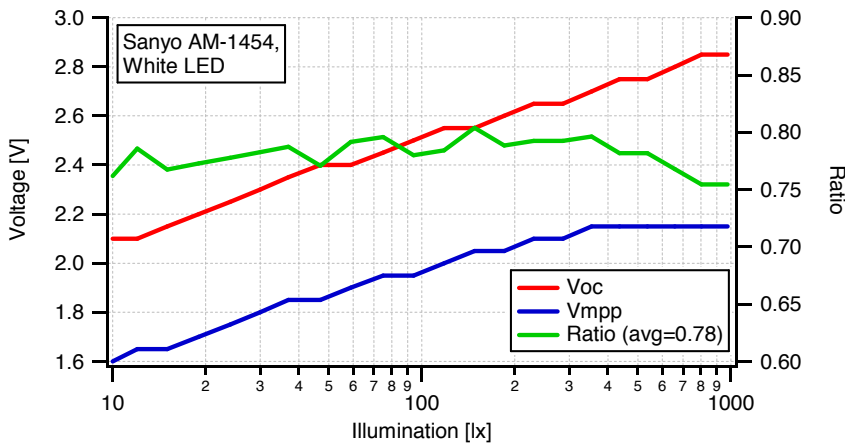


Figure 5.4: V_{oc} and V_{mpp} for a single Sanyo AM–1454, at different illuminance levels.

AM–1454 parallel solution, as showed in fig. B.1. This will sensibly increase the current output, but the voltage will remain the same.

The $2 \times$ Sanyo AM–1454 maximum voltage is around 2.9V for an illuminance of around 1000 lux. The current varies between $4\mu A$ (at 10 lux) and $386\mu A$ (at 975 lux). The power varies between $4.4\mu W$ (at 10 lux) and $690\mu W$ (at 975 lux). As expectable from this data, the current values are higher than the AM–1815 because the cells are in parallel, whilst the total power as well as the voltage are smaller because the area.

In figure 5.4, are plotted the open circuit voltage V_{oc} and the MPP voltage V_{mpp} . The average ratio is 0.78. It is possible to notice also here that V_{mpp} it is increasing with illuminance. The sampling resolution for this module is 0.05V, depending on the maximum V_{oc} , the quantization error is between 1.7–2.4%.

5.2.3 Solarprint SP–7375

This solar panel is a new technology DSSC especially made for indoor solutions. Solarprint is still refining their production process, so the tested model will sensibly differ from the commercialized one. However this tests will prove what status they reached in development and refinement, compared to what is already on the market.

The version used for the test is a prototype received from Solarprint in early June 2012 (ver. PDP067_1_7). The outer dimensions are $73mm \times 79mm$. Active region dimensions are

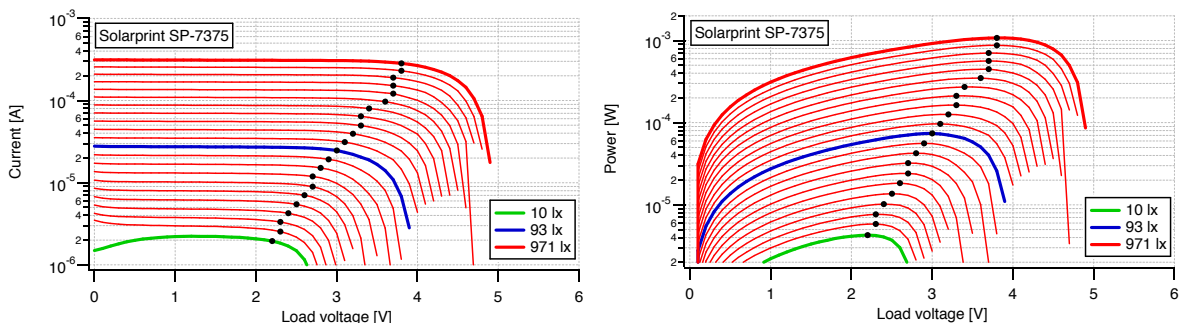


Figure 5.5: Current (left) and power (right) curves for Solarprint SP–7375, at different illuminance levels. The black dots represent the MPP.

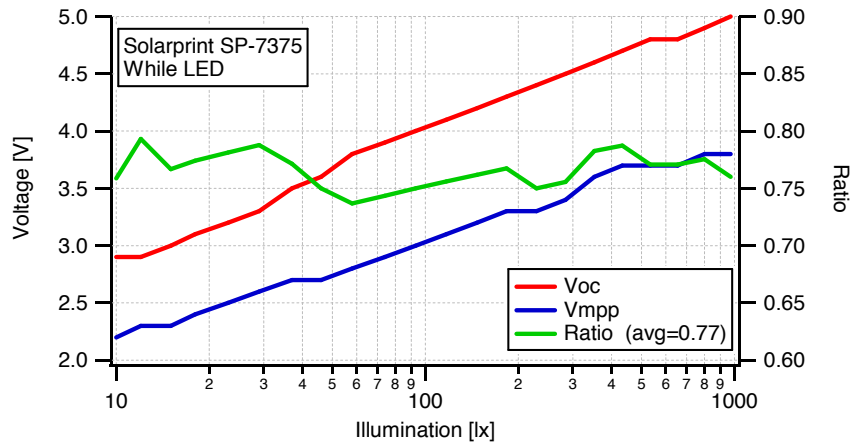


Figure 5.6: V_{oc} and V_{mpp} for Solarprint SP-7375, at different illuminance levels.

$60mm \times 60mm$, but since the cells are spaced the effective area is $24cm^2$. It is composed by 8 cells in series.

The Solarprint SP-7375 maximum voltage is around 5V for an illuminance of around 1000 lux. The current varies between $2.2\mu A$ (at 10 lux) and $314\mu A$ (at 971 lux). The power varies between $4.3\mu W$ (at 10 lux) and $1077\mu W$ (at 971 lux). This last data is very interesting if compared with the direct competitor (SANYO AM-1815), there is a difference of more than $300\mu W$ at high light level. The tradeoff is that the Sanyo panel is smaller size, but on the other side, Solarprint's one has smaller effective area.

In figure 5.6, are plotted the open circuit voltage V_{oc} and the MPP voltage V_{mpp} . The average ratio is 0.77.

The sample resolution is the same for Sanyo AM-1815, depending on the maximum V_{oc} , the quantization error is between 2–3.4%.

5.2.4 Solarprint SP-7375-0.5V

This second panel by Solarprint is very particular. It is a 1 cell DSSC panel, in order to maximize the space utilization. The version used for the test is also a prototype received from Solarprint in early June 2012 (ver. PDP066.1.5). Its outer dimensions are $73mm \times 79mm$ and the active region dimensions are $60mm \times 60mm$, with an effective area of $36cm^2$.

Since is a single cell the maximum voltage is 0.65V for an illuminance of around 1000 lux.

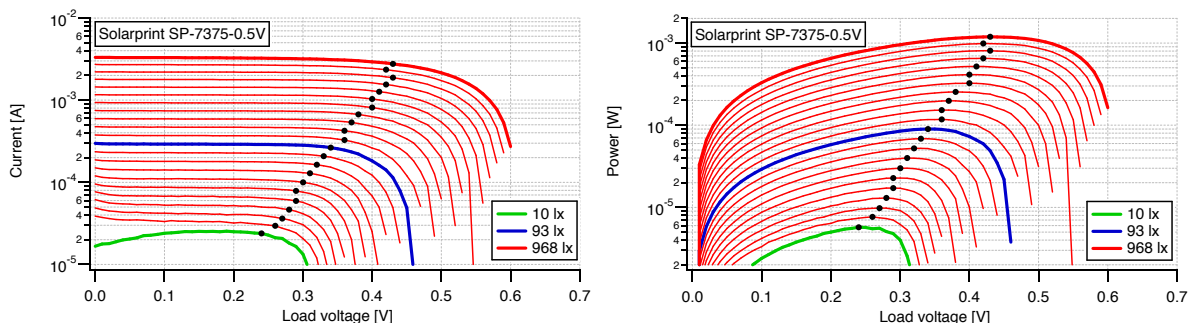


Figure 5.7: Current (left) and power (right) curves for Solarprint SP-7375-0.5V, at different illuminance levels. The black dots represent the MPP.

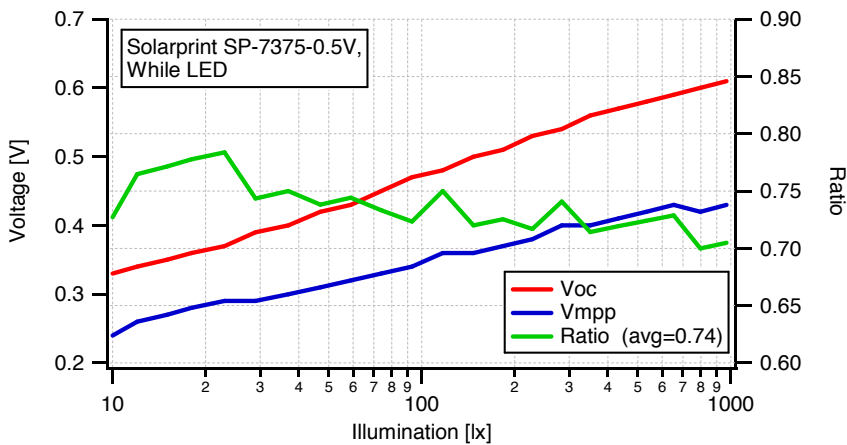


Figure 5.8: V_{oc} and V_{mpp} for Solarprint SP-7375-0.5V, at different illuminance levels.

The current varies between $2.5\mu A$ (at 10 lux) and $3316\mu A$ (at 968 lux). The power varies between $5.7\mu W$ (at 10 lux) and $1092\mu W$ (at 968 lux).

The characteristic of this cell is to have a high current, that at high illuminance can be 10 times larger than the 8 cells module. With the advent of low power boost converters, the low voltage of this device will not be a problem. In next chapters there will be more information about converter performances.

In figure 5.8, are plotted the open circuit voltage V_{oc} and the MPP voltage V_{mpp} . The average ratio is 0.74.

Due to the small voltage the sampling resolution for this cell is $0.01V$, depending on the maximum V_{oc} , the quantization error is between 1.6–3%.

5.2.5 Partial Shading

The conclusion after simulations of partial shading patterns, is that PV–panels of this size are not affected by multiple maxima phenomena. Contrary on what is demonstrated in [17], the author feels to disagree on what is presented in the paper. Following results will demonstrate this statement.

Three shading patterns were used:

- *Single cell shading*: one covering material stripe to completely shade a cell;
- *Double non-consecutive cells shading*: two covering material stripes to completely shade two non consecutive cells;
- *Area shading*: a piece of covering material shading a portion of panel surface orthogonal with respect of the cells length.

The Solarprint SP-7375-0.5V and the Sanyo AM-1454 are not interesting because they are less affected by this phenomena. Solarprint one is actually not affected at all because, since it is a single cell module, a shading will be saw by the device as decrease in illuminance. For this reasons it was decided to proceed with the tests of the two 8 cells panels.

The tests were conducted using the same setup described in the beginning of this chapter, for only one light level. The reference illuminance value found in the datasheets is 200 lux, so it was chosen also to execute the partial shading experiments.

In figure 5.9 are plotted the power and current curves for the Sanyo AM-1815 at the same illuminance (185 lux), and different shading patterns:

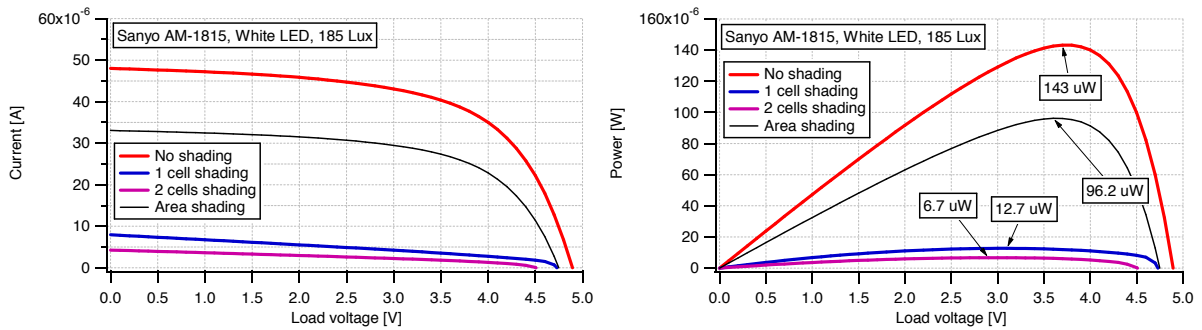


Figure 5.9: Current (left) and power (right) curves for Sanyo AM-1815, at 185 lux. Every curve is a different shading pattern.

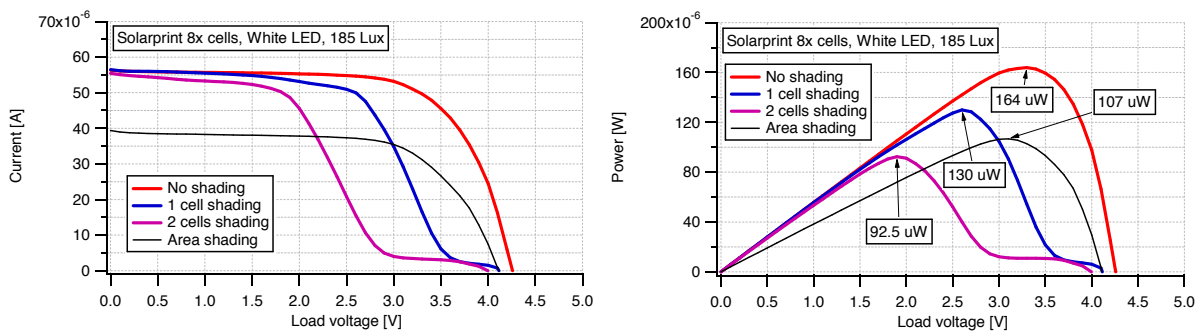


Figure 5.10: Current (left) and power (right) curves for Solarprint SP-7375, at 185 lux. Every curve is a different shading pattern.

- *single cell shading*: equivalent of a 3.53cm^2 shaded area (like fig. 4.18c);
- *double non-consecutive cells shading*: equivalent of a 7.06cm^2 shaded area (like fig. 4.18d);
- *area shading*: equivalent of a 8.7cm^2 shaded area (like fig. 4.18a).

From this graph it is possible to see that cell shading is more disruptive than area shading on the Sanyo module. Even considered that the effective area of the cell shading patterns are smaller than the area shading, the output current is sensibly less. The reason for this behavior is in the cell structure: covering a complete cell is not letting the equivalent diode to activate. Is almost like interrupting a circuit, however the panel keeps working because the cells are made of semiconductive material which will still let a certain amount of current to flow, the cells will act as a resistance. In the area shading case, instead, all the cells are working but they just have a decreased area, because part of them is covered. This results in lowering the current output.

In figure 5.10 are plotted the power and current curves for the Solarprint SP-7375 at the same illuminance (185 lux), and different shading patterns:

- *single cell shading*: equivalent of a 3cm^2 shaded area (like fig. 4.18c);
- *double non-consecutive cells shading*: equivalent of a 6cm^2 shaded area (like fig. 4.18d);
- *area shading*: equivalent of a 6cm^2 shaded area (like fig. 4.18a).

In this case the results were not expected. Solarprint panel is clearly performing better than Sanyo's one. The curves underline the typical behavior when using bypass diodes. Bypass diodes will let the current to flow in reverse direction of the cell even when the cell is not working due to

shadow or damage. However in the solar module, there are no bypass diodes, but as confirmed by Solarprint, is an intrinsic property of DSSC technology. Furthermore due to the fact that this property is available without any additional manufacturing process, it will not affect in any case the cost of the PV panels, but it will surely increase their market value, because it is a feature that silicon panels do not have.

To sum up, the tests showed that there is no evidence of multiple maxima, that can interfere with a MPPT algorithm. Multiple maxima are likely to appear in mixed kind of architectures such as the one used for outdoor solar arrays, where panels are made by parallel and series cells at the same time. Partial shading is a relative problem for the Solarprint module, which handles it in very good way. However in real life scenario it will be very hard to predict the size of the problem. As consequence probably the most common scenario will be the *area shading* case: an attenuated curve, more similar to a diminishing in illuminance.

5.2.6 Nominal Output Power

The aim of this section is to summarize with two graphs the power performances of the tested device, at indoor range of illuminance.

Figure 5.11 (up) shows the nominal powers of the different solar arrays. Although the power curves are very close together. To solve this superposition of curves, the Sanyo AM–1815 was taken as reference since is considered as mature technology and also a market leader. All

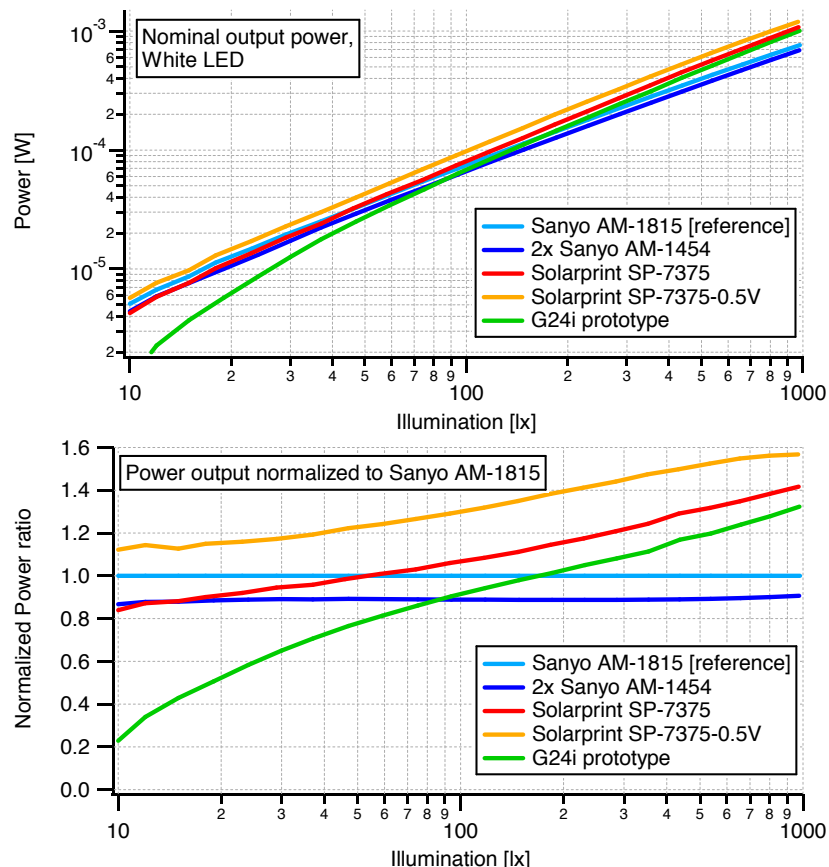


Figure 5.11: Nominal output power curves (up), normalized curves (down) with respect to Sanyo AM–1815, at different illuminance levels.

the nominal power values are then normalized to the ones of the Sanyo AM-1815. The result is shown in picture 5.11 (bottom), the AM-1815 assumes always the value 1.

The normalized plot presents a very interesting result: same solar technology arrays have similar power curves. In fact all the DSSC panels (the two Solarprint and the G24i ones), have mostly parallel power curves. The same is for a-Si modules. However DSSCs, excluding Solarprint-7375-0.5V, have lower performances at low light levels.

5.2.7 Power Density

Instead of considering the power output of every module, here the intent is to analyze the power density. Power density is useful to understand the building quality of a panel and the technology trends. For instance, Solarprint modules are still prototypes and they can still improve their characteristics.

To generate the density data, all the panels maximum power curves of 5.11 are taken and divided by the respective area, the result is the power density expressed in W/cm^2 . Figure 5.12 (up) shows the outcome of the calculation.

In the same way it was done for nominal output power, the densities are normalized with respect of the Sanyo AM-1815 device. The result of the normalization is shown in figure 5.12 (bottom).

It is evident that G24i panel has the worse power density among the tested modules, nevertheless this does not obligatory mean less power. The G24i cells need bigger area to generate

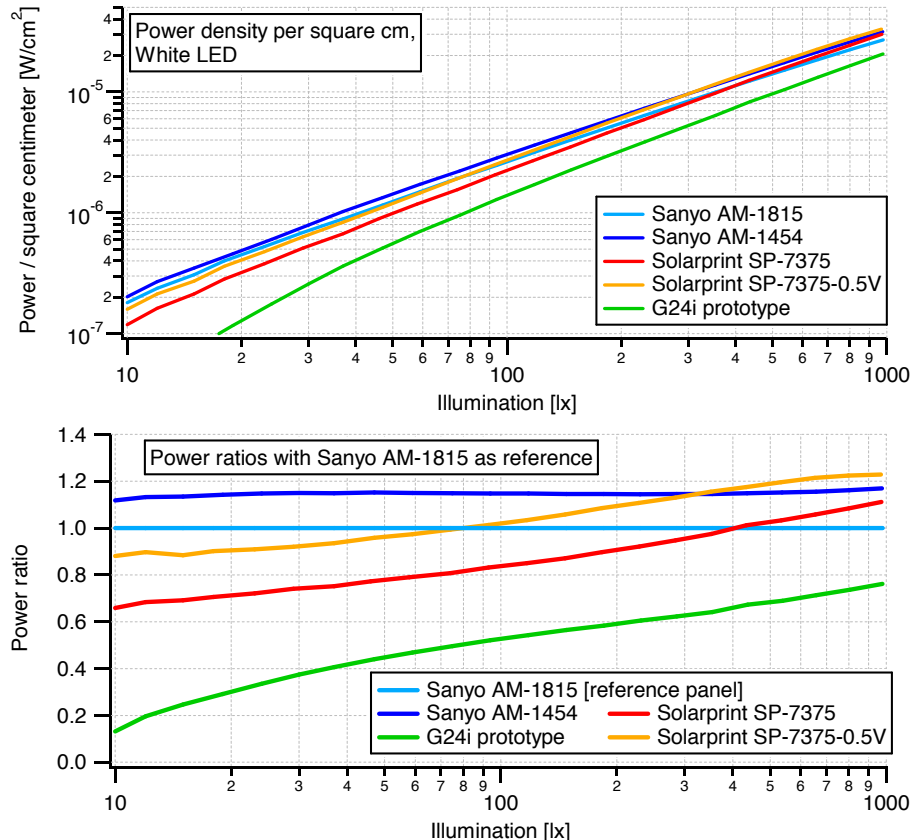


Figure 5.12: Power density curves (up), normalized curves (down) with respect to Sanyo AM-1815, at different illuminance levels.

the same amount of power of the others, however they are extremely flexible and handy. Even if the tested is a prototype, their products have recently entered the market. So together with a-Si they are already available.

Similarly to what described in the previous section, also in the normalized efficiency plot, the different solar technologies have the same trend. Per unit area a-Si is still more efficient, but the trend is demonstrating that DSSCs have not yet reached market maturity.

Finally Solarprint modules have a 20% difference in efficiency due to the fill factor. The 1 cell panel has a better surface efficiency, because all the active area is covered by photovoltaic material. Although in the 8 cells panel, this is not possible: a containing material, is separating the cells from leaking the photovoltaic material. This separation is not optimized yet, in fact now only 66% of the area is active. This is one of the reason that lead Solarprint to the decision of producing also a single cell module, to maximize the area efficiency. There is also a difference in the modules produced by Sanyo, in this case probably is due to the fact that the area was utilized more efficiently in the AM–1454 model rather than the AM–1815.

To sum up, for a fixed area specifications like in this project case, at low illuminance levels (less than 100lux) amorphous silicon cells are better compared to DSSC ones, whilst for more than 100lux DSSCs are the beste choice.

Chapter 6

The Harvesting System

In this chapter are proposed different solutions for EH power management. Various products according to the PV cells technologies are going to be investigated in order to obtain always the maximum charging current and the best efficiency. The aim of this thesis, in fact, is not only giving a solution for nowadays available technologies, but also for the future ones such as the DSSCs, considered the third generation of PV cells.

6.1 Commercial Energy Harvesting Chips

Energy Harvesting is still a growing sector in the market, it still suffers for being very young, however, there are already interesting solutions able to perform decently at very low power levels.

In this section will be presented all the relevant commercial chips found on the market and in prototyping phase. The reason is to give the reader a good knowledge of the research direction in this sector. All the chips are going to be analyzed according to the specifications provided in the datasheets. Finally the ICs characteristics are collect in a summarizing table (table 6.1).

6.1.1 BQ25504

The BQ25504 is a chip produced by Texas Instruments Incorporated. It integrates a low power boost converter and a charging protection circuit. The declared current consumption is around $330nA$. One of its pros, is the ability to manage low voltage sources such as: single or double solar cells or thermoelectric generators. The boost converter can be started with V_{IN} as low as $330mV$, and once started, can continue to harvest energy down to $V_{IN} = 80mV$, with an average efficiency of more than 80%. It works with a lot of battery types since it is possible to program undervoltage and overvoltage levels.

The BQ25504 also implements a programmable maximum power point tracking sampling network to optimize the transfer of power into the device [36]. The MPPT algorithm in the IC, is the fractional open circuit voltage [section 3.2.3], it samples the V_{oc} every 16 seconds in a 256ms windows.

Texas Instruments is providing very detailed application notes on how to calculate the resistors network to set the V_{mpp} and V_{oc} ratio, and also the charging thresholds.

6.1.2 MAX17710

The MAX17710 is a chip produced by Maxim Integrated Products. It is a very flexible EH solution, it can accept unregulated inputs of low voltage as well as high voltage ones. It works with

single, double or 8 solar cells, piezo, thermoelectric generators and even AC sources like radio waves. The MAX17710 is a complete system for charging and protecting micropower–storage cells such as Infinite Power Solution’s THINERGY microenergy cells (MECs) [37].

It features two different charging modes: linear and boost. Linear charging is used for sources with a voltage V_{IN} bigger than battery one V_{BATT} , this method dissipate only about $625nA$ of current. The boost converter can harvest energy down to approximately $1\mu W$ when operated in pulsed mode and as high as $100mW$ in continuous conversion. The boost converter can be started with an input voltage as low as 750 mV, and once started, it can continue to harvest energy down to 250 mV input voltage [37].

It provides an undervoltage and overvoltage shunt protection, limiting the maximum cell voltage to 4.125V. It also includes an internal voltage protection preventing the cell from overdischarging by not allowing the cell voltage falling under 2.15V. The IC includes also a low-dropout (LDO) linear regulator with selectable voltages of 3.3V, 2.3V, or 1.8V. This is useful for systems that are not able to run at the MECs voltage (4.0V).

Finally Maxim choose not implement any MPPT circuit, because they say: “while an MPPT system can utilize the harvesting source more intelligently in high–power situations, it inevitably results in higher quiescent current and a poorer break–even threshold” [37].

6.1.3 MAS6011

The MAS6011 is a chip produced by Micro Analog Systems. The MAS6011 solar cell system manager monitors the supply voltage and charging of a battery–powered system containing a small solar cell. The current consumption of this IC is extremely low, 110 nA [38]. This device is very simple but also cheap and rather complete for the purposes of this project. However it has some constraints: it was made only for solar cells and Li–Va batteries.

The starting voltage is 2.0V, making the chip able to work only with 4 or 8 cells PV panels. It integrates an overcharging protection, but under discharging one. However with an external microcontroller is it possible to set also this last one. It requires a protecting diode (such as BAT54) to stop battery reverse current from damaging the solar device, when there is low light.

6.1.4 LTC4071

The LTC4071 is a chip produced by Linear Technology Corporation. It allows simple charging of Li-Ion/Polymer batteries from very low current, intermittent or continuous charging sources. The current consumption is quite low, around $550nA$.

The LTC4071 provides a simple battery protection and charging solution by preventing the battery voltage from exceeding a programmed level. Its shunt architecture requires just one resistor from the input supply to charge and protect the battery in a wide range of battery applications [39].

6.1.5 CBC915

The CBC915 is a chip produced by Cymbet Corporation. It can use any type of EH transducer: light, vibration, thermal and RF. It works only with Cymbet EnerChip CBC050 Thin Film Energy Storage Devices. It has a protection circuit. Like for the MAX17710 and MAS6011, this IC is compatible only with a battery technology.

The CBC915 uses an advanced MPPT algorithm that constantly matches the transducer output impedance. They claim that the MPPT used is: very efficient method of converting energy from an EH transducer and is superior to charge accumulation techniques that do not match the impedance of the transducer to the power conversion stage. However there is no data

showing the real performances. The CBC915 operates in multiple modes and can communicate with microcontrollers [40].

6.1.6 ANG1010

The ANG1010 is a chip produced by Anagear Semiconductors. This component is still a prototype and not in production at the moment this thesis was written. All the following information may change with time and from the final datasheet, they are extracted from the company website.

It is designed especially for solar panels but can work also with others sources. The photovoltaic input should be in the range of 1.5–3.5V. The ANG1010 outputs two different programmable voltages in the range of 0.9–3.0V. It has an integrated MPPT control. The declared current consumption in deep sleep mode is less than $50nA$, and in standby is around $400nA$.

This IC is also capable to be connected to a primary battery. This is a very interesting feature, since due to discontinuity of EH sources, there is the possibility the system will run out of power from the rechargeable battery. That is why usually, EH is not the primary energy source but it used more as a backup. This reasons make this chip a very complete solution for EH systems. Surplus energy generated by a PV panel, is stored in a buffer capacitor or a rechargeable battery (like MECs or Li–Va). Internal circuitry will automatically select the highest available input voltage.

A 12-bit ADC monitors the battery voltage to protect from undercharging and overcharging. It has an integrated microcontroller with EEPROM and RAM and serial interface. Another important feature is that the chip also has onboard low power oscillators, that can be used as timers (instead of using similar functions in code, which require more power).

6.1.7 Considerations

Among all these possible solutions, it was decided to test in this thesis the following chips, for the following reasons:

- *BQ25504*: is a very efficient boost charger with possibility to control the overcharging and underdischarging voltages, making it usable with various rechargeable batteries. It is very low power and integrates a MPPT circuit;
- *MAX17710*: is the most handy device: with possibility to use both high and low voltage sources. Although it works only with MECs cells and provides them a good protection;
- *MAS6011*: its energy consumption is the lowest for this kind of devices. It is simple and low cost, but needs an underdischarging protection, and works only with Li–Va cells.

LTC4071 is a good low power linear converter, but compared to the MAX17710, it offers less features and to the MAS6011, it is more power consuming. CBC915 is very complex IC with a lot of features not required in this project, but the biggest problem is that it uses all proprietary technologies, such as storage chips which have a capacity of only 50 maximum. ANG1010 is an interesting chip on the paper, but is still under developing and prototyping.

Table 6.1 summarizes the characteristics.

Table 6.1: Summarizing table for EH chips. Prices are for single component and they are extracted from <http://www.digikey.com>.

	Types of EH sources	Current/power consumption	Starting voltage	Converter type	MPPT	Charging protections	Battery types	IDO	Cost
BQ25504	Low voltage DC (solar, thermal)	$330nA$	$330mV$	boost	yes	yes	Li-Ion, Li-Va MECs, Scap	no	\$ 6.35
MAX17710	Low/high voltage DC/AC (solar, thermal, vibration)	$625mA$ linear $1\mu W$ boost	$750mV$	boost + linear	no	yes	MECs	1.8, 2.3 or 3.3V	\$ 8.89
MAS6011	Solar	$110nA$	$2.0V$	diode	no	only overcharging	Li-Va	no	\$ 1-1.5
LTC4071	Solar, piezo	$550mA$	—	diode	no	yes	Li-Ion, MECs	no	\$ 4.92
CBC915	Low/high voltage DC/AC (solar, thermal, vibration)	—	—	charge pump	yes	yes	proprietary cells	no	\$ 4.91
ANG1010	Solar optimized	$400nA$	$1.5V$	boost + buck	yes	yes	Lithium cells	2 adj out 0.9 - 3.0V	—

6.2 Tested Solutions

Based on the considerations in section 6.1.7, the selected chips were tested to verify their behavior, reliability, efficiency, closeness to the declared values and compare between them.

The experiments were performed by connecting the different devices in series with the Fluke 8846A multimeter to measure the output current. In parallel, a voltage source was simulating the battery load voltage as described for the model in section 4.2. Batteries are really unpredictable sources due to lot of factors involved (chemicals deterioration, internal resistance, etc.), so the choice of using a voltage source as load is to be able to replicate the experiments several times with less unpredictable conditions. The serial port (RS232) is used to vary the light intensity of 12 white LEDs on top of the measuring chamber. The RS232 is also acquiring current data of the device under test. The collected values are averaged over 10 samples in order to reduce the errors.

Finally the data is processed in the computer, elaborated by the analysis tool and presented in this section.

6.2.1 Energy Harvesting with BQ25504

The board used for the tests of the BQ25504 is the evaluation module (BQ25504EVM) built by Texas Instruments; for easy reference the schematic is found in [41] fig. 11. However a few modifications were done to set some parameters. The programmable voltages of the chip are the: V_{MPP}/V_{oc} ratio, the undervoltage, overvoltage and the battery OK level.

For what concerns the MPPT circuit, is it possible to set the V_{MPP}/V_{oc} ratio with a resistors network, in the following way. Rewriting the equation 3.1 for the fractional open circuit voltage MPPT:

$$V_{MPP} \approx k_1 \times V_{OC} \quad (6.1)$$

in this case k_1 is set by the resistors network: $R2 = 4.43M\Omega$, $R10 = 5.6M\Omega$ and $R1 = 10M\Omega$, the V_{MPP} is the voltage drop between the series resistor $R10 + R1$:

$$V_{MPP} = \frac{R10 + R1}{R2 + R10 + R1} V_{OC} \quad (6.2)$$

by substituting the resistor values we obtain that $k_1 = 0.78$ as verified in the datasheet, so:

$$V_{MPP} = 0.78 \times V_{OC} \quad (6.3)$$

Recalling the characterizations done in section 5.2, Sanyo AM-1454 has a ratio of $V_{MPP}/V_{oc} = 0.78$, Solaprint SP-7375-0.5V has a ratio of $V_{MPP}/V_{oc} = 0.74$ and Solaprint SP-7375 has a ratio of $V_{MPP}/V_{oc} = 0.77$. Eventually it was decided to keep the ratio of 0.78, since the difference is very small and not going to influence very much the output power.

As mentioned in section 6.1.1, the BQ25504 has adjustable battery voltage, thus allowing to work with different types of batteries, such as Li-Va cells and MECs. This two batteries have respectively 3.0V and 4.0V nominal voltages. For this reason two loads type were simulated with the voltage source.

Although the BQ25504EVM is already equipped with programming resistors, the thresholds voltages selected are suitable for a 3.0V battery as showed in figure 6.1. To make the board suitable also for 4.0V batteries, a modification of the overvoltage level was required. This level is used to prevent rechargeable batteries from being exposed to excessive charging voltages or to prevent over charging a capacitive storage element. However in the experiments the storage

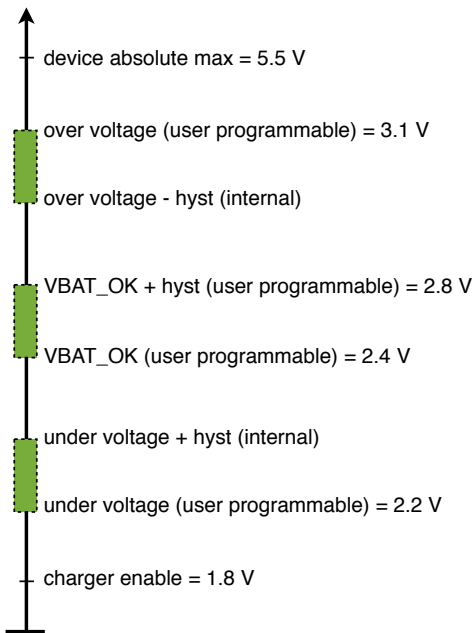


Figure 6.1: Thresholds voltages of BQ25504 with respect of the described setup.

element was emulated with the voltage source, so there was no risk of damaging it, in case a battery is connected, this tune is not suggested.

To set the VBAT_OV, two resistor are used R3 and R4, in addition Texas Instruments provides the space to place a trimmer for fine tuning of the level.

Taking the equation given in [36], and modifying it to fit with the used components, the overvoltage is:

$$VBAT_OV = \frac{3}{2} VBIAS \left(1 + \frac{R4}{R3 + R_{Trim}} \right) \quad (6.4)$$

where $VBIAS = 1.25V$ typically. The sum of the resistors must be $10M\Omega$. The values used are $R3 = 3.9M\Omega$, $R4 = 5.9M\Omega$, then a trimmer of $R13 = 1M\Omega$ was soldered, since the sum $R3 + R4 = 9.5M\Omega$ to fine tune it. The result is a threshold voltage of around 4.2V.

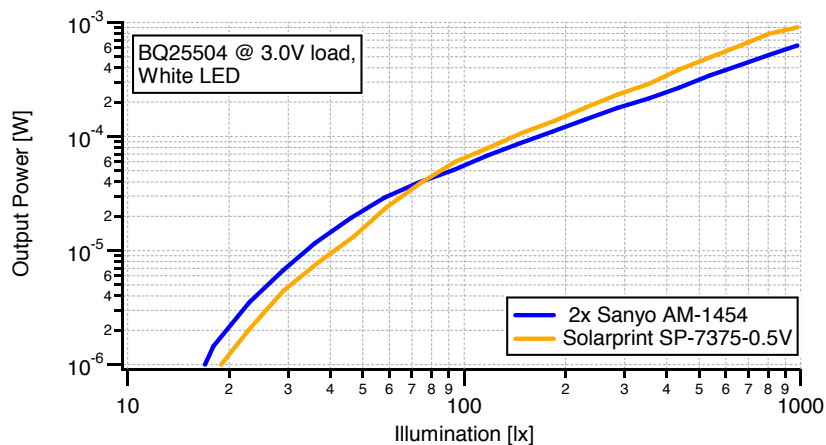


Figure 6.2: Output power of the BQ25504 with a load voltage of 3.0V. Tested performed with 2 types of solar panels.

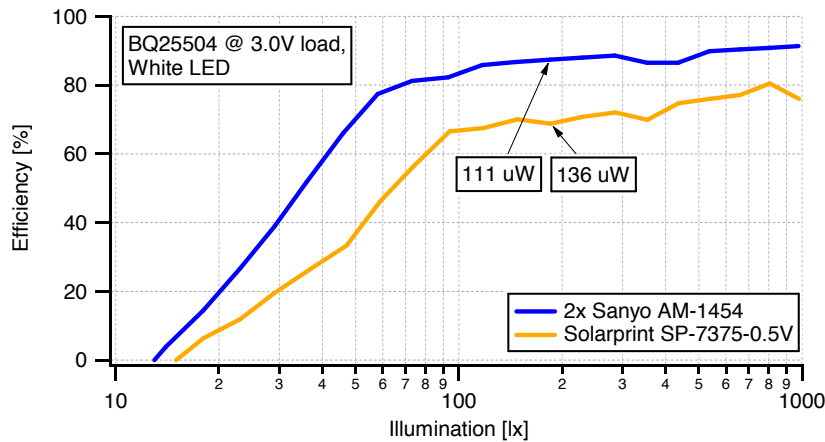


Figure 6.3: Power efficiency with respect of the MPP for the BQ25504 at load voltage of 3.0V.

To prevent rechargeable batteries from being deeply discharged and damaged, or to prevent completely depleting charge from a capacitive storage element, the undervoltage (VBAT_UV) threshold must be set using external resistors. The IC allows the user to set a programmable voltage (VBAT_OK) independent of the overvoltage and undervoltage settings to indicate whether the battery voltage is at an acceptable level. Those other thresholds were left as they were from the factory, since they are not going to influence the operation.

All the tests performed with the BQ25504, will be now differentiated, according to the load voltage, in two categories to simplify analysis and considerations.

In figure 6.2 are shown the output power curves of the device for two different types of solar arrays: Sanyo AM-1454 (average output voltage 2.0V), and Solarprint SP-7375-0.5V (average output voltage 0.5V), using a load of 3.0V. The Sanyo's panel perform better in low light conditions, but the power difference is very small, whilst at high light level the Solarprint product is sensibly better, with more than $270\mu W$ difference.

Although this disparity, in relation to their respective MPP curves, the BQ25504 reaches efficiency level (figure 6.3) of more than 80%, already at 70 lux with the Sanyo's device. Instead with the Solarprint SP-7375-0.5V, the efficiency is less, around 15% than the AM-1454.

Thanks to the overvoltage tuning, it was possible to measure also the behavior of a 4.0V load

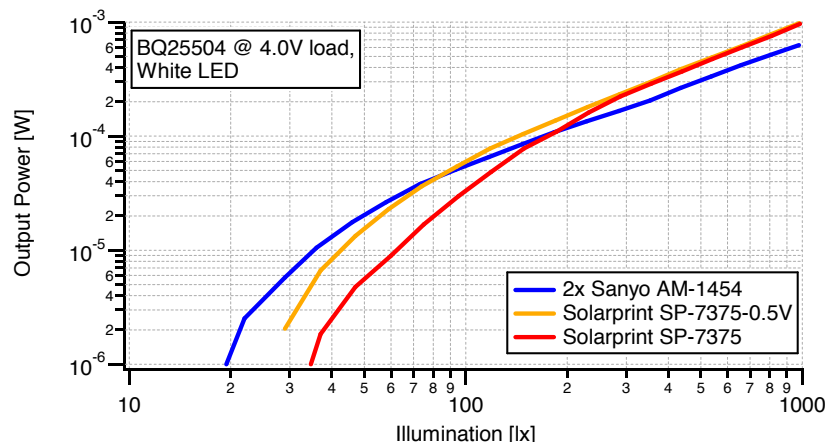


Figure 6.4: Output power of the BQ25504 with a load voltage of 4.0V. Tested performed with 3 types of solar panels.

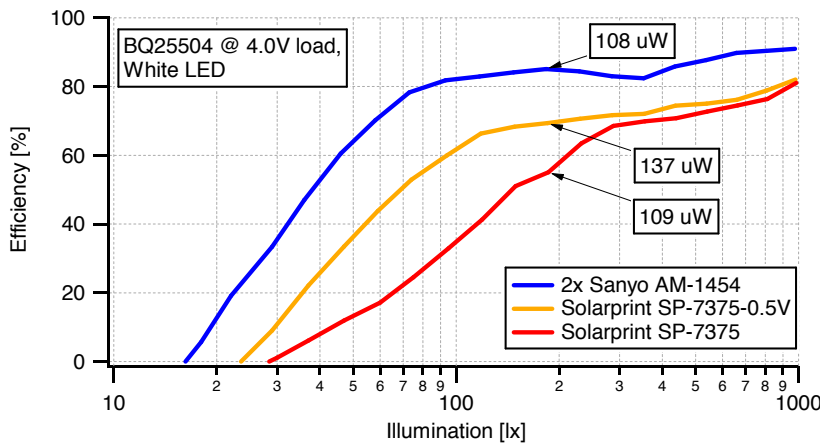


Figure 6.5: Power efficiency with respect of the MPP for the BQ25504 at load voltage of 4.0V.

such as a MEC battery. In this case, though, also the Solarprint SP-7375 sample was tested by using a voltage divider to achieve a lower input voltage, suitable for the input characteristics of the BQ25504.

Figure 6.4, shows the power performances; a part from the Sanyo one, both Solarprint devices present a reverse current at low light, this means that the chip is using energy to start-up, the current generated by the solar panels is not enough to power the IC. However at high illuminance both Solarprint modules exploit high power. At 970 lux the power is around $977\mu W$, and the difference between the SP-7375 and the SP-7375-0.5V is only $12\mu W$. Whilst between the two DSSCs and the a-Si panels, power difference is of $350\mu W$. Compared to the 3V load case, the charger using the Sanyo cells give constant performances, in contrasts with the Solarprint devices that work differently for changing light levels.

The efficiencies are shown in figure 6.5, if the illuminance is less than 200 lux the Sanyo will give both more power and better efficiency, whilst Solarprint panels are better at higher light levels.

6.2.2 Energy Harvesting with MAS6011

The peculiarity of this linear converter is the extreme active low power. This characteristic allow the IC to work efficiently even at low illuminance.

The MAS6011 does not offer the same configurations possibilities as the BQ25504, however the manufacturing company does not provide any evaluation board. For this reason a printed circuit board (PCB), was designed to test the component. Figure A.1 shows the schematic of the PCB.

All the same testing procedures were applied also to this chip. The solution with MAS6011, was especially designed to work with Li-Va battery cells, this automatically excludes the 4.0V load test.

Figure 6.6 shows the output power. It is very evident, compared to the BQ25504, that at low light levels there is still some available power that can charge a battery. In fact, thanks to the low active consumption of the IC, a small amount of power is used to run the converter, whilst the rest is delivered to the load. The average illuminance of a dark room with only an emergency light on, is around 50 lux, this means that a system with MAS6011 at 50 lux can still charge or run a microcontroller in sleep mode. Whilst the difference between PV modules for low light is very small, the Solarprint device generates $925\mu W$ at 978 lux versus the $654\mu W$ obtained out of the Sanyo AM-1815 at the same illuminance.

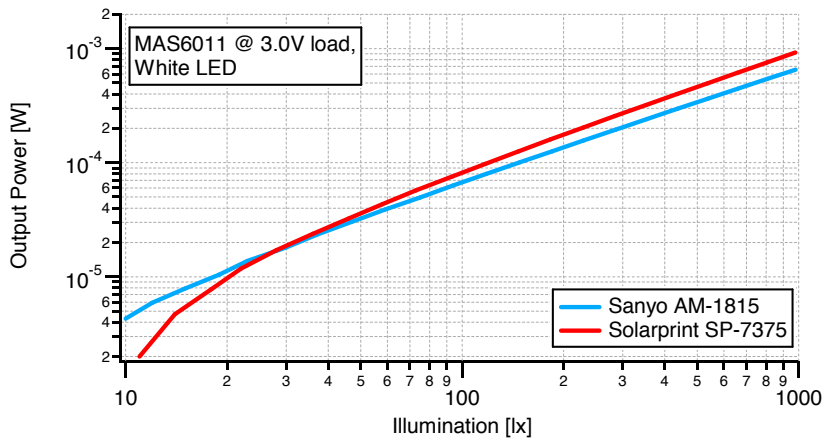


Figure 6.6: Output power of the MAS6011 with a load voltage of 3.0V. Tested performed with 2 types of solar panels.

The efficiency, plotted in figure 6.7, is very linear for the Sanyo Amorton panel. On the other side the DSSC shows peculiar trend: under 20 lux is less than 80%, around 70 lux is 100%, and finally stabilizes to 88% for high illuminance.

6.2.3 Energy Harvesting with MAX17710

This device integrates both a linear converter and a boost converter. They are used to charge a 4.0V MEC cell, according to the input source voltage. For EH sources with a voltage higher than 4.0V, the linear charger can work up to 5.3V. Instead, for low voltages EH sources, a step-up converter activates to charge the battery using burst or continuos mode according to the available power. To operate the switching-regulator, the input voltage must be higher than 0.7V, so for this experiment the Solarprint SP-7375-0.5V was automatically excluded.

The electronic board used for testing is the evaluation module MAX17710EVKIT (fig. 2 in [42]), produced by Maxim as well. No other component was added to change parameters, but some jumpers were changed, to exclude the integrated PV cells and MEC soldered on board.

In **linear mode** the MAX17710 works similarly to the MAS6011, by limiting the voltage (to 4.125V for MECs) and forwarding a constant current. Due to this load voltage, the two tested

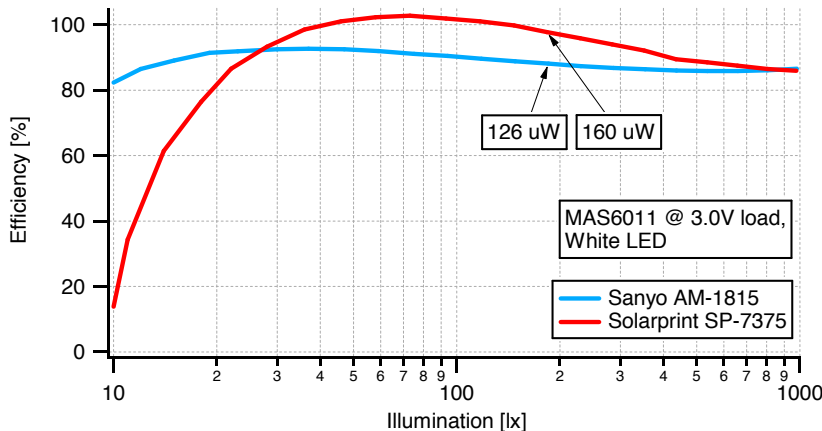


Figure 6.7: Power efficiency with respect of the MPP for the MAS6011 at load voltage of 3.0V.

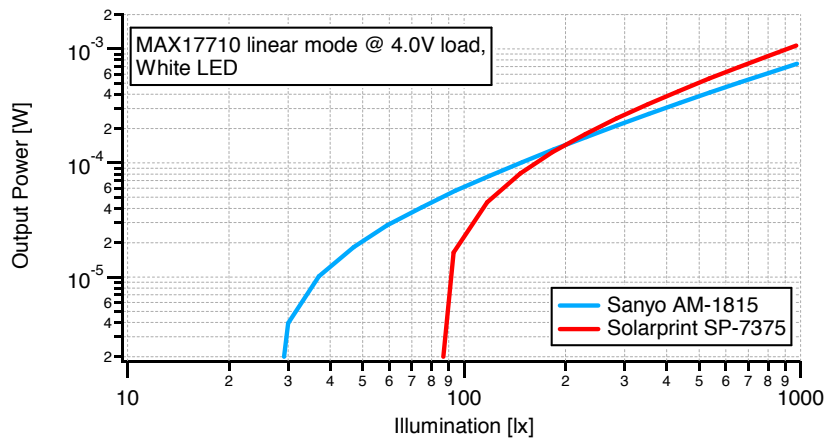


Figure 6.8: Output power of the MAX17710 with a load voltage of 4.0V. Tested performed with 2 types of solar panels.

solar panels: Sanyo AM-1815 and Solarprint SP-7375 present a significant output power drop at low illuminance, because of their V_{oc} also decrease under 4.0V. Figure 6.8 shows exactly this behavior, the difference between the two panel depend on the average V_{oc} . The Sanyo array has a voltage of 5.0V average so it is less affected by this problem compared to SP-7375. The linear charger is not able to work anymore in low light due to low voltage, however the the MAX17710 does not switch automatically to the step-up charger for low input voltages. This could be a possible interesting feature to implement in the future versions of the chip.

Excluding this decay at illuminances lower than 100 lux, high light performances are rather good. The SP-7375 generates $1069\mu W$ at 975 lux versus the $740\mu W$ obtained out of the Sanyo AM-1815 at the same illuminance.

Compared to the MAS6011, this IC shows a higher power at 200 lux and more. The reason is evident in figure 6.9, where the efficiency of the MAX17710 in linear mode reach almost 100% at 1000 lux, whilst at lower illuminances than 200 lux, it decays very fast, due to the strict voltage requirement.

Finally, even if the current consumptions of the two chips are $110nA$, for the MAS6011, and $625nA$, for the MAX17710, the building quality of this latter linear converter is better and guarantee a bigger power transfer.

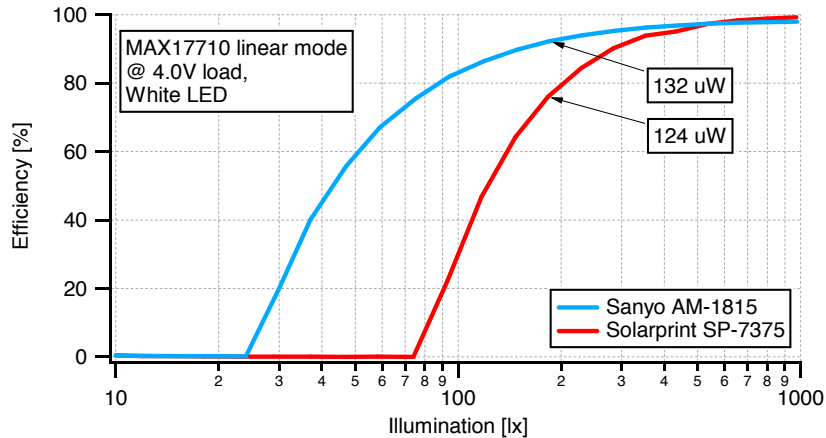


Figure 6.9: Power efficiency with respect of the MPP for the MAX17710 at load voltage of 3.0V.

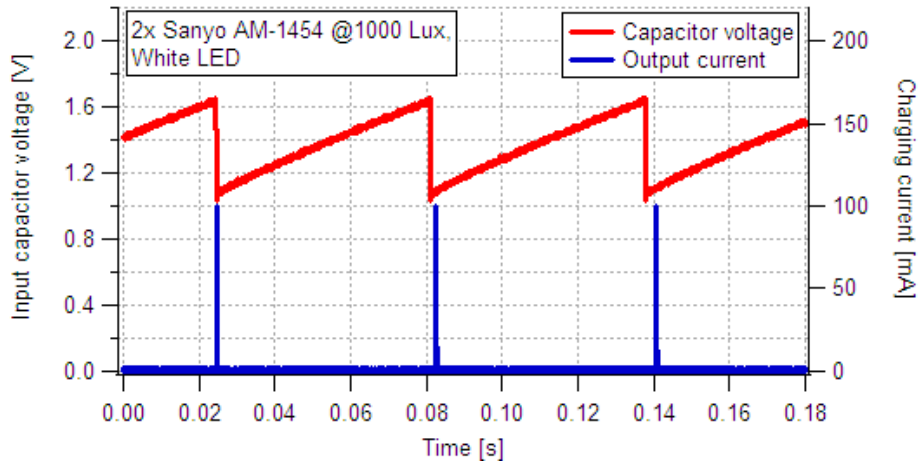


Figure 6.10: MAX17710 charging behavior. The red line represent the input voltage on the PV panel or on the C5 capacitor, the blue line is the output current to the battery.

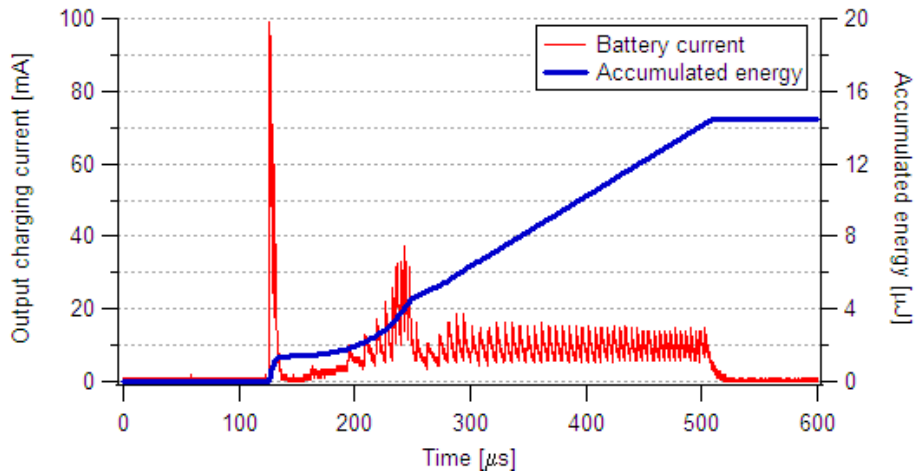


Figure 6.11: MAX17710 output charging current profile.

The **step-up converter** in the MAX17710 needs a bit of explanation. It can harvest energy down to approximately $1\mu W$ when operated in pulsed harvest mode and as high as $100mW$ in continuous conversion [37]. The converter works by charging a capacitor (C5) until the voltage on the capacitor reaches a certain threshold. After the current flows into an external inductor (L1), and every clock cycle ($1MHz$), inductor is forcing voltage into the external capacitor (C4) connected to pin CHG. When CHG voltage rises above the voltage of the battery, the charge is delivered to the cell. According to the Maxim datasheet [37]: “charge sources with operational voltages between $1.0V$ and $2.0V$ require boosting, but are too high a voltage to control the boost circuit efficiently, under these conditions, a voltage-divider is required”. The evaluation board of the MAX17710 is already equipped with a voltage divider to half the input voltage, in this way is possible to connect the $2\times$ Sanyo AM-1454 parallel module, by enabling the divider with a jumper.

Measuring the charging current in the battery was not possible using the precision multimeter due to the bursting mode of the converter. A different approach was used to gather information about the conversion efficiency. Figure 6.10 exploits the working behavior of the chip: the red

line is the output voltage from the solar panel that charges the $47\mu F$ input capacitor (C5). Then the boost converter increase this voltage to the suitable level for the battery and store it in C4. As the voltage on C4 reaches the CHG threshold, then the IC discharge C4 and deliver a current spike to the output (blue line) on the BATT pin.

The charging current profile out of the burst regulator is shown in figure 6.11); this data was acquired as voltage signal across a 10Ω resistor, with a digital oscilloscope. The pulses frequency is changing according to the light availability, this is reasonable since with lower illuminance, the IC needs more time to accumulate the same amount of energy in C4. To measure the amount of energy delivered from the MAX17710 to the battery it can be easily done by integrating the current profile over time and multiplying by the voltage. The energy is measured in joules [J] and its formula is:

$$E = P \times t = (V \times I) \times t \quad (6.5)$$

where P is the power, t is the time, V the voltage and I the current. The integration was done in the analysis tool and the resulting energy is $14.46\mu J$, to obtain the correspondent value in power, it must be multiplied by the frequency of current peaks. For 1000 lux, the frequency is $f = 1/0.058s = 17.24s^{-1}$ (fig. 6.10). Finally the power is equal to:

$$P_{out} = E_{out} \frac{1}{t} = 14.46[\mu J] \times 17.24[s^{-1}] = 249.3[\mu W] \quad (6.6)$$

The available input power can instead be calculated in two ways by computing the energy stored in the capacitor or how fast is charged the capacitor, in any of the two cases the result is the same. The energies collected in the capacitor just after the discharge and before the discharge are:

$$E_{chg} = \frac{1}{2} CV_1^2 = \frac{1}{2} \times 47[\mu F] \times 1.05^2[V^2] = 25.9[\mu J] \quad (6.7)$$

$$E_{dischg} = \frac{1}{2} CV_2^2 = \frac{1}{2} \times 47[\mu F] \times 1.65^2[V^2] = 64[\mu J] \quad (6.8)$$

the resulting energy is the difference between the two levels: $38.1\mu J$, the resulting input power is:

$$P_{in} = E_{in} \frac{1}{t} = 38.1[\mu J] \times 17.24[s^{-1}] = 656.8[\mu W] \quad (6.9)$$

In this way the resulting efficiency, between the output power and the input one, is very low equal to 38%. This number is not comparable to other converting methods, however this was the procedure used to get the value. Due to time constraint, no further investigation was possible to be done on this converting chip.

6.3 Results

Table 6.2 sums up all the results presented in this section. All the solutions with different chips, solar modules and load voltages, are listed.

In general DSSCs are able to output more power at high illuminance levels, in opposition to a-Si cells that perform better at lower light.

Among the two different linear chips, the MAX17710 is able to squeeze more power at high light levels, rather than a more linear MAS6011 which is the only solution able to work in poorly

Table 6.2: Summarizing table for EH solutions tested in this chapter. The “–” symbol means that the power value is less than $1\mu W$.

	Converter type	Solar module	Load voltage	P_{out} at 10 lux	P_{out} at 94 lux	P_{out} at 980 lux	Average efficiency
BQ25504	boost	2×AM-1454	3.0V	-	51 μW	629 μW	62.8%
	=	SP-7375-0.5V	3.0V	-	59 μW	905 μW	47.7%
	=	2×AM-1454	4.0V	-	50 μW	629 μW	57.5%
	=	SP-7375-0.5V	4.0V	-	54 μW	977 μW	45.4%
	=	SP-7375	4.0V	-	29 μW	965 μW	33%
MAX17710	linear	AM-1815	4.0V	-	57 μW	740 μW	62.9%
	=	SP-7375	4.0V	-	16 μW	1069 μW	44%
	boost	2×AM-1454	4.0V	n.a.	n.a.	249 μW	n.a.
MAS6011	linear	AM-1815	3.0V	4 μW	63 μW	654 μW	88.6%
	=	SP-7375	3.0V	2 μW	75 μW	925 μW	84.9%

illuminated environments. In fact, due to its extremely low power construction, MAS6011 is able to maintain an average efficiency of more than 80% for all the illuminance range.

It is not really possible, instead, to compare boost converters due to the problems to collect data from the MAX17710, however there are enough data about the BQ25504. This latter chip works decently in both low and high illuminance, but is not able to deliver a positive power in very dark rooms. Output power varies also according to the load voltage, because the more the light the higher is the solar module voltage. So 3.0V load gather more power than 4.0V load around 100 lux, and viceversa happens around 1000 lux.

The MPPT techniques tested (fixed voltage and fractional open circuit voltage), demonstrated to have a high efficiency generally for an illuminance of more than 100 lux. Therefore at low light the simple fixed voltage gives more than 80% efficiency, as showed in figure 6.7, for this reason there is no need to use more accurate techniques of MPPT for this kind of applications.

Finally, all the three tested solutions perform good at medium and high light levels, and different loads. Therefore they all demonstrated to be valid alternatives provided they match the application specific requirements.

Chapter 7

Conclusions

In this Master Thesis, the work was focused on developing an Energy Harvesting system, for indoor usage, capable of efficiently transfer the energy generated by the solar panel, to the storage element. The main issues with this kind of sources is the inconsistency of energy and the low availability of power.

Furthermore this thesis successfully reached the established goals and completed the sequent tasks:

- Research and study the MPPT methods, and analyze their characteristics and performances in order to select the most appropriates for EH usage.
- Model of EH system power components: solar cells, batteries. Several models are proposed in order to provide the reader with the right tools to understand the behavior of those devices, both mathematically and electronically.
- Characterization of four samples of industrial solar cells, enriching this thesis with more information than what is possible to get from manufacturers datasheets. A study also on partial shading and power density was conducted, dismissing the problem of multiple maxima and verifying the development of DSSCs as next generation of solar cells. Furthermore using the same measurements approach, the reader is able to reproduce all the experiments thanks to exhaustive explanations.
- Demonstrated that DSSC have good potentiality, they are already able to perform better than a-Si cells and will probably dominate the future of indoor solar devices. For instance manufactures started already to develop products integrating them, even if they are not mature yet.
- Accurate study of the majority of the EH power management ICs available on the market at the moment this thesis was written.
- Broad and exhaustive measurements for three very interesting PMICs. All the chips were tested in terms of different illuminances, solar panels and voltage loads. The results are presented in clear graphs and a summary section helps to collect and compare them.

Finally during the research in this field, the author noticed that all the information available were fragmented and there was no single complete reference or book. For this reason this thesis represents a good background for EH developers, both hardware and software, due to the passion and the intent of the author, to collect the most useful material in this topic. With the final aim of helping readers, approaching energy harvesting, to have all the tools to successfully

understand the challenges. Furthermore this work achieved also the intent to bring knowledge in Assa Abloy in order to help the work of others employees to develop future products.

7.1 Future Work

The first objective of this project was to study the MPPT techniques, however during the development the objectives changed. It was decided to give the thesis a wider topic and focus on evaluating commercial solutions performances. The project itself is almost complete and fulfill the specifications, but in a future perspective, there could be further studies such as:

- Develop a better testing circuit for the MAX17710, in order to validate the efficiency and the nominal power out of the step-up regulator. Collect the new data and compare them with switching-convertisers, such as BQ25540.
- Taking into account the study on the PMIC performances did in this project, select one of the tested solutions to design and realize a complete energy harvesting device.
- Measure how much energy a energy harvesting system, like the one discussed in this project, can harvest. The measurements should be at different daytimes and places. This will allow to create a useful statistics that would be, together with this thesis, a good reference for a solar energy harvesting developer.

Bibliography

- [1] Sanyo Ltd, “Amorphous Silicon Solar Cells Amorphous Photosensors,” Feb. 2011.
- [2] J. David, “Nickel-cadmium battery recycling evolution in Europe,” *Journal of Power Sources*, vol. 57, no. 1, pp. 71–73, 1995.
- [3] J. H. Pedersen, “Power Converter for Energy Harvesting,” *Technical University of Denmark*, pp. 1–36, Mar. 2011.
- [4] S. Senli, “Ethernet Energy Harvesting,” Master’s thesis, KTH School of ICT, 2012.
- [5] D. Bouchouicha, F. Dupont, M. Latrach, and L. Ventura, “Ambient RF energy harvesting,” *International Conference on Renewable Energies and Power quality, Granada, Spain*, 2010.
- [6] J. Hagerty, T. Zhao, R. Zane, and Z. Popovic, “Efficient broadband rf energy harvesting for wireless sensors,” *Department of Electrical and Computer Engineering, University of Colorado at Boulder, Boulder, CO*, pp. 80309–80425, 2005.
- [7] T. Starner and Massachusetts Institute of Technology. Perceptual Computing Section, “Human powered wearable computing,” 1995.
- [8] L. Bao and X. Li, “Towards Textile Energy Storage from Cotton T-Shirts,” *Advanced Materials*, vol. 24, pp. 3246–3252, May 2012.
- [9] S. Roundy, “Energy scavenging for wireless sensor nodes with a focus on vibration to electricity conversion,” 2003.
- [10] M. Grätzel, “Conversion of sunlight to electric power by nanocrystalline dye-sensitized solar cells,” *Journal of Photochemistry and Photobiology A: Chemistry*, vol. 164, pp. 3–14, June 2004.
- [11] Solarprint, “DSSC Module Leaflet 1 page,” *solarprint.ie*, pp. 1–1, Dec. 2011.
- [12] M. Grätzel, “Solar cells to dye for,” *nature*, vol. 421, no. 6923, pp. 586–587, 2003.
- [13] L. Castañer and S. Silvestre, *Modelling photovoltaic systems using PSpice*. Wiley, 2002.
- [14] R. Twohig, “Comparison of Indoor PV modules,” *solarprint.ie*, pp. 1–6, Oct. 2011.
- [15] A. Dolara, R. Faranda, and S. Leva, “Energy comparison of seven MPPT techniques for PV systems,” *J. Electromagn. Anal. Appl.*, vol. 3, pp. 152–162, 2009.
- [16] T. Esram and P. L. Chapman, “Comparison of Photovoltaic Array Maximum Power Point Tracking Techniques,” *IEEE Transactions on Energy Conversion*, vol. 22, pp. 439–449, June 2007.

- [17] N. Sridhar and D. Freeman, "A study of dye sensitized solar cells under indoor and low level outdoor lighting: comparison to organic and inorganic thin film solar cells and methods to address maximum power point tracking," *solarprint.ie*.
- [18] Texas Instruments, Incorporated, "Introduction to Photovoltaic Systems Maximum Power Point Tracking," *Application Report*, pp. 1–8, Nov. 2010.
- [19] J. Kim, J. Kim, and C. Kim, "A Regulated Charge Pump With a Low-Power Integrated Optimum Power Point Tracking Algorithm for Indoor Solar Energy Harvesting," *IEEE Transactions on Circuits and Systems II: Express Briefs*, vol. 58, pp. 802–806, Dec. 2011.
- [20] H. Yu, Q. Yue, and H. Wu, "Power management and energy harvesting for indoor photovoltaic cells system," *Mechanic Automation and Control Engineering (MACE), 2011 Second International Conference on*, pp. 521–524, 2011.
- [21] A. Weddell, G. Merrett, and B. Al-Hashimi, "Ultra low-power photovoltaic MPPT technique for indoor and outdoor wireless sensor nodes," *Design, Automation & Test in Europe Conference & Exhibition (DATE), 2011*, pp. 1–4, 2011.
- [22] D. Brunelli, L. Benini, C. Moser, and L. Thiele, "An efficient solar energy harvester for wireless sensor nodes," *Proceedings of the conference on Design, automation and test in Europe*, pp. 104–109, 2008.
- [23] S. Laurier, "Experimental analysis of photovoltaic energy scavengers for sensor nodes," *Electronics and Information systems. University of Ghent, Belgium*, 2007.
- [24] H. Yu, H. Wu, Y. Wen, and P. Li, "Indoor micro-light energy harvesting system for low power wireless sensor node,"
- [25] A. Weddell, G. Merrett, and B. Al-Hashimi, "Photovoltaic Sample-and-Hold Circuit Enabling MPPT Indoors for Low-Power Systems," *Circuits and Systems I: Regular Papers, IEEE Transactions on*, no. 99, pp. 1–1, 2011.
- [26] Y. Lim and D. Hamill, "Synthesis, simulation and experimental verification of a maximum power point tracker from nonlinear dynamics," *Power Electronics Specialists Conference, 2001. PESC. 2001 IEEE 32nd Annual*, vol. 1, pp. 199–204 vol. 1, 2001.
- [27] P. Midya, P. Krein, R. Turnbull, R. Reppa, and J. Kimball, "Dynamic maximum power point tracker for photovoltaic applications," *Power Electronics Specialists Conference, 1996. PESC'96 Record., 27th Annual IEEE*, vol. 2, pp. 1710–1716 vol. 2, 1996.
- [28] D. Dondi, D. Brunelli, L. Benini, P. Pavan, A. Bertacchini, and L. Larcher, "Photovoltaic cell modeling for solar energy powered sensor networks," *Advances in Sensors and Interface, 2007. IWASI 2007. 2nd International Workshop on*, pp. 1–6, 2007.
- [29] D. Sera, "Real-time Modelling, Diagnostics and Optimised MPPT for Residential PV Systems," 2009.
- [30] V. Yong, S.-T. Ho, and R. P. H. Chang, "Modeling and simulation for dye-sensitized solar cells," *Applied Physics Letters*, vol. 92, no. 14, p. 143506, 2008.
- [31] M. Chen and G. Rincon-Mora, "Accurate electrical battery model capable of predicting runtime and IV performance," *IEEE Transactions on Energy Conversion*, vol. 21, no. 2, pp. 504–511, 2006.

- [32] “OrCAD PSpice - User’s Guide,” *OrCAD*, pp. 1–436, Nov. 1998.
- [33] B. Al-Hashimi, *The art of simulation using PSpice*. analog and digital, CRC, 1995.
- [34] Fluke, “8842A Instruction Manual,” *Instruction Manual*, pp. 1–269, Apr. 2012.
- [35] Fluke, “Fluke 8845A/8846A,” *User Manual*, pp. 1–103, July 2008.
- [36] T. Instruments, “BQ25504 - Ultra Low Power Boost Converter with Battery Management for Energy Harvester Applications,” *Datasheet*, pp. 1–24, Oct. 2011.
- [37] Maxim, “MAX17710 Energy Harvesting Charger and Protector,” *Datasheet*, pp. 1–17, Aug. 2011.
- [38] M. A. Systems, “MAS6011B Solar Cell Energy Harvesting System Manager,” *Datasheet*, pp. 1–10, Oct. 2011.
- [39] Linear Technology Corporation, “LTC4071 - Li-Ion/Polymer Shunt Battery Charger System with Low Battery Disconnect,” *Datasheet*, pp. 1–18, Oct. 2011.
- [40] Cymbet Corporation, “EnerChip™ Energy Processor for Energy Harvesting Applications - CBC915,” *Datasheet*, pp. 1–16, Mar. 2012.
- [41] Texas Instruments Ltd, “bq25504 EVM,” *User’s Guide*, pp. 1–17, Oct. 2011.
- [42] Maxim Integrated Ltd, “MAX17710GB20 Evaluation Kit,” *User’s Guide*, pp. 1–8, Mar. 2012.
- [43] M. Grätzel, “Dye-sensitized solar cells,” *Journal of Photochemistry and Photobiology C: Photochemistry Reviews*, vol. 4, pp. 145–153, Oct. 2003.
- [44] Y. K. Tan and S. K. Panda, “Energy Harvesting From Hybrid Indoor Ambient Light and Thermal Energy Sources for Enhanced Performance of Wireless Sensor Nodes,” *IEEE Transactions on Industrial Electronics*, vol. 58, pp. 4424–4435, Sept. 2011.
- [45] O. Lopez-Lapena, M. T. Penella, and M. Gasulla, “A New MPPT Method for Low-Power Solar Energy Harvesting,” *IEEE Transactions on Industrial Electronics*, vol. 57, pp. 3129–3138, Sept. 2010.
- [46] N. Femia, G. Petrone, G. Spagnuolo, and M. Vitelli, “Optimization of Perturb and Observe Maximum Power Point Tracking Method,” *IEEE Transactions on Power Electronics*, vol. 20, pp. 963–973, July 2005.
- [47] A. K. Abdelsalam, A. M. Massoud, S. Ahmed, and P. N. Enjeti, “High-Performance Adaptive Perturb and Observe MPPT Technique for Photovoltaic-Based Microgrids,” *IEEE Transactions on Power Electronics*, vol. 26, pp. 1010–1021, Apr. 2011.
- [48] Solarprint, *Dye Sensitised Solar Cells “DSSC” Explained*. solarprint.ie, Sept. 2011.
- [49] A. Ryer, “Light measurement handbook.” international light, 1997.
- [50] C. Lu, V. Raghunathan, and K. Roy, “Maximum power point considerations in micro-scale solar energy harvesting systems,” *Circuits and Systems (ISCAS), Proceedings of 2010 IEEE International Symposium on*, pp. 273–276, 2010.

- [51] C. Alippi and C. Galperti, “An Adaptive System for Optimal Solar Energy Harvesting in Wireless Sensor Network Nodes,” *IEEE Transactions on Circuits and Systems I: Regular Papers*, vol. 55, pp. 1742–1750, July 2008.
- [52] Y. Lim and D. Hamill, “Simple maximum power point tracker for photovoltaic arrays,” *Electronics Letters*, vol. 36, no. 11, pp. 997–999, 2000.
- [53] B. O’regan and M. Grätzel, “Photoelectrochemical cells,” *Nature (London)*, vol. 353, p. 737, 1991.
- [54] D. Chan and J. Phang, “Analytical methods for the extraction of solar-cell single-and double-diode model parameters from IV characteristics,” *Electron Devices, IEEE Transactions on*, vol. 34, no. 2, pp. 286–293, 1987.
- [55] A. Taylor, “Illumination fundamentals,” *Lighting Research Center*, p. 9, 1990.
- [56] G. Gosset, O. Bulteel, P. Baijot, and D. Flandre, “Ultra-high-efficiency co-integrated photovoltaic energy scavenger,” *SOI Conference (SOI), 2011 IEEE International*, pp. 1–2, 2011.
- [57] M. Gorlatova, A. Wallwater, and G. Zussman, “Networking low-power energy harvesting devices: Measurements and algorithms,” *INFOCOM, 2011 Proceedings IEEE*, pp. 1602–1610, 2011.
- [58] G. Kovacs, “BASIC GUIDE TO VIRTUAL ELECTRONICS IN SPICE,” pp. 1–14, Apr. 1998.
- [59] MicroSim Corporation. Irvine, Calif., “MicroSim application notes,” 1996.
- [60] K. Win, S. Dasgupta, and S. Panda, “An optimized MPPT circuit for thermoelectric energy harvester for low power applications,” *Power Electronics and ECCE Asia (ICPE & ECCE), 2011 IEEE 8th International Conference on*, pp. 1579–1584, 2011.
- [61] D. Sera, R. Teodorescu, and P. Rodriguez, “PV panel model based on datasheet values,” *Industrial Electronics, 2007. ISIE 2007. IEEE International Symposium on*, pp. 2392–2396, 2007.
- [62] N. D’Souza, L. Lopes, and X. Liu, “An intelligent maximum power point tracker using peak current control,” *Power Electronics Specialists Conference, 2005. PESC’05. IEEE 36th*, p. 172, 2005.
- [63] A. Wacker, “Supplying TPS61200 With a Single Solar Cell,” *Application Report*, pp. 1–8, Mar. 2012.
- [64] M. Grätzel, “Solar energy conversion by dye-sensitized photovoltaic cells,” *Inorganic Chemistry*, vol. 44, no. 20, pp. 6841–6851, 2005.
- [65] T. Starner, “The challenges of wearable computing: Part 1,” *Micro, IEEE*, vol. 21, no. 4, pp. 44–52, 2001.

Appendix A

Schematics of the testing boards

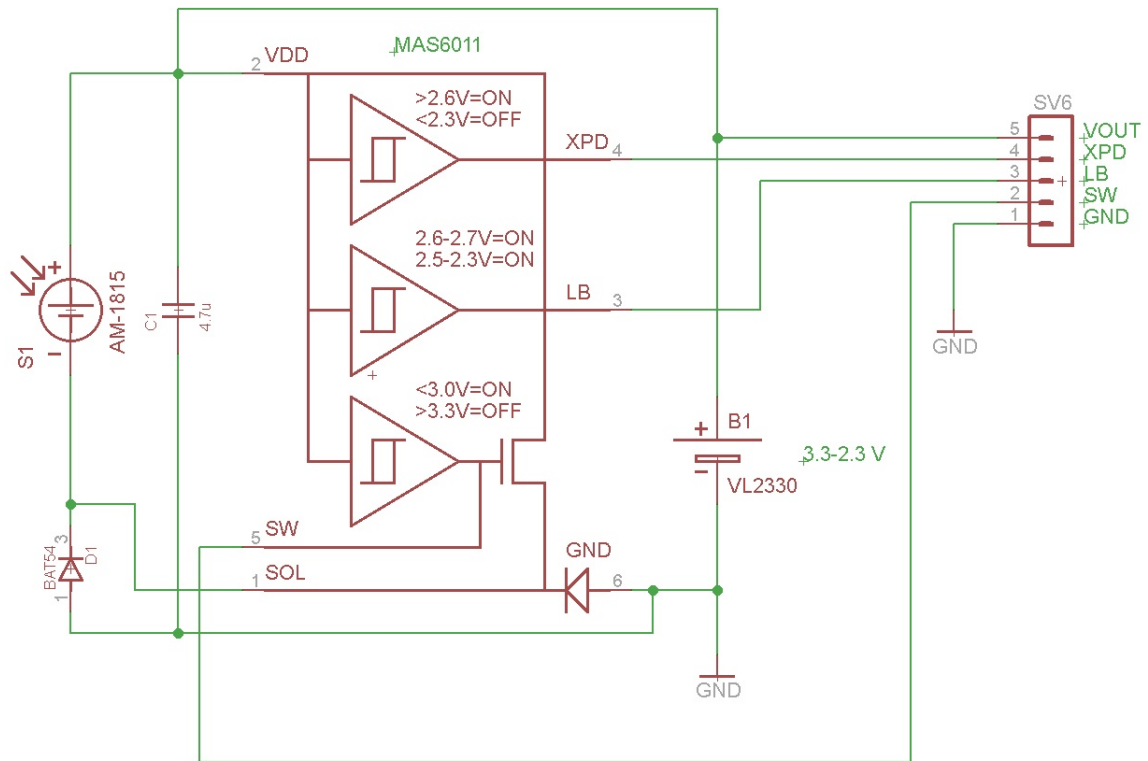


Figure A.1: Circuit schematic used to generate the testing board for MAS6011. The BAT54 diode is used to block reverse current from the battery to the solar cell.

Appendix B

PV panels and testing setup

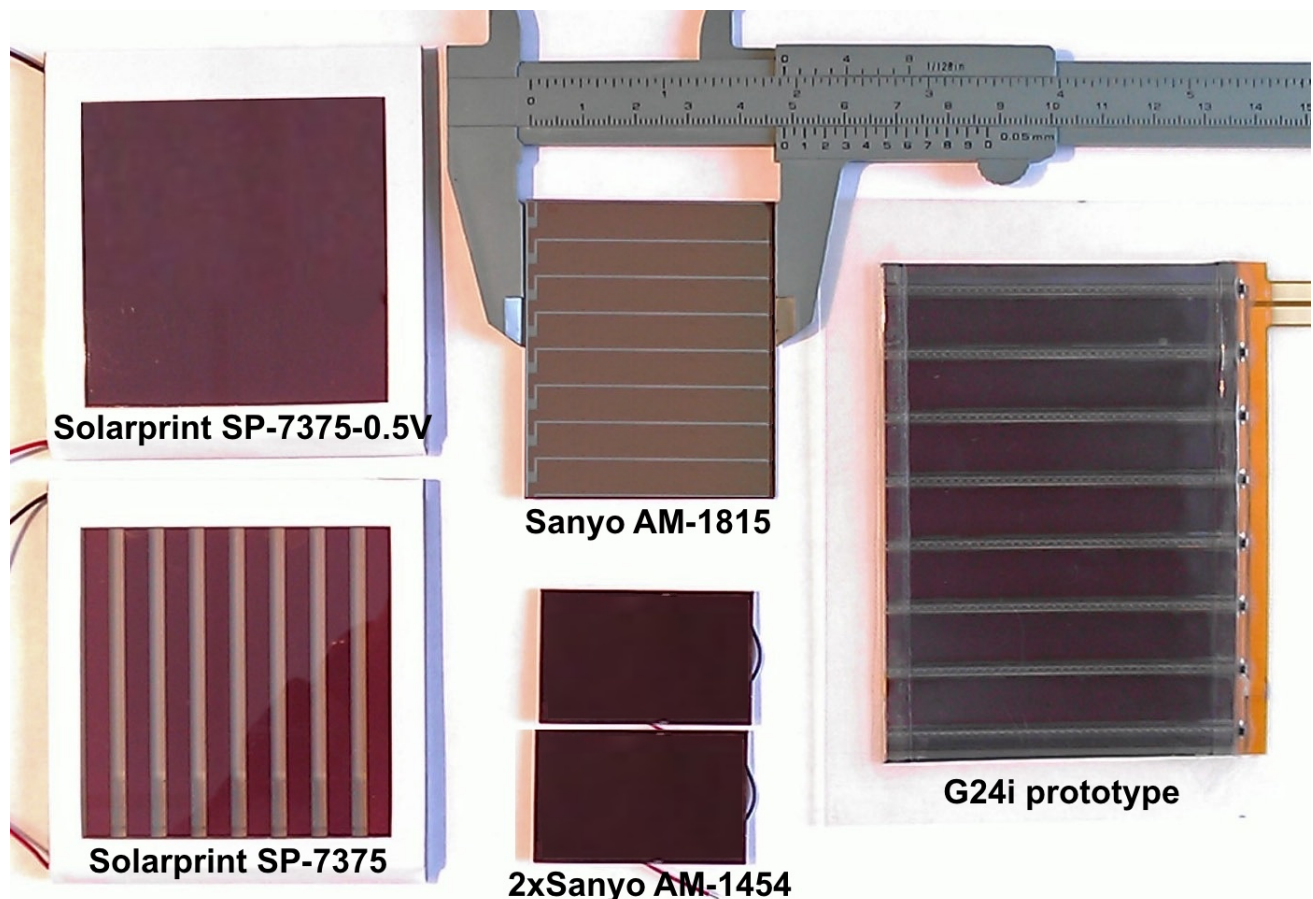


Figure B.1: The photovoltaic devices tested in this thesis.

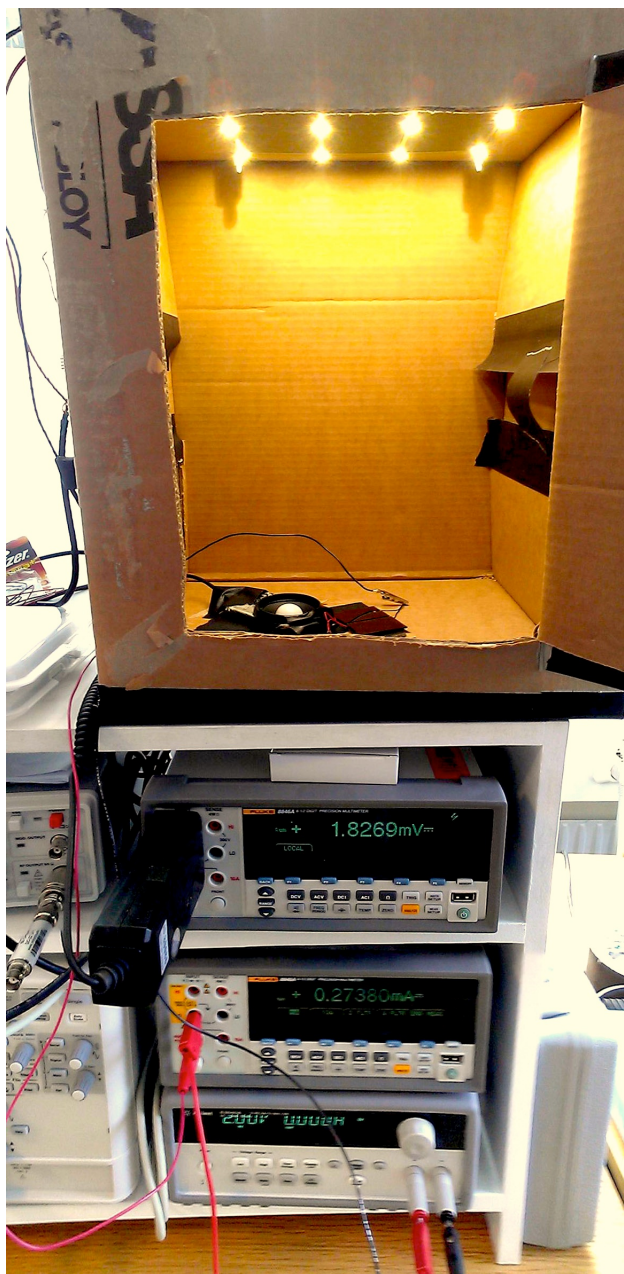


Figure B.2: The testing equipment. On top the light controlled chamber, with the lux-meter sensor. On the bottom the two precision multimeters and the DC power supply.

